Journal Information

Maejo International Journal of Science and Technology (ISSN 1905-7873 © 2014), the international journal for preliminary communications in Science and Technology is the first peer-refereed scientific journal of Maejo University (www.mju.ac.th). Intended as a medium for communication, discussion, and rapid dissemination of important issues in Science and Technology, articles are published online in an open access format, which thereby gives authors the chance to communicate with a wide range of readers in an international community.

Publication Information

MIJST is published triannually. Articles are available online and can be accessed free of charge at http://www.mijst.mju.ac.th. Printed and bound copies of each volume are produced and distributed to selected groups or individuals.

Abstracting/Indexing Information

MIJST is covered and cited by Science Citation Index Expanded, SCOPUS, Journal Citation Reports/Science Edition, Zoological Record, Directory of Open Access Journals (DOAJ), CAB Abstracts, ProQuest, Google Scholar and EBSCO.

Contact Information

Editorial office: Maejo International Journal of Science and Technology (MIJST), 1st floor, Orchid Building, Maejo University, San Sai, Chiang Mai 50290, Thailand

Tel: +66-53-87-3880; Fax: +66-53-49-8133
E-mail: duang@mju.ac.th

MAEJO INTERNATIONAL JOURNAL OF SCIENCE AND TECHNOLOGY

MAEJO INTERNATIONAL JOURNAL OF SCIENCE AND TECHNOLOGY

The International Journal for the Publication of Preliminary Communications in Science and Technology

http://www.mijst.mju.ac.th
ISSN 1905-7873

MAEJO INTERNATIONAL JOURNAL
OF SCIENCE AND TECHNOLOGY

Volume 8, Issue 2 May-August 2014

CONTENTS

http://www.mijst.mju.ac.th
ISSN 1905-7873

http://www.mijst.mju.ac.th
ISSN 1905-7873

MAEJO INTERNATIONAL JOURNAL
OF SCIENCE AND TECHNOLOGY

Volume 8, Issue 2 May-August 2014

Author Index

Instructions for Authors

A proper introductory e-mail page containing the title of the submitted article and certifying its originality should be sent to the editor (Duang Buddhasukh, e-mail: duang@mju.ac.th). The manuscript proper together with a list of suggested referees should be attached in separate files. The list should contain at least 5 referees with appropriate expertise. Three referees should be non-native from 3 different countries. Each referee's academic/professional position, scientific expertise, affiliation and e-mail address must be given. The referees should not be affiliated to the same university/institution as any of the authors, nor should any two referees come from the same university/institution. The editorial team, however, retain the sole right to decide whether or not the suggested referees are approached.

Failure to conform to the above instructions will result in non-consideration of the submission.

Please also ensure that English and style is properly edited before submission. UK style of spelling should be used. Authors who would like to consult a professional service can visit www.proof-reading-service.com, www.editage.com, www.bioedit.co.uk (bioscience and medical papers), www.bioscienceeditingsolutions.com, www.scribendi.com, www.letpub.com, www.papersconsulting.com, www.stickleredi ting.com, Cambridge Proofreading (http://proofreading.org/), www.ProofreadingServices.com, www.horizonproofreaders.org, www.manuscript-proofreding.com, Quality Proofreading, Help.Plagtracker, www.ninjaessays.com/editing/, http://bid4papers.com/editing-services.html or www.enago.com.

Important : Manuscript with substandard English and style will not be considered.

Warning : Plagiarism (including self-plagiarism) may be checked for at *the last* stage of processing and, if detected, will result in a rejection and blacklisting.

Manuscript Preparation

Manuscripts must be prepared in English using a word processor. MS Word for Macintosh or Windows, and .doc or .rtf files are preferred. Manuscripts may be prepared with other software provided that the full document (with figures, schemes and tables inserted into the text) is exported to a MS Word format for submission. Times or Times New Roman font is preferred. The font size should be 12 pt and the line spacing 'at least 17 pt'. A4 paper size is used and margins must be 1.5 cm on top, 2.0 cm at the bottom and 2.0 cm on both left and right sides of the paper. Although our final output is in .pdf format, authors are asked NOT to send manuscripts in this format as editing them is much more complicated. Under the above settings, a manuscript submitted should not be longer than **15 pages** for a full paper or **20 pages** for a review paper.

A template file may be downloaded from the *Maejo Int. J. Sci. Technol.* homepage. (DOWNLOAD HERE)

Authors' full mailing addresses, homepage addresses, phone and fax numbers, and e-mail addresses homepages can be included in the title page and these will be published in the manuscripts and the Table of Contents. The corresponding author should be clearly identified. It is the corresponding author's responsibility to ensure that all co-authors are aware of and approve of the contents of a submitted manuscript.

A brief (200 word maximum) Abstract should be provided. The use in the Abstract of numbers to identify compounds should be avoided unless these compounds are also identified by names.

A list of three to five keywords must be given and placed after the Abstract. Keywords may be single words or very short phrases.

Although variations in accord with contents of a manuscript are permissible, in general all papers should have the following sections: Introduction, Materials and Methods, Results and Discussion, Conclusions, Acknowledgments (if applicable) and References.

Authors are encouraged to prepare Figures and Schemes in colour. Full colour graphics will be published free of charge.

Tables and Figures should be inserted into the main text, and numbers and titles supplied for all Tables and Figures. All table columns should have an explanatory heading. To facilitate layout of large tables, smaller fonts may be used, but in no case should these be less than 10 pt in size. Authors should use the Table option of MS Word to create tables, rather than tabs, as tab-delimited columns are often difficult to format in .pdf for final output.

Figures, tables and schemes should also be placed in numerical order in the appropriate place within the main text. Numbers, titles and legends should be provided for all tables, schemes and figures. Chemical structures and reaction schemes should be drawn using an appropriate software package designed for this purpose. As a guideline, these should be drawn to a scale such that all the details and text are clearly legible when placed in the manuscript (i.e. text should be no smaller than 8-9 pt).

For bibliographic citations, the reference numbers should be placed in square brackets, i.e. [ ], and placed before the punctuation, for example [4] or [1-3], and all the references should be listed separately and as the last section at the end of the manuscript.

Format for References

Journal :

1. D. Buddhasukh, J. R. Cannon, B. W. Metcalf and A. J. Power, "Synthesis of 5-n-alkylresorcinol dimethyl ethers and related compounds *via* substituted thiophens", *Aust. J. Chem.*, **1971**, *24*, 2655-2664.

Text :

2. A. I. Vogel, "A Textbook of Practical Organic Chemistry", 3rd Edn., Longmans, London, **1956,** pp. 130-132.

Chapter in an edited text :

3. W. Leistritz, "Methods of bacterial reduction in spices", in "Spices: Flavor Chemistry and Antioxidant Porperties" (Ed. S. J. Risch and C-T. Ito), American Chemical Society, Washington, DC, **1997**, Ch. 2.

Thesis / Dissertation :

4. W. phutdhawong, "Isolation of glycosides by electrolytic decolourisation and synthesis of pentinomycin", *PhD Thesis*, **2002**, Chiang Mai University, Thailand.

Patent :

5. K. Miwa, S. Maeda and Y. Murata, "Purification of stevioside by electrolysis", *Jpn. Kokai Tokkyo Koho 79 89,066* (**1979**).

Proceedings :

6. P. M. Sears, J. Peele, M. Lassauzet and P. Blackburn, "Use of antimicrobial proteins in the treatment of bovine mastitis", Proceedings of the 3rd International Mastitis Seminars, **1995**, Tel-Aviv, Israel, pp. 17-18.

Websites :

7. S. Simon, "What is an odds ratio?", **2008**, http://www.childrensmercy.org/stats/definitions/or.htm (Accessed: October 2011).

Manuscript Revision Time

Authors who are instructed to revise their manuscript should do so within **45** days. Otherwise the revised manuscript will be regarded as a new submission.

Manuscript Processing Time

As a result of a large number of submissions, there may be a long delay in the evaluation or publication of a paper. A duration of at least 6-8 months between submission and acceptance (or rejection) can normally be expected.

Maejo International Journal of Science and Technology

ISSN 1905-7873
Available online at www.mijst.mju.ac.th

Short Communication

Temporal physiological and biochemical changes in *Hippeastrum vittatum* 'Red Lion' bulbs stored at different temperatures

Qi Wang [1], Jianjun Zhang [1], Jaime A. Teixeira da Silva [2] and Xiaonan Yu [1,*]

[1] Beijing Key Laboratory of Ornamental Plants Germplasm Innovation and Molecular Breeding, National Engineering Research Centre for Floriculture, College of Landscape Architecture, Beijing Forestry University, Beijing 100083, China

[2] P. O. Box 7, Miki-cho post office, Ikenobe 3011-2, Kagawa-ken, 761-0799, Japan

* Corresponding author, e-mail: yuxiaonan626@126.com

Received: 3 July 2013 / Accepted: 4 May 2014 / Published: 6 May 2014

Abstract: Starch and soluble sugar concentrations, α-amylase activity and soluble protein of *Hippeastrum vittatum* 'Red Lion' bulbs were assessed under different storage temperatures and storage periods. Bulbs were stored for 45 days at 20°, 12°, 8° or 4°C. Starch concentration decreased most at 4°C on the 45th day, changing from 29.7% to 10.9% in the exterior scales and from 33.0% to 13.0% in the interior scales. The α-amylase activity in the exterior scales, except at 4° and 8°C, decreased significantly between 0 and 15 days of storage, and then increased significantly from the 15th day until the end of the trial. The soluble sugar concentration increased most at 4°C: in the exterior scales it changed from 54.73 to 153.93 mg·g^{-1} while in the interior scales it increased from 39.67 to 148.11 mg·g^{-1}. The soluble protein concentration in all treatments peaked on the 30th day at 8°C in the exterior scales (2.15 mg·g^{-1}) and at 12°C in the interior scales (2.17 mg·g^{-1}). Understanding these physiological and biochemical changes in the bulbs of *H. vittatum* after storage would serve as a reference for bulb dormancy mechanisms in future studies.

Keywords: *Hippeastrum vittatum*, 'Red Lion' bulbs, low-temperature sweetening, α-amylase activity, bulb dormancy

INTRODUCTION

Hippeastrum vittatum Herbert inhabits the lightly-forested Bolivian slopes at 610-1830 m, where conditions are cool and shady. It has 2-6 large, white-and-red striped, moderately fragrant blooms per scape, which is 90 cm tall with an intense green throat [1]. Due to its beautiful flowers and the continuous development of new varieties, *H. vittatum* can be used as an indoor potted ornamental, as a cut flower, or in landscape compositions as a flowering bush or border plant. Although the ornamental and economic value is high, China's *H. vittatum* bulb self-sufficiency rate

is very low and the storage technology gap relative to advanced international levels is large while flowering and the quality of cut flowers are also unsatisfactory. Domestic and foreign research on forcing culture of *H. vittatum* bulbs focused more on the relationship between storage temperature, storage time and the effect of cultivation on plant characters (leaf length, flower bud number, etc.). For example, De Hertogh and Gallitano [2] found that highest quality plants were produced at 22/18°C with long days (3-hr night break with incandescent light). These plants reached the market stage in 25 days and had 15.4-cm-long leaves. They reached full flower in 32 days with 18.6-cm-long leaves, 43.6-cm-tall flower stalks, and 19.3-cm-diameter flowers. Lu et al. [3] showed that bulbs used for forcing culture need to be stored at 4-7°C for 45-60 days, that buds germinate at 22°C over 10-14 days, and that flower buds sprout above 25°C. The effect of temperature on *in vitro* bulb production has also been examined [4]. However, the physiological and biochemical changes that take place within *H. vittatum* bulbs have still not been reported even though the bulb is the central organ for the success of this ornamental. In order to provide a theoretical basis for bulb germination, flowering control of fresh cut flowers, and postharvest handling, this article studies the physiological and biochemical changes to *H. vittatum* bulbs at different storage temperatures and storage periods.

MATERIALS AND METHODS

The experiment was conducted from November 2011 to January 2012 and *H. vittatum* bulbs were harvested when leaves turned yellow. *H. vittatum* 'Red Lion', which has red, velvety blooms and a sturdy scape, is very popular in China and is used to decorate the Spring Festival. After removing the aerial parts, 45 bulbs (purchased from Binfen Horticultural Co., Beijing) that had tightly-held scales, no pests or bulb plate injury and that were 6 cm in diameter were selected. Older outer scales, dead roots and some devitalised tissues attached to the root disk surface were all removed. Bulbs were soaked and sterilised for 1 hr in 80% Carbendazim (disinfectant) (Lianhelichen Crop Science Chemical Co. Ltd, Jiangsu) diluted 800fold with distilled water, and were used for the experiment after having dried off.

Ten bulbs were used for each storage temperature, i.e. 20°, 12°, 8° and 4°C. Bulbs were placed at each temperature for 45 days. From November 26th 2011 onwards, physiological and biochemical indices were determined for each temperature treatment every 15 days. Five bulbs were set aside at room temperature (20±0.5°C). Before physiological and biochemical tests, three bulbs were randomly selected and scales were carefully removed. Since many differences exist between exterior and interior scales (first 2-3 layers from the outside to the inside and first 2-3 layers from the inside to the outside respectively), for example the inner scales are much more tender than the outer scales, they were analysed separately. Three bulbs per treatment were shredded and mixed evenly and each analysis was done in triplicate.

The anthrone method was used to determine soluble sugar [5, 6]. Starch content was determined by the method of Men and Liu [7] using perchloric acid. α-Amylase activity was determined by the 3,5-dinitrosalicylic acid colorimetric method [6]. Soluble protein content was determined by the method of Bradford [8] using Coomassie Brilliant Blue G-250 staining.

SPSS version 17 was used to analyse all biochemical indicators which changed over time at different storage temperatures. Duncan's multiple range test was used to calculate the significance ($P < 0.05$) between single factors while two-way ANOVA was applied to test the effects of between-subject factors.

RESULTS AND DISCUSSION

The change in carbohydrate concentration is one of the most sensitive physiological indicators of plant metabolism under low temperature conditions, and starch and soluble sugar play an important role in the maintenance of balance between carbohydrate supply and demand [9]. Generally, in the process of dormancy at low temperature, starch-degrading enzyme activity increases and starch is hydrolysed in bulbs with subsequent accumulation of soluble sugar [10, 11]. This is also intimately related to carbon and nitrogen metabolism [12]. In the present experiment, the soluble sugar concentration of both the inner and outer scales of *H. vittatum* increased during storage (Figure 1), a process commonly termed 'low temperature sweetening' [13]. This response is similar to that in lily bulbs [14, 15, 16]. As seen from Figure 1, the lower the storage temperature, the higher the soluble sugar concentration becomes. At the same temperature, as storage progresses from 0 to 45 days, starch content consistently declines (Figure 2) while soluble sugar concentration increases in both exterior and interior scales, suggesting that a longer experiment (exceeding 45 days) might reveal more information about the internal biochemical changes in *H. vittatum* bulb.

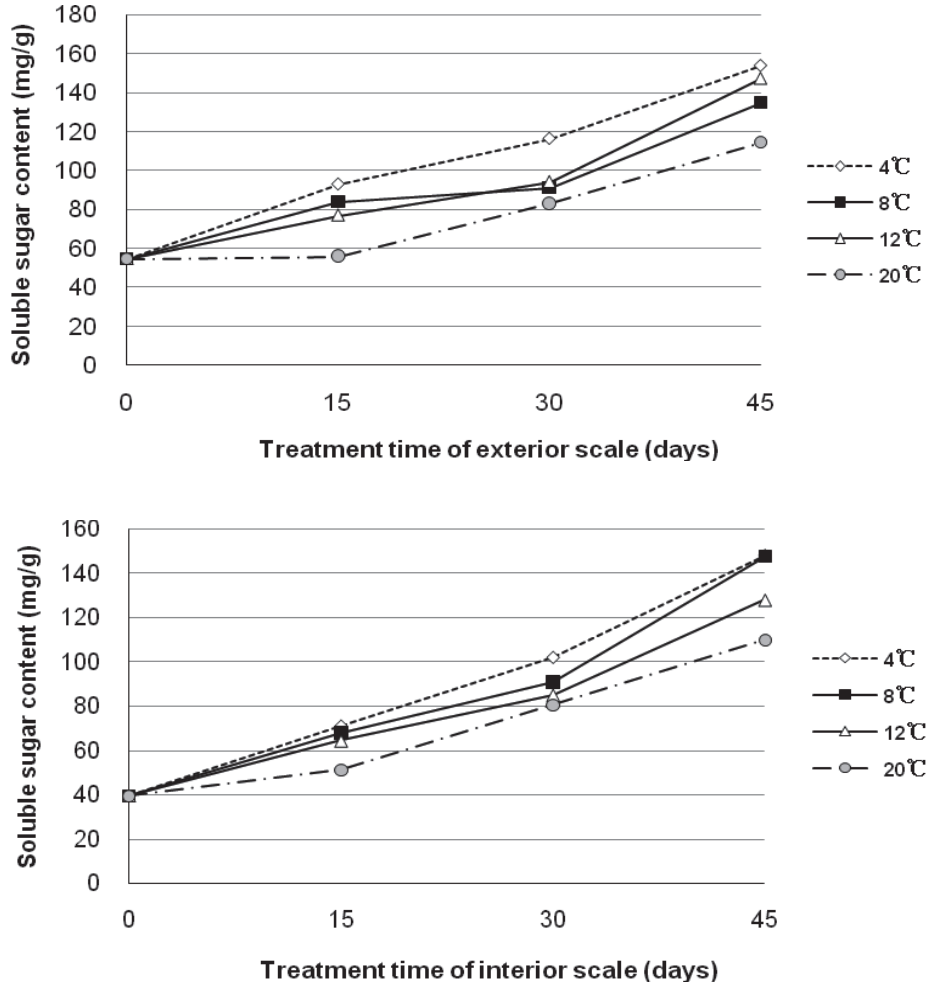

Figure 1. Changes in soluble sugar content of exterior scale and interior scale of *H. vittatum* 'Red Lion' bulb stored at different temperatures

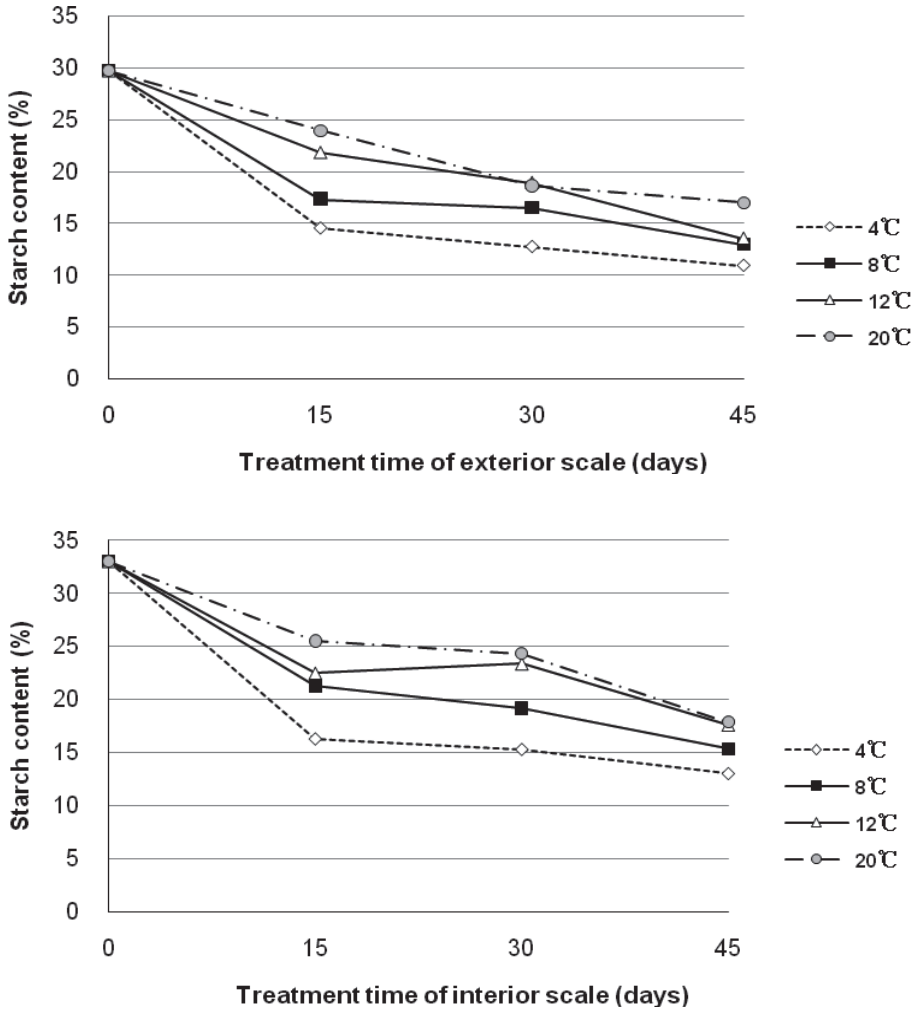

Figure 2. Changes in starch content of exterior scale and interior scale of *H. vittatum* 'Red Lion' bulb stored at different temperatures

Starch degradation and α-amylase activity are related within scale cells. In our experiments, α-amylase activity increases during 15-45 days after temperature treatment (DATT) (Figure 3) while starch content decreases steadily during 0-45 DATT at all temperatures (Figure 2). The discrepancy at 0-15 DATT may be due to the complexity of starch decomposition [17,18]. α-Amylase activity at 4°C increases consistently. Interestingly, most studies of forcing culture do not employ a storage temperature of less than 5°C. However, whether this would negatively impact bulb quality still requires further studies.

The soluble protein in most plants is involved in various metabolic enzymes, and its concentration is an important indicator to understanding plant metabolism. In this study, the concentrations of soluble protein at their highest levels at 30 DATT was almost the same for all temperature treatments, showing a constant metabolism of the *H. vittatum* bulb between 4° and 20°C (Figure 4).

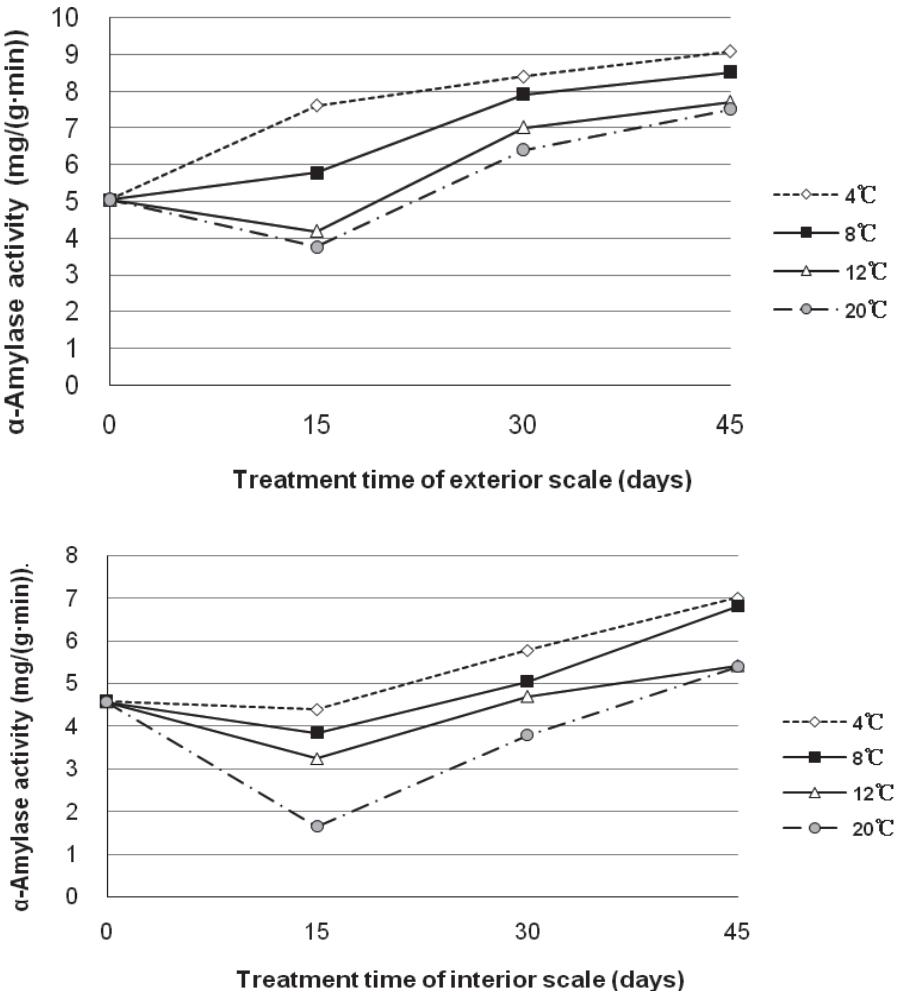

Figure 3. Changes in α-amylase activity in exterior scale and interior scale of *H. vittatum* 'Red Lion' bulb stored at different temperatures

Almost every study to date on *H. vittatum* bulb has focused on forcing culture and little is known about the internal mechanism of its dormancy. From the perspective of physiological and biochemical changes in bulbs, forcing culture can also be used to illustrate the internal changes in bulbs to some extent. The temperature of *H. vittatum* bulbs during the cultivation period between bud development and flowering ranges from 15° to 25°C [19]. When 'Red Peacock' bulbs were stored at 9-10°C for 6 weeks and then placed in the greenhouse for 2 weeks, 60% of flower buds sprouted, but only 30% sprouted when kept at 9-10°C for 8.5 weeks [20]. Read [1] claimed that 6 weeks at 13°C is sufficient for scapes to emerge when bulbs are cultivated at 18-19°C. Lu and Wang [21] noted that for most *Hippeastrum* varieties, bulbs stored at 12°C for 8-13 weeks could effectively break dormancy. When *H. vittatum* 'Red Lion' was propagated *in vitro* by twin scales, carbohydrate content throughout bulblet formation changed in response to temperature, plant growth regulators and substrate [4].

This experiment provides a theoretical basis for physiological and biochemical mechanisms of *H. vittatum* bulbs after dormancy and would thus allow for the improvement of post-harvest technology.

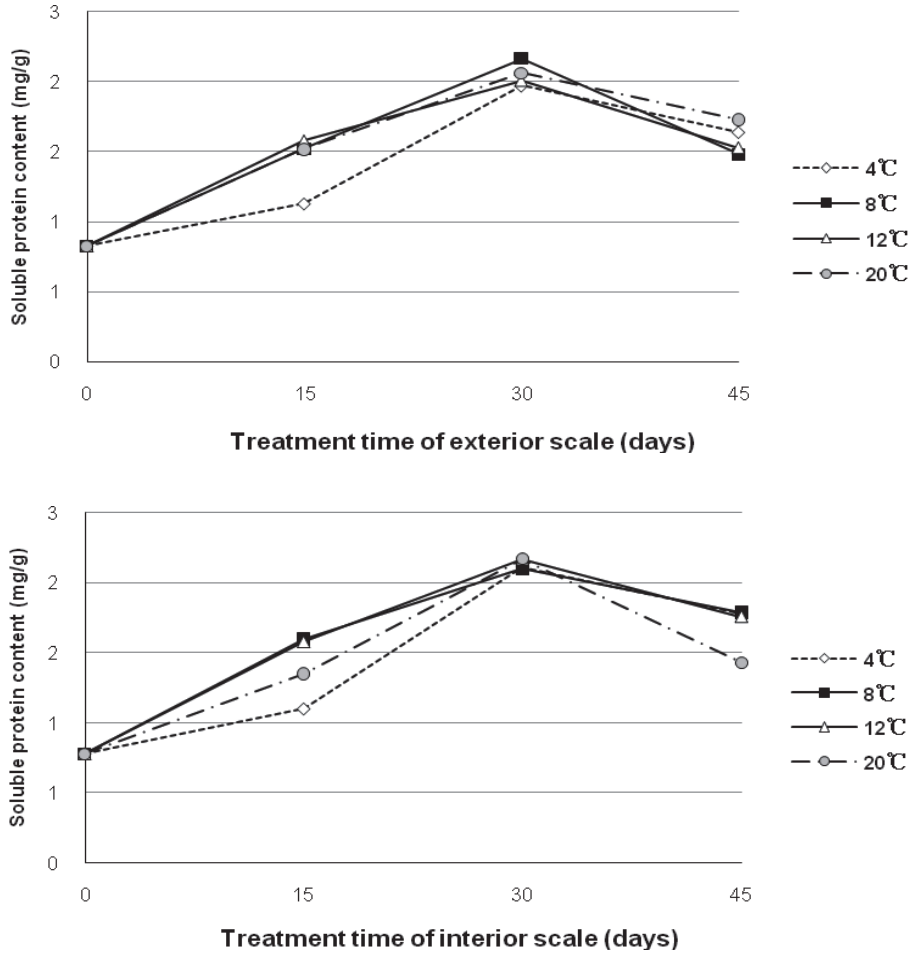

Figure 4. Changes in soluble protein content of exterior scale and interior scale of *H. vittatum* 'Red Lion' bulb stored at different temperatures

CONCLUSIONS

Temperature and storage time induce the biochemical changes in the bulb of *Hippeastrum vittatum* 'Red Lion'. Starch concentrations in both the interior and exterior scales decrease with storage time and the lowering of temperature. Except for 4° and 8°C, α-amylase activity both in the exterior and interior scales decreases significantly between 0 and 15 days of storage then increases significantly from 15 to 45 days. Soluble sugar concentrations in both the interior and exterior scales increase with storage time and the lowering of temperature. Soluble protein concentrations in both the interior and exterior scales peak at approximately the same level on day 30 regardless of temperature and storage time. There seems to be no significant difference in the degree of biochemical changes occurring in the interior and exterior scales of the *H. vittatum* 'Red Lion'.

ACKNOWLEDGEMENTS

This work was financially supported by the Fundamental Research Funds for the Central Universities (YX2014-20) and the Introducing Advanced Technology Project from the State Forestry Administration (2012-4-59).

REFERENCES

1. V. M. Read, "*Hippeastrum*: the Gardener's Amaryllis", Timber Press, Portland, **2004**, pp.16-45.
2. A. A. de Hertogh and L. Gallitano, "Influence of photoperiod and day/night temperatures on flowering of Amaryllis (*Hippeastrum*) cv. Apple Blossom", *Acta Hort.*, **2000**, *515*, 129-134.
3. W. T. Lu, Y. Z. Zhou, H. Z. Cheng, X. M. Lou and H. W. Jiang, "Study on flowering time regulators of *Hippeastrum hybridum*", *Northern Hort.*, **2010**, *20*, 110-112.
4. W. Zhang, L. Song, J. A. Teixeira da Silva and H. M. Sun, "Effects of temperature, plant growth regulators and substrates and changes in carbohydrate content during bulblet formation by twin scale propagation in *Hippeastrum vittatum* 'Red lion'", *Sci. Hort*., **2013**, *160*, 230-237.
5. D. L. Morris, "Quantitative determination of carbohydrates with Dreywood's anthrone reagent", *Science*, **1948**, *107*, 254-255.
6. H. S. Li, Q. Sun, S. J. Zhao and W. H. Zhang, "Principles and Techniques of Plant Physiological Biochemical Experiment", Higher Education Press, Beijing, **2000**, pp.195-197 (in Chinese).
7. F. Y. Men and M. Y. Liu, "Potato Cultivation Physiology", China Agriculture Press, Beijing, **1995**, pp.32-57 (in Chinese).
8. M. M. Bradford, "A rapid and sensitive method for the quantitation of microgram quantities of protein utilizing the principle of protein-dye binding", *Anal. Biochem.*, **1976**, *72*, 248-254.
9. M. Le Nard, "Physiology and storage of bulbs: Concepts and nature of dormancy in bulbs", in "Post-Harvest Physiology and Crop Preservation" (Ed. M. Lieberman), Plenum Press, New York, **1983**, pp.191-230.
10. N. K. Chrungoo, "Concepts of dormancy regulation in vegetative plant propagules: A review", *Env. Exp. Bot.*, **1992**, *32*, 309-318.
11. N. Shiomi and N. Benkeblia, "Chilling effect on soluble sugars, respiration rate, total phenolics, peroxidase activity and dormancy of onion bulbs", *Sci. Agricola*, **2004**, *61*, 281-285.
12. T. Ohyama, S. Komiyama, N. Ohtake, K. Sueyoshi, J. A. Teixeira da Silva and S. Ruamrungsri, "Physiology and genetics of carbon and nitrogen metabolism in tulip", in "Floriculture, Ornamental and Plant Biotechnology: Advances and Topical Issues" (Ed. J. A. Teixeira da Silva), Vol. 3, Global Science Books, Isleworth, **2006**, pp.12-25.
13. T. ap Rees, W. L. Dixon, C. J. Pollock and F. Franks, "Low temperature sweetening of higher plants", in "Recent Advances in the Biochemistry of Fruits and Vegetables" (Ed. J. Friend and M. J. C. Rhodes), Academic Press, New York, **1981**, pp.41-61.
14. H. M. Sun, J. A. Teixeira da Silva, Y. F. Li and T. L. Li, "Effects of low temperature on dormancy release in lily bulbs", *Floricult. Ornament. Biotechnol.*, **2007**, *1*, 41-45.
15. H. M. Sun, T. L. Li and Y. F. Li, "Starch metabolism and sprouting of bulb in *Lilium davidii* var. unicolor stored at different cold temperatures", *Acta Hort. Sin.*, **2004**, *34*, 337-342.
16. Y. P. Xia, C. H. Huang, G. F. He and H. J. Zheng, "Changes of carbohydrates metabolism and enzymes activities in low temperature storage for bulbs of *Lilium* Oriental hybrids", *Acta Hort. Sin.*, **2006**, *33*, 571-576.
17. T. H. Nielsen, U. Deiting and M. Stitt, "A β-amylase in potato tubers is induced by storage at low temperature", *Plant Physiol.*, **1997**, *113*, 503-510.
18. F. Chen and X. S. Hu, "The research and development of the 'low temperature sweetening' mechanism in potato tubers", *Chin. Potato J.*, **1998**, *12*, 52-55 (in Chinese).
19. J. C. Doorduin and W. Verkerke, "Effects of bulb temperature on development of *Hippeastrum*", *Acta Hort.*, **2002**, *570*, 313-315.

20. S. Q. Tian, X. D. Zhu, H. Z. Cheng and W. M. Guo, "The study of forcing culture technology on introduced species of *Hippeastrum* spp.", *Jiangsu Agric. Sci.*, **2008**, *4*, 151-153 (in Chinese).
21. Y. M. Lu and Y. J. Wang, "*Hippeastrum*", China Forestry Press, Beijing, **2004**, pp.12-33 (in Chinese).

Maejo International Journal of Science and Technology

ISSN 1905-7873
Available online at www.mijst.mju.ac.th

Short Communication

Proximate composition, total phenolics content and antioxidant activities of microalgal residue from biodiesel production

Pamon Pumas [1] and Chayakorn Pumas [2, *]

[1] Discipline of Health Science and Environment, Faculty of Science and Technology, Chiang Mai Rajabhat University, Chiang Mai 50300, Thailand
[2] Department of Biology, Faculty of Science, Chiang Mai University, Chiang Mai 50200, Thailand

* Corresponding author, e-mail: chayakorn.pumas@gmail.com; tel: +66 (0)53 941950 ext.116; fax: +66 (0)53 852 259

Received: 4 Mach 2013 / Accepted: 10 May 2014 / Published: 12 May 2014

Abstract: In biodiesel production, lipid is extracted from algal biomass but some beneficial substances may remain in its residue. In this study proximate composition, total phenolics content and antioxidant activities of a microalgal residue after lipid extraction were determined. It was found that the residue has a high protein content and the hot aqueous extract of the residue is high in both the phenolics content and the level of antioxidant activities.

Keywords: biodiesel production, microalgal residue, proximate composition, antioxidant activities, total phenolics content, ferric reducing power, Trolox equivalent antioxidant capacity

INTRODUCTION

Microalgae are interesting as the third generation of biofuel production, especially biodiesel. Lipid is extracted from microalgal biomass and converted into biodiesel by chemical methods [1]. However, microalgal residue is produced after lipid extraction. A good use of this by-product will certainly be beneficial to the solving of both the economic and environmental issues involved in biodiesel production from microalgal biomass [2].

Generally, microalgae are used as feed or feed supplement due to their high nutritional value [3]. In addition, microalgae have been known for their production of bio-active substances, especially antioxidants. For example, the extracts of *Spirulina platensis* and *Dunaliella salina* show high antioxidant activity when analysed by Trolox equivalent antioxidant capacity (TEAC) assay [4]. Natrah et al. [5] reported that extracts from many microalgal strains including *Isochrysis galbana*,

Chaetoceros calcitrans, *Scenedesmus quadricauda*, *Chlorella vulgaris*, *Nannochloropsis oculata* and *Tetraselmis tetrathele* show inhibitory activity against lipid peroxidation of linoleic acid. Among the microalgae tested, *I. galbana* and *C. calcitrans* exhibit the highest antioxidant activity in the ferric thiocyanate and thiobarbituric acid assays. Recently, some commercial applications of microalgae, such as nutritional supplements, natural dyes and skin care products, were being promoted [3]. However, there seem to have been no reports on the antioxidant activities of lipid-extracted microalgal biomass (microalgal residue) or its extract. Antioxidants could be used in biodiesel production as oil protectant against oxidative deterioration [6]. Thus, antioxidant activities (including phenolics content) and nutritional content of the microalgal residue are worth investigating. The results could lead to applications in biodiesel production or animal feed supplement, and the residue would be used completely and worthily.

MATERIALS AND METHODS

Preparation of Microalgal Residue and Proximate Analysis

A microalgal consortium consisting of *Golenkinia* sp. (45.9%), *Acutodesmus (Scenedesmus) dimorphus* (Turpin) Tsarenkom (34.6%), *Chlorella* sp. (13.4%), *Micractinium* sp. (3.3%) and *Scenedesmus acutus* Meyen (2.7%) was cultivated in a 4×8 m open pond using 10,000 L of CMU03 medium [7] at the Faculty of Fisheries Technology and Aquatic Resources, Maejo University. After 1 month the cells were harvested by spontaneous flocculation and dried with solar heat. Lipid was extracted from the microalgal biomass by Soxhlet extraction with hexane: chloroform: methanol 4:1:1 (v/v) at 80°C for 10 hr [8]. The microalgal residue was filtered and dried at 40°C.

The proximate chemical composition and energy of the dry microalgal residue were analysed at Central Laboratory (Thailand) Co. Ltd. by using the AOAC methods [8] and a bomb calorimeter according to a standard method [9] respectively.

Extraction and Analysis of Microalgal Residue

The dry microalgal residue was ground into powder in a mortar. One hundred grams of the powdered microalgal residue was soaked in 95% ethanol or distilled water at 55°C for 15 hr. The cold aqueous extract was prepared separately by extracting the same amount of material three times with distilled water at ambient temperature with intermittent shaking for 3 days each time. All solutions from the extraction were concentrated with a rotary evaporator at 40^{o}C and the extracts finally dried in a lyophiliser.

Total phenolics content was determined using the Folin-Ciocalteu method as described by Chandler and Dodds [10]. The total phenolics content values were standardised with gallic acid and reported as mg of gallic acid equivalent per gram of sample.

The ferric reducing power of the microalgal residue was evaluated according to the method of Oyaizu [11]. The reducing power was calculated and expressed as mg of gallic acid equivalent per gram of sample.

The 2,2'-azino-bis(3-ethylbenzthiazoline-6-sulphonic acid) (ABTS) radical anion scavenging assay was executed by the method given by Re et al. [12] with some modifications and was expressed as Trolox equivalent antioxidant capacity (TEAC), defined as mg of Trolox equivalent per gram of sample.

Statistical Analysis

The data were expressed as mean ± standard deviation of three replicates. Statistical comparison between the groups was analysed using one-way analysis of variance (ANOVA) and post-hoc Tukey's b-test using SPSS version 14.0. *p*-Values less than 0.05 were considered significant.

RESULTS AND DISCUSSION

From the proximate analysis, the microalgal residue was found to possess a high nutritional value, especially with respect to protein and carbohydrate (Table 1). The yields of the hot aqueous extract, cold aqueous extract and ethanolic extract of the microalgal residue were 9.46%, 9.36%, and 1.562% respectively. The low yield of the ethanolic extract was expected because most of the non-polar substances in the residue, such as lipids and carotenoids, had been previously extracted, which also corresponds to the low fat content of the residue, as shown in Table 1.

Table 1. Proximate composition of microalgal residue after lipid extraction

Nutrient	%
Protein (N x 6.5)	27.26
Fat	1.36
Ash	26.20
Fibre	9.22
Carbohydrate	35.93
Energy	265.00 (cal.g^{-1})

From Figure 1, the hot aqueous extract of the microalgal residue shows the highest total phenolic content. Phenolic compounds have been noted for their positive correlation with antioxidant capacity [13]. Therefore, the determination of phenolics content is an indirect method of evaluating the antioxidant capacity of a sample.

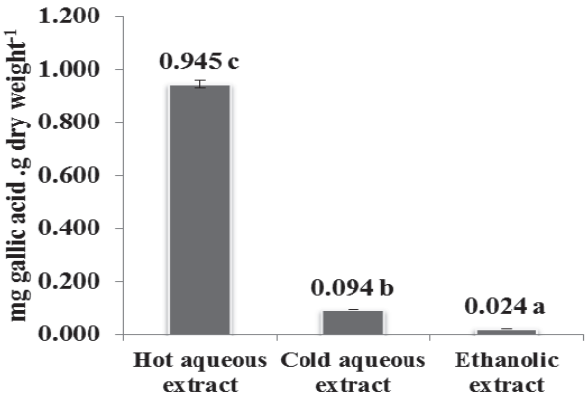

Figure 1. Total phenolics content of extracts of microalgal residue
Note: Values with the different letters are significantly different at $p>0.05$.

The hot aqueous extract of the microalgal residue shows a significantly high ferric reducing power, the highest among the three extracts (Figure 2). The reducing power of an antioxidant is the ability to provide electrons to free radicals, thus stopping the damages incurred by the radical chain

reactions [11]. The hot aqueous extract of the microalgal residue also shows the highest and most significant scavenging ability against ABTS radical (Figure 3). Scavenging activity is the ability to give electrons or hydrogen atoms to free radicals via single electron transfer or hydrogen atom transfer [12].

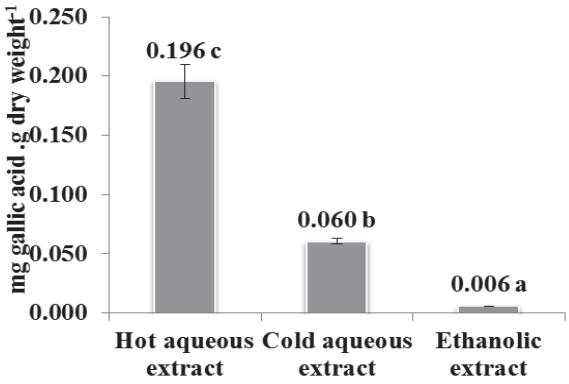

Figure 2. Ferric reducing power of extracts of microalgal residue
Note: Values with the different letters are significantly different at $p>0.05$.

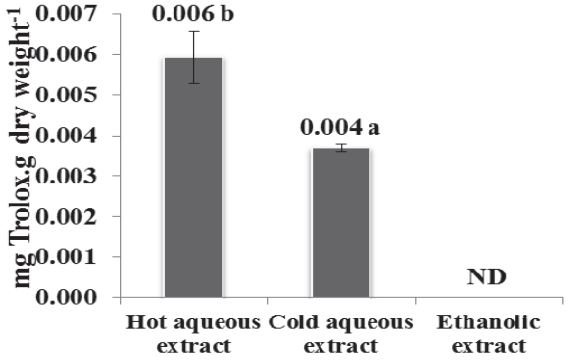

Figure 3. ABTS radical scavenging assay of extracts of microalgal residue
Note: Values with the different letters are significantly different at $p>0.05$. ND = not detected

Hot water was found to be the most suitable solvent for extraction of phenolics and antioxidants from the microalgal residue. Since the polarity of phenolic compounds varies significantly, it is difficult to optimise a method for extraction of all phenolic compounds [14]. Water is a highly polar solvent and generally not a suitable solvent for non-polar organic compounds at room temperature. However, when the temperature of water is increased, there is a steady decrease in its permittivity, viscosity and surface tension and a rise in its diffusive characteristics, which results in its capacity for dissolving a wider range of substances including some less polar compounds [15]. This may account for a slightly higher extraction yield and higher antioxidant capacities as well as higher total phenolics content of the hot aqueous extract compared to the cold extract. The results are similar to the study by Shon et al. [16], who found that hot water could extract a larger amount of total phenolic compounds than that obtained by other solvents and that the hot-water extract also exhibited good antioxidant activities. On the other hand, non-polar antioxidants and other non-polar metabolites such as chlorophyll, carotenoids, ω-3 fatty acids and γ-linolenic acid found in the

microalgae [17] were removed in the bio-oil extraction process, leading to the observed low antioxidant capacities of the ethanolic extract.

Interestingly, although the lipid-extracted microalgal biomass is a leftover material from the production process, its antioxidant activities are still comparable to that of some whole biomass algae. The total phenolics content of the hot aqueous extract (0.945 ± 0.015 mg gallic acid.g dry weight^{-1}) obtained in this study is close to that of *Turbinaria conoides* aqueous extract (1.116 ± 0.011 mg gallic acid.g dry weight^{-1}) [18] and its ABTS radical scavenging activity (0.006 ± 0.001 mg Trolox.g dry weight^{-1}) is about twice higher than that of *Padina minor* aqueous extract (0.003 ± 0.001 mg Trolox.g dry weight^{-1}) [19]. Similarly, the value for reducing power from this study (0.196 ± 0.014 mg gallic acid.g dry weight^{-1}) is higher than those derived from *Amphiroa* sp. and *Halimeda macroloba* aqueous extracts (0.022 ± 0.000 and 0.092 ± 0.000 mg gallic acid.g dry weight^{-1} respectively) [18].

However, the ratio of the microalgal population in a microalgal consortium may influence the antioxidant activities. Although the population may change with physical factors such as light intensity and water temperature, CMU03 medium was found to control the population of microalgal consortia to be in the group of green microalgae. From our previous study [7], the dominant species may be different in each consortium but they are still in the Chlorophyceae and this may not significantly affect the proximate composition, although the antioxidant activities may still change. Aboul-Enein et al. [20] reported that microalgae show different antioxidant activities, even though they belong to the same genus. It was found that *Scenedesmus dimorphus* shows higher anti-lipid peroxidation than *S. acutus* due to different antioxidant contents in each species, such as carotenoids, vitamin E and vitamin C. Thus, the microalgal population and residue at the time of harvest should be standardised.

CONCLUSIONS

A microalgal residue after lipid extraction (for biodiesel production) is found to be high in protein and may be suitable for use as a feed supplement. The hot aqueous extract of the residue is also high in total phenolics content and antioxidant activities, i.e. ferric reducing power and ABTS radical scavenging activity.

ACKNOWLEDGEMENTS

This work was partially funded by the Centre of Excellence for Renewable Energy, Chiang Mai University. We acknowledge the Faculty of Fisheries Technology and Aquatic Resources, Maejo University, for providing the space and the facilities for microalgal cultivation. We are thankful to Assistant Professor Dr. Thepparath Ungsethaphand and Dr. Sudaporn Tongsiri for providing microalgal biomass, and to Assistant Professor Dr. Suparin Chaiklangmuang for providing microalgal residue.

REFERENCES

1. Y. Chisti, "Biodiesel from microalgae", *Biotechnol. Adv.,* **2007**, *25*, 294-306.
2. L. Govindarajan, R. Senthilkumar, R. Nitin and B. H. F. Bakheet, "Kinetic study of algae biomass grown in natural medium using spectroscopic analysis", *J. Algal Biomass Utln.*, **2010**, *1*, 1-11.

3. P. Spolaore, C. Joannis-Cassan, E. Duran and A. Isambert, "Commercial applications of microalgae", *J. Biosci. Bioeng.*, **2006**, *101*, 87-96.
4. J. A. Mendiola, I. Rodríguez-Meizoso, F. J. Señoráns, G. Reglero, A. Cifuentes and E. Ibáñez, "Antioxidants in plant foods and microalgae extracted using compressed fluids", *Electron. J. Environ. Agric. Food Chem.*, **2008**, *7*, 3301-3309.
5. F. M. I. Natrah, F. M. Yusoff, M. Shariff , F. Abas and N. S. Mariana, "Screening of Malaysian indigenous microalgae for antioxidant properties and nutritional value", *J. Appl. Phycol.*, **2007**, *19*, 711-718.
6. G. El Diwani, S. El Rafie and S. Hawash, "Protection of biodiesel and oil from degradation by natural antioxidants of Egyptian Jatropha", *Int. J. Environ. Sci. Technol.*, **2009**, *6*, 369-378.
7. C. Sriphuttha, C. Pumas, J. Pekkoh and Y. Peerapornpisal, "Selection of high CO_2 tolerant microalgae for bio-fuel production", *J. Fish. Technol. Res.*, **2013**, *7(S1)*, 71-80 (in Thai).
8. W. Horwitz (Ed.), "Official Methods of Analysis of AOAC International", 18th Edn., Association of Official Analytical Chemists (AOAC), Gaithersburg (MD), **2005**.
9. ANSI/ASTM, "Standard Test Method for Gross Calorific Value of Solid Fuel by the Adiabatic Bomb Calorimeter: ASTM D2015–77", American National Standards Institute and American Society for Testing and Materials, Philadelphia, **1977**, pp.9-17.
10. S. F. Chandler and J. H. Dodds, "The effect of phosphate, nitrogen and sucrose on the production of phenolics and solasodine in callus cultures of *Solanum laciniatum*", *Plant Cell Reports*, **1983**, *2*, 205-208.
11. M. Oyaizu, "Studies on products of browning reaction. Antioxidative activities of products of browning reaction prepared from glucosamine", *Jpn. J. Nutr. Diet.*, **1986**, *44*, 307-315.
12. R. Re, N. Pellegrini, A. Proteggente, A. Pannala, M. Yang, and C. Rice-Evans, "Antioxidant activity applying an improved ABTS radical cation decolorization assay", *Free Radic. Biol. Med.*, **1999**, *26*, 1231-1237.
13. C. Rice-Evans, N. Miller and G. Paganga, "Antioxidant properties of phenolic compounds", *Trends Plant Sci.*, **1997**, *2*, 152-159.
14. P. Garcia-Salas, A. Morales-Soto, A. Segura-Carretero and A. Fernández-Gutiérrez, "Phenolic-compound-extraction systems for fruit and vegetable samples", *Molecules*, **2010**, *15*, 8813-8826.
15. C. C. Teo, S. N. Tan, J. W. Yong, C. S. Hew and E. S. Ong, "Pressurized hot water extraction (PHWE) ", *J. Chromatogr. A*, **2010**, *1217*, 2484-2494.
16. M. Y. Shon, T. H. Kim and N. J. Sung, "Antioxidants and free radical scavenging activity of *Phellinus baumii* (*Phellinus of Hymenochaetaceae*) extracts", *Food Chem*., **2003**, *82*, 593-597.
17. M. Herrero, A. Cifuentes and E. Ibanez, "Sub- and supercritical fluid extraction of functional ingredients from different natural sources: Plants, food-by-products, algae and microalgae: A review", *Food Chem*., **2006**, *98*, 136-148.
18. W. Boonchum, Y. Peerapornpisal, D. Kanjanapothi, J. Pekkoh, C. Pumas, U. Jamjai, D. Amornlerdpison, T. Noiraksar and P. Vacharapiyasophon, "Antioxidant activity of some seaweed from the Gulf of Thailand", *Int. J. Agric. Biol.*, **2011**, *13*, 95-99.
19. Y. Peerapornpisal, D. Amornlerdpison, U. Jamjai, T. Taesotikul, Y. Pongpaibul, M. Nualchareon and D. Kankanapothi, "Antioxidant and anti-inflammatory activities of brown marine alga, *Padina minor* Yamada", *Chiang Mai J. Sci.*, **2010**, *37*, 507-516.

20. A. M. AbouL-Enein, F. K. El-Baz, G. S. El-Baroty, A. M. Youssef and H. H. A. El-Baky, "Antioxidant activity of algal extracts on lipid peroxidation", *J. Med. Sci*., **2003**, *3*, 87-98.

Maejo Int. J. Sci. Technol. **2014**, *8*(02), 129-142

Maejo International Journal of Science and Technology

ISSN 1905-7873
Available online at www.mijst.mju.ac.th

Full Paper

Volatile profiles of tomato wine before and after ageing

John Owusu [1, 3, *], Haile Ma [1, 2], Zhenbin Wang [1], Newlove Akowuah Afoakwah [1, 4] and Agnes Amissah [3]

[1] School of Food and Biological Engineering, Jiangsu University, 301 Xuefu Road, Zhenjiang 212013, China
[2] Key Laboratory for Physical Processing of Agricultural Products, 301 Xuefu Road, Zhenjiang, Jiangsu 212013, China
[3] School of Applied Science and Technology, Hospitality Department, Koforidua Polytechnic, Ghana
[4] School of Applied Science and Arts, Bolgatanga Polytechnic, Bolagatanga, Ghana

* Corresponding author: e-mail: mhl@ujs.edu.cn; tel: +86-511-88790958; fax: +86 511 88 78 0201

Received: 15 September 2013 / Accepted: 5 June 2014 / Published: 6 June 2014

Abstract: The volatile profiles of tomato wine before and 90 days after storage at 10° and 15° were determined. The results indicate that storage temperature significantly influences the volatile composition of tomato wine. A total of 75 volatile compounds are identified, viz. 38 esters, 7 carbonyls, 1 furan, 4 sulphur-containing compounds, 18 higher alcohols, 6 fatty acids and 1 terpene. Twenty-five volatile compounds are present beyond their odour threshold, but the major contributors to the overall aroma of tomato wine are ethyl octanoate, ethyl hexanoate and isoamyl acetate, which are characterised by fruity notes. The potent odoriferous volatile compound, linalool, contributes much to the wine stored at 15° than at 10°. Storage significantly improves the fruitiness of tomato wine.

Keywords: tomato wine, volatile profile, aroma, odour threshold, wine ageing

INTRODUCTION

The aroma of wine influences its quality, cost and consumer choice. A mix of numerous and unique odour compounds contributes to the complexity of wine aroma [1]. Over 800 volatile compounds have been identified in wines [2]. The volatile composition of wine is influenced by several factors including the type and variety of fruit [3], yeast strain [4], inoculum size [5], fermentation temperature [6], maturation process and type of ageing [7]. In order to produce wine

of the best flavour, the concentration of desirable volatile compounds should be enhanced and that of undesirable ones minimised [8]. During fermentation, the growth and development of yeast and the formation of flavour compounds are influenced by many factors such as yeast strain, pH, temperature and inoculum size.

Tomato is one of the most important vegetables in the world, with the total production of 145.8 million tonnes recorded in 2010 and 161.79 million tonnes in 2012 [9]. Fruits and vegetables including tomato are reported to experience post harvest losses of about 20-50%, especially in the developing world. Many fruits have been utilised for winemaking [3, 4] as a means of stemming postharvest losses, and tomato can also be considered a potential candidate with its unique phytochemical and flavour composition [10, 11]. The unique flavour is due to a complex mixture of volatile and non-volatile compounds: over 400 volatile compounds have been identified in tomato [12, 13]. However, compounds that appear to be the most important determining factors of flavour in tomato are *cis*-3-hexenal, hexenal, 2-isobutylthiazole, *β*-ionone, *trans*-2-hexenal, *cis*-3-hexenol, *trans*-2-*trans*-4-decadienal, 6-methyl-5-hepten-2-one and 1-penten-3-one [13]. The aroma of fresh tomato is quite different from that of the processed one as a result of loss and creation of volatiles [14]. Increased concentration of linalool and *α*-terpineol was reported for heated tomato [12]. Likewise, winemaking, which involves maceration, fermentation, maturation and ageing, is likely to modify the volatile composition of tomato wine. This modification should be controlled in order to produce tomato wine of acceptable aroma. Among the many factors which can be controlled to modify tomato wine aroma are pH of the must, fermentation and ageing temperature.

Many authors have studied the volatile composition of many fruits and their wines [3-5, 15-18]. However, to the best of our knowledge, even though the volatile profile of tomato has been studied extensively [e.g. 19, 20], that of its wine has not been reported before. The aim of this study is therefore to assess the volatile profile of tomato wine before and after storage in order to evaluate how it influences tomato wine quality.

MATERIALS AND METHODS

Preparation of Yeast Culture

The dry yeast used, *Saccharomyces bayanus*, BV 818, was purchased from Angel Yeast Company Limited, Hubei province (China) and kept in a refrigerator at 5^{o}C according to the manufacturer's instructions. The yeast culture was prepared in YDP medium (yeast extract = 0.5% (w/v), peptone = 1.0% (w/v) and glucose = 2% (w/v)) in a 250-mL Erlenmeyer flask. The pH of the culture medium was adjusted to 5.0 with tartaric acid. The medium was sterilised in an autoclave at 121^{o} for 20 min. *S. bayanus*, BV 818 (0.03 g) was suspended in 100 mL of sterilised medium and heated to 40^{o} for 20 min. to rehydrate the yeast cells [21]. It was then cooled to room temperature (25^{o}) for adaptation [22] and incubated in an incubator shaker (QYC 211, Shanghai Test Equipment Co. Ltd) at 30^{o} for 24 hr.

Tomato Wine Production

Tomatoes (*L. esculentum* Mill.), was purchased from a market in Zhenjiang, Jiangsu province, were selected based on colour and size uniformity. They were washed several times with running tap water to remove dirt, sterilised with 2% potassium metabisulphite, rinsed several times with distilled water, dried with napkin paper and blended with a sterilised blender. Potassium metabisulphite (0.050 g/L) was added to the must as an antioxidant and antimicrobial agent [22].

Pectic enzyme (0.5 g/L) (Sinopharm Chemical Reagent Co., Ltd (Shanghai)) was added to break down pectin to improve aroma and colour extraction [23], and ammonium phosphate (0.5 g/L) was added as a source of ammonia and phosphorus for the growth of the yeast [24]. The total soluble solid (TSS) of the milled tomato was measured with Abbe refractometer (WAY-2S, China) in accordance with a known method [25] and the value obtained was 4.90 ± 0.20^{o} Brix. The TSS of the original tomato must was ameliorated with sucrose to 20.6 ± 0.30^{o}Brix [26]. The pH of the must at 25^{o} was determined with a pH meter (PHS-2C Precision pH/mV meter, China) after standardisation with standard buffer solutions of pH 7 and 4, according to an established method [27]. The must pH obtained was 4.11. Into a 5-L Erlenmeyer flask was placed 4.5 L (5.30 kg) of tomato must, which was inoculated with 180 mL (1.3x10^{6} cells/mL) of the 24-hr *S. bayanus*, BV 818 inoculum to give an inoculum level of 3.8%. The must was batch-fermented in triplicate in an incubator at 15±2^{o} [22]. The fermentation was monitored until the TSS value of the must became stable. After fermentation, the wine was separated from the pomace and stored at 7^{o} for two months for particles to settle down. The wine titratable acidity was measured as described previously [28] and the ethanol content was determined by a known method [29].

Ageing of Tomato Wine

The tomato wine samples were aged in bottles in triplicate. They were put in 250-mL brown bottles, potassium metabisulphite (0.027 g/L) was added, and the bottles were tightly capped. They were incubated at 10^{o} and 15^{o} for 90 days. Samples were taken for analysis on day 0 and 90. Analysis was done in triplicate.

Analysis of Volatile Compounds

A modified method of solid phase microextraction (SPME) technique described by Márquez et al. [30] was used for extraction of volatile compounds from tomato wine. The SPME fibre used was a Stable Flex divinylbenzene/Carboxen/polydimethylsiloxane (DVB/CAR/PDMS) (Supelco, Bellefonte, USA), which is designed for flavour analysis. The fibre was conditioned for 1 hr at 270^{o} before use. For each SPME analysis, 5 mL of the wine sample was placed in a 15-mL glass vial containing a small stirring magnet at 350 rpm. The sample was spiked with 50 µL of an internal standard (aqueous solution of 1-propanol (100μg/L)). Sodium chloride (1 g) was then added to increase the volatility of the flavour compounds. The vial was then sealed with a silicone septum and put into a water-bath (40^{o}). An SPME needle was then pierced through the septum and the SPME fibre was extended through the needle to place the stationary phase in contact with the headspace of the sample. The fibre was withdrawn into the needle after 30 min. and removed from the vial and inserted for 3 min. in the injection port of a gas chromatograph (6890/5973 GC-MS, Agilent, USA). The extracted chemicals were desorbed thermally at 250^{o} and transferred directly to a DB-1701 cross-linked (14% cyanopropylphenylmethylpolysiloxane) column (30 m, 0.25 mm i.d., 25-µm film thickness) (Agilent, USA).

The injection port was operated in splitless mode and the flow rate of helium (99.9995%) as carrier gas was 1 mL/min. The initial oven temperature was held at 50^{o} for 10 min., ramped at 6^{o}/ min to 150^{o}, and then at 8^{o}/min to 200^{o} and held for 3 min. The total run time was 35.9 min. The Agilent 5973 quadrupole mass spectrometer was operated in the electron ionisation mode at 70 eV with a source temperature of 230^{o} (quadrupole at 150^{o}), with a continuous scan from *m*/*z* 33 to *m*/*z* 330. The data were collected with HP ChemStation software (D.00.00) and searched against the NIST98 libraries. Compounds were preliminarily identified by a library search and their identities

were confirmed by mass spectra and GC retention time of standards or a homologous series of straight chain alkanes (C5-C19). The quantitation of the volatile compounds was based on peak surface areas in the chromatograms. All tests were carried out in triplicate.

Determination of Odour Activity Values

The odour activity values (OAVs) were determined as the ratio of the mean concentration of an aroma compound to its odour threshold value (the lowest concentration that can be detected through smell) obtained from the literature. The aroma compounds with OAVs greater than 1 were considered as those which contribute to the aroma of the wine [31].

Data Analysis

All data were expressed as mean ± standard deviation and subjected to Analysis of Variance (ANOVA) using SPSS Version 17.0. The differences in means were separated with Duncan's Multiple Range test and $P<0.05$ indicated that the difference was significant.

RESULTS AND DISCUSSION

General Attributes

After ageing the pH and titratable acidity of the tomato wine decrease slightly but are not significantly different ($P>0.05$) from those before (Table 1). The pH values are comparable to those regarded suitable for white and red wines [22]. In addition, the TSS and ethanol content of the wine after ageing are similar to those before ageing.

Table 1. General wine attributes before and after ageing

Attribute	pH	TA (g/L)	TSS (^{o}Brix)	EC (g/L)
C	3.67±0.01^{a}	4.43±0.33^{a}	6.0±0.3^{a}	71.10±6.32^{a}
C10	3.60±0.00^{a}	4.40±0.40^{a}	6.50±0.30^{b}	67.15±3.16^{a}
C15	3.60±0.00^{a}	4.40±0.40^{a}	6.20±0.30^{a}	68.73±3.95^{a}

Note: C = tomato wine before ageing; C10 = tomato wine after ageing at 10^{o}; C15 = tomato wine after ageing at 15^{o}; TA = titratable acidity; TSS = total soluble solid; EC = ethanol content. Means with the same alphabets in a column are not significant at $P<0.05$. Mean ± standard deviation were obtained from triplicate measurements.

Volatile Compounds

The total number of volatile compounds identified in tomato wine before and after storage are 75 (Table 2). These comprise 38 esters, 7 carbonyls, 1 furan, 4 sulphur compounds, 18 higher alcohols, 6 fatty acids and 1 terpene. Most of the volatiles identified are known compounds in wines and are mainly formed during the fermentation and winemaking processes [32].

Table 2. Concentrations of volatile compounds (mg/L) in fresh tomato wine and those aged at 10° and 15°

Compound	C	C10	C15	Odour threshold	Odour descriptor
Esters					
Ethyl acetate	14.13 [a] ±0.03	15.86 [b] ±0.04	16.89 [c]±0.06	7.5	Fruity, sweet
Ethyl propanoate	-	0.18[b] ±0.00	0.22[c]±0.01	0.01	Fruity
Ethyl butanoate (Ethyl butyrate)	2.71[a] ±0.02	2.98[b] ±0.03	3.55[c] ±0.04	0.02	Floral, fruity
Ethyl pentanoate	0.45[c] ± 0.00	0.26[b] ±0.01	0.12[a] ±0.00	-	-
Ethyl hexanoate	71.54[a] ± 0.43	81.09[b] ±0.27	104.34[c]±0.43	0.014	Apple, fruity, sweetish
(Z)-Ethyl-3-hexenoate	0.33[a] ±0.01	0.40[b] ±0.02	0.51[c] ±0.02	-	-
Ethyl heptanoate	1.08[a] ±0.03	1.67[b] ±0.03	1.87[c] ±0.04	-	Wine-like, fruity
Ethyl-6heptenoate	0.16 ±0.01	ND	ND	-	-
Ethyl octanoate (EO)	346.63[a] ±1.13	367.90[b] ±0.97	366.63[b] ±1.21	0.02	Sweet, fruity and fresh
% EO of all esters	68.19	59.08	59.44	-	-
(Z)-Ethyl-3-octenoate	ND	ND	0.49 ±0.02	-	-
Ethyl nonanoate	ND	1.14[a] ±0.03	0.70[a] ±0.01	0.38	Cognac, fatty, oily
Ethyl-8-nonenoate	ND	0.50 ±0.03	-	-	
Ethyl decanoate	30.44[a] ±1.01	100.09[c] ±1.04	75.39[b] ±0.43	1.5	Flowery, fruity
Ethyl-9-decenoate	5.50 [a] ±0.06	16.66 [c] ±0.08	12.50 [b] ±0.05	-	Fatty, fruity
Ethylbenzoate	ND	0.37[a] ±0.02	0.41[b] ±0.01	-	Floral, fruity
Ethyl-3-cyclo-pentyl propionoate	0.63 ±0.03	ND	ND	-	-
Diethyl ethanoate	0.26 ±0.01	ND	ND	-	-
Diethyl succinate	1.73[a] ±0.03	2.82[c] ±0.02	2.21[b] ±0.01	0.07	Light fruity
Methyl acetate	ND	0.11 ±0.01	ND	-	Ethereal, estery, fruity
Isoamyl acetate	17.32[b] ±0.02	15.76[a] ±0.05	18.58[c] ±0.02	0.03	Banana, pear
Ethyl 3-methyl butanoate	0.93[c] ±0.01	ND	ND	-	Fruity
Isoamyl octanoate	2.44[b]±0.02	3.87[c]±0.03	2.23[a] ±0.04	-	-
Methyl hexanoate	-	0.24[a] ±0.02	0.32[c] ±0.01	-	-
Methyl octanoate	6.13[b] ±0.03	5.66[a] ±0.12	6.13[b] ±0.13	0.20	Intense citrus
Methyl decanoate	ND	1.17 ±0.03	ND	-	Fatty, cognac, oily
Propyl hexanoate	0.13[a] ±0.01	0.28[b] ±0.02	0.37[c] ±0.00	-	-
Propyl octanoate	ND	ND	0.83 ±0.02	-	Coconut, fatty, winey
Butyl butanoate	0.46 ±0.02	ND	ND	-	-
Isobutyl pentanoate	ND	0.30 ±0.00	-	-	-
Isobutyl octanoate	ND	0.28[b] ±0.00	0.17[a] ±0.00	-	Fatty, fruity, winey
2-Butyl octanoate	0.11 ±0.00	ND	ND	-	-
Isopentyl hexanoate	ND	ND	1.86[c] ±0.12	-	-
Hexyl acetate	0.24[a] ±0.00	0.46[b] ±0.01	0.45[b] ±0.01	0.7	Sweet, perfume
Hexyl octanoate	0.61[a] ±0.03	ND	ND	-	-
2-Phenylethyl acetate	ND	2.50 ±0.02	ND	0.25	Floral, rose, fruity, honey

Note: Values are means ± standard deviation obtained from triplicate measurements. C = tomato wine before ageing; C10 and C15 = tomato wines aged at 10° and 15° respectively; ND = not detected; ' -' = no data/information. Means with the same alphabets in a row are significant (P<0.05).

Table 2. (Continued)

Compound	C	C10	C15	Odour threshold	Odour descriptor
2-Hydroxymethyl benzoate	ND	0.18 ±0.01	ND	-	-
2-Phenylethyl 4-fluorobenzoate	4.39 ±0.04	ND	ND	-	-
Subtotal (mg/L)	**508.35^{a}±2.98**	**622.73^{c}±2.91**	**616.77^{b}±2.68**		
Subtotal (%)	**68.46**	**82.39**	**78.82**		
Carbonyls					
Acetaldehyde	0.8^{a} ±0.07	1.45^{b} ±0.05	1.36^{b} ±0.05	100	Sherry, nutty, bruised apple
Butanal	ND	ND	0.02 ±0.01	-	-
Decanal	1.28 ±1.05	ND	ND	1.0	Grassy, orange skin-like
2-Cyclohexene-1-one	ND	0.50 ±0.00	ND	-	-
6-Methyl-5-hepten-2-one	3.33^{c} ±0.07	1.61^{a} ±0.11	2.23^{b} ±0.05	-	-
% 6-Methyl-5-hepten-2-one of carbonyls	50.45	22.61	39.40	-	-
3-Octanone	0.72^{a} ±0.05	ND	ND	-	-
(E)-5,9-Undecadien-2-one	0.46^{a} ±0.02	3.56^{c} ±0.01	2.05^{b} ±0.03	-	-
Subtotal (mg/L)	**6.60^{b} ±1.26**	**7.12^{b} ±0.17**	**5.66^{a} ±0.14**	-	-
Subtotal (%)	**0.89**	**0.94**	**0.72**		
Furans					
2,3-Dihydrobenzofuran	4.23 ±0.04	ND	ND	-	-
Subtotal (mg/L)	**4.23 ±0.04**	ND	ND		
Subtotal (%)	**0.57**	ND	ND		
Sulphur compounds					
Thiazole	0.20 ±0.01	ND	ND	0.038	Popcorn, peanut
2-Isobutylthiazole	ND	0.17 ±0.03	ND	-	-
3-Methylisothiazole	0.33^{b} ±0.01	ND	0.25^{a} ±0.03	-	-
5-Methylthiazole	0.20 ±0.00	ND	ND	-	-
Subtotal (mg/L)	**0.73^{c} ±0.02**	**0.17^{a} ±0.03**	**0.25^{b} ±0.03**		
Subtotal (%)	**0.10**	**0.02**	**0.04**		
Fatty acids					
Acetic acid	2.29^{a} ±0.24	3.23^{b} ±0.15	ND	200.0	Acid, fatty
3-Methylbutanoic acid	0.93^{b} ±0.01	ND	0.66^{a} ±0.00	3.0	Cheese, rancid
Hexanoic acid	12.40^{c} ±0.12	10.80^{b} ±0.43	8.70^{a} ±0.20	3.0	Cheese, rancid, fatty, fruity
Heptanoic acid	ND	1.26^{b} ±0.05	0.38^{a} ±0.32	3.0	Fatty, dry
Octanoic acid	41.75^{c} ±0.22	4.44^{a} ±0.52	36.78^{b} ±0.22	10	Rancid, fatty acid, dairy
Acetohydroxamic acid	ND	0.28 ±0.00	ND	-	-
Subtotal (mg/L)	**57.37^{b} ±0.59**	**20.01^{a} ±0.72**	**46.52^{b} ±0.22**		
Subtotal (%)	**7.73**	**2.65**	**5.94**		
Higher Alcohols					
3-Methyl-1-butanol (isoamyl alcohol)	151.35^{c} ±1.01	88.50^{a} ±1.02	98.81^{b} ±0.01	60.0	Solvent, sweet, nail polish
% 3-Methyl-1-butanol of total alcohol	92.77	85.61	89.73		
2-Methyl-1-propanol (isobutyl alcohol)	ND	3.58 ±0.02	ND	0.55	Malty
3-Ethoxy-1-propanol	ND	0.64^{b} ±0.00	0.38^{a} ±0.00	0.1	Fruity

Note: Values are means ± standard deviation obtained from triplicate measurements. C = tomato wine before ageing; C10 and C15 = tomato wines aged at 10^{o} and 15^{o} respectively; ND = not detected; ' -' = no data/information. Means with the same alphabets in a row are significant (P<0.05).

Table 2. (Continued)

Compound	C	C10	C15	Odour threshold	Odour descriptor
(S)-1,3-Butanediol	ND	0.19 ±0.00	ND	-	-
2,3-Butanediol	0.46[a] ±0.06	ND	0.52[a] ±0.03	150	Floral, waxy, fruity, herbal
Amyl alcohol	0.62[b] ±0.04	0.25 [a] ±0.02	0.28[a] ±0.02	80.0	Fruity, balsamic
4-Methyl-1-pentanol	ND	ND	0.30 ±0.00	-	-
1-hexanol	3.73 [b] ±0.08	2.15 [a] ±0.31	2.60 [a] ±0.39	8.0	Green grass
(S)-(+)-3-Methyl-1-pentanol	0.66[b] ±0.00	0.40 [a] ±0.03	0.47 [a] ±0.10	-	Fruity, balsamic
(E)-3-Hexen-1-ol	0.82 [a] ±0.24	0.50 [a] ±0.21	0.56 [a] ±0.28	0.4	Green, floral
1-Heptanol	1.70 [a] ±0.20	2.19 [b] ±0.10	1.77 [ab] ±0.30	1.0	Grape, sweet
1-Octanol	2.32 [c] ±0.05	1.88 [a] ±0.13	2.08 [b] ±0.03	0.12	Intense citrus, roses
6-Octen-1-ol	ND	0.94 (0.08)	ND	-	-
1-Nonanol	ND	ND	0.70 [a] ±0.05	0.058	-
(E)-2-Nonen-1-ol	ND	0.30 ±0.05	ND	-	-
(Z)-3-Nonen-1-ol	1.15 [c] ±0.04	0.86 [b] ±0.03	0.90 [b] ±0.05	-	-
9-Decen-1-ol	0.34 [a] ±0.03	0.59 [b] ±0.06	0.42 [a] ±0.05	-	-
Benzyl alcohol	0.40 [a] ±0.05	0.41 [a] ±0.05	0.33 [a] ±0.10	200	Citrusy, sweet
Subtotal (mg/L)	**163.15[c]**	**103.38[a]**	**110.12[b]**		
Subtotal (%)	**21.97**	**13.68**	**14.07**		
Terpene					
Linalool	2.11 [a] ±0.25	2.39 [a] ±0.14	3.23 [b] ±0.45	0.025	Fruity, citric
Subtotal (mg/L)	**2.11 [a] ±0.25**	**2.39 [a] ±0.14**	**3.23 [b] ±0.45**		
Subtotal (%)	**0.28**	**0.32**	**0.41**		

Note: Values are means ± standard deviation obtained from triplicate measurements. C = tomato wine before ageing; C10 and C15 = tomato wines aged at 10° and 15° respectively; ND = not detected; ' -' = no data/information. Means with the same alphabets in a row are significant (P<0.05).

Most esters found in wines are formed mainly through yeast fermentation [22] and are the main cause of fruitiness in wines, so they play an essential role in the aroma character of young wines [33]. In this study esters are the most abundant volatile compounds, the total concentration being 508.35 mg/L (68.46% of the total volatiles). This is greater than that reported for three varietal wines (26.30-34.20%) [15]. It also increases to 622.73 mg/L (82.39% of the total volatiles) and 616.77 mg/L (78.82% of the total volatiles) when stored at 10° and 15° respectively. The rise in the level of esters during ageing is apparently due to chemical esterification of alcohols and acids [34]. A previous study reported an increase in total ester concentration of white wines after 12 months [35]. The major esters found in the tomato wine are ethyl octanoate, ethyl decanoate and ethyl hexanoate (Table 2). Ethyl octanoate alone constitutes 68.19% of all the esters. The concentration of ethyl octanoate increases significantly (P<0.05) after storage, but storage temperature effect is not significant (P>0.05). Ethyl octanoate is known for its sweet, fruity and fresh notes [36]. The concentration of ethyl decanoate with flowery and fruity notes [37] is also influenced significantly (P<0.05) by storage temperature (Table 2). The wine stored at 10° records a higher value (P<0.05) of ethyl decanoate than does the one stored at 15°. Ethyl hexanoate imparts apple fragrance to wine [38] and after storage its concentration increases significantly. The wine stored at 15° gives a higher value (P<0.05) of ethyl hexanoate than does the one stored at 10°. The other important esters detected are isoamyl acetate, ethyl acetate, ethyl 9-decenoate, ethyl butanoate, isoamyl octanoate, diethyl butanedioate and ethyl 3-methylbutanoate. The storage temperature has a significant effect (P<0.05) on the isoamyl acetate concentration. Isoamyl acetate

is characterised by a banana fragrance [31]. During ageing the tomato wine stored at both temperatures records significant increase ($P<0.05$) in their ethyl acetate content. The ethyl acetate concentrations before and after storage are all less than 150.00 mg/L and is likely to impart a pleasant and fruity fragrance to the wine [39]. The ethyl 9-decenoate concentration is 5.50 mg/L and this increases to 16.66 mg/L and 12.50 mg/L after storage at 10^{o} and 15^{o} respectively. Ethyl butanoate contributes floral and fruity notes to wine aroma [40]. After fermentation, the ethyl butanoate concentration is 2.71 mg/L and this increases significantly ($P<0.05$) after storage, with the wine stored at 15^{o} recording the highest.

The total concentration of carbonyls recorded for the tomato wine is 6.60 mg/L (0.89% of the total volatiles). The major carbonyl detected is 6-methyl-5-hepten-2-one (3.33 mg/L, 50.45% of total carbonyls). Its concentration is influenced by storage temperature ($P<0.05$) and storage leads to its diminution. It is one of the compounds that represent the fresh tomato flavour [13] and is an important product of lycopene catabolism [41]. The general reduction in its content after ageing might reduce the fresh tomato flavour of the wine. The aldehydes found in wine are mostly produced through fermentation and the processing of or extraction from oak cooperage [22]. The acetaldehyde concentration of the tomato wine is 0.81 mg/L while the sensory threshold of acetaldehyde is 100 mg/L [33]. Above this threshold acetaldehyde is usually considered as an off-odour but when it combines with other oxidised compounds, it imparts fragrance to sherries. The acetaldehyde concentration in the tomato wine is far below the threshold and it is thus not expected to contribute negatively to the flavour of the wine. Many ketones are fermentation by-products and only a few seem to have sensory significance [22]. The ketone, 3-octanone, was detected in the tomato wine only after fermentation but not after storage. The (E)-5,9-undecadien-2-one level in the tomato wine, however, experiences significant increase during storage.

Before ageing, 2,3-dihydrobenzofuran, a bioactive phytochemical which is known to possess antiangiogenic properties [42], was identified in the tomato wine. However, after bottle ageing it was not detected. This might be due to its being converted to other compounds.

The sulphur compounds identified in the tomato wine are thiazole, 2-isobutylthiazole, 3-methylisothiazole and 5-methylthiazole. Thiazole and 5-methylthiazole were detected only after fermentation. 2-Isobutylthiazole was detected only in the tomato wine stored at 10^{o}. One of the major compounds which determine the flavour of tomato is 2-isobutylthiazole [13]. The presence or absence of this compound in the wine may influence its tomato flavour.

Organic acids in wine produce a refreshing taste and modify especially the perception of sweetness and other mouthfeel sensations [22]. In wines fatty acid production is based on the must composition and fermentation conditions [43]. The total concentration of fatty acids detected in the tomato wine after fermentation is 57.37 mg/L (7.73% of all volatiles) (Table 2). After storage at 15^{o}, even though there is a reduction in the total fatty acid content of the wine, it is not significant ($P>0.05$). However, there is a significant reduction ($P<0.05$) after storage at 10^{o}. This is in contrast with the results of a previous study [35]. The reduction in fatty acids may be due to chemical esterification between alcohols and acids [34]. Octanoic and hexanoic acids are the major acids found in the tomato wine and after storage these two acids show significant reduction. It has been shown that hexanoic and octanoic acids can contribute to the aroma of some white wines [44]. Heptanoic and acetohydroxamic acids were not detected in the wine after fermentation but were formed during storage. The acetic acid content after fermentation is 2.29 mg/L but this increases to 3.23 mg/L after storage at 10^{o}. These are far below 0.7-1.1 g/L, the level considered objectionable in wines [45]. *S. bayanus*, which was used in this study, is known to produce lower quantities of

acetic acid than does *S. cerevisiae* [46]. This may account for the low acetic acid concentration in the tomato wine.

Higher alcohols are secondary products which originate from yeast metabolism during alcoholic fermentation and are important aroma components of wines [8, 22]. They may contribute positively or negatively based on the type and concentration [47]. After fermentation, the total concentration of higher alcohols in the tomato wine is 163.15 mg/L (21.97% of all volatile compounds) (Table 2), and is extremely high compared with the results reported for raspberry wines [48]. After ageing at 10^{o} and 15^{o}, it decreases to 103.38 mg/L (13.68% of total volatile compounds) and 110.12 mg/L (14.07% of total volatile compounds) respectively. It is known that the higher alcohol concentration of less than 300 mg/L contributes positively to the aroma of wines but that greater than 400 mg/L may reduce its aroma quality [34]. Therefore the higher alcohol concentrations obtained in this study are likely to contribute positively to the overall aroma of tomato wine. The major higher alcohol detected after fermentation is 3-methyl-1-butanol (isoamyl alcohol), which constitutes 92.77% of all higher alcohols. In a study involving three varietal wines, one of the main alcohols reported is also 3-methyl-1-butanol [15]. After storage the concentration of higher alcohols decreases significantly (P<0.05), and the major alcohol, 3-methyl-1-butanol, constitutes 85.61% and 89.73% of all higher alcohols stored at 10^{o} and 15^{o} respectively. Storage temperature has a significant effect (P<0.05) on the higher alcohol concentration after ageing. The reduction in the concentration after ageing is consistent with the result of a previous study [35] and may be due to chemical esterification [34]. On the other hand, 2-methyl-1-propanol (isobutyl alcohol), 3-ethoxy-1-propanol and 6-octen-1-ol were not detected after fermentation, but only detected after ageing. Reductive denitrification of amino acids or synthesis from sugars [22] might account for this.

Terpenes are secondary products of plants and their biosynthetic pathway starts from acetyl-CoA [49]. It is known that terpenes could play an essential role in the characterisation of wine varieties [15]. In this study only one terpene, 3,7-dimethyl-1,6-octadien-3-ol (linalool), is detected in the tomato wine (Table 2). Linalool was among the terpenes previously reported in three varietal wines [15] and Muscat and Pedro Ximenez wines [21]. The linalool content of the tomato wine stored at 15^{o} is significantly higher (P<0.05) than that stored at 10^{o}. Linalool is noted for its fruity, rose and citric notes [26].

OAVs and Relative Odour Contribution of Volatile Compounds

The contribution of each volatile compound was assessed by its OAV, the ratio of its concentration to its odour threshold, which was obtained from literature [31, 37, 40, 49, 50]. Those compounds with OAVs greater than 1 are considered to contribute to the wine aroma [31], though it is known that those compounds with OAVs less than 1 can synergistically make a contribution [51]. Compounds in tomato wine with OAVs greater than 1 and their odour descriptors are shown in Table 3. In all, 23 compounds register OAVs greater than 1. Nonanal, decanal, ethyl acetate and octanoic acid, which are among the odour-active compounds found in this study were also identified in a previous study [15]. Vilanova et al. [38] also reported constituents with OAVs greater than 1 in Spanish Albariño wines.

The relative odour contribution (ROC), which indicates the per cent contribution of each volatile compound with OAV greater than 1 is expressed as the ratio of the OAV of the individual compound to the total OAV expressed as percentage [31]. After fermentation the combined ROC of ethyl octanoate, ethyl hexanoate and isoamyl acetate to the aroma of the tomato wine is 98.44%

(Table 3). After ageing the combined ROC values of these three compounds decrease only slightly, i.e. 98.07% and 98.04% for wine stored at 10^{o} and 15 ^{o} respectively. It was reported that the joint contribution of the same three compounds to the aroma of three varietal wines was in the range of 92.9-98.7% [15], which is comparable to the present results. Another study also reported these three constituents as the most contributory compounds to the aroma of Spanish Albariño wines [38]. The odour description of ethyl octanoate is 'sweet, fruity and fresh' [50] while that of ethyl hexanoate is 'apple, fruity and sweetish' [38] and that of isoamyl acetate is 'banana and pear' [31]. Linalool, one of the most odoriferous terpenes with a fruity, rose and citric descriptor [26] gives an ROC value of 0.36%, which increases to 0.38% and 0.48% after storage at 10^{o} and 15^{o} respectively. Linalool thus also contributes much to the global aroma of the tomato wine after storage.

Table 3. Odour activity values (OAVs) and relative odour contribution (ROC) of tomato wine

Compound	C	C10	C15	Odour descriptor
Esters				
Ethyl acetate	1.88 (<0.01%)	2.11 (<0.01%)	2.25(<0.01%)	Fruity, sweet
Ethyl propanoate	ND	18.00 (0.07%)	22.00 (0.08%)	Fruity
Ethyl butanoate	135.50 (0.58%)	149.00 (0.59%)	177.50(0.66%)	Floral, fruity
Ethyl hexanoate	5110.00 (21.85%)	5792.14 (22.99%)	7452.86 (27.67%)	Apple, fruity, sweetish
Ethyl octanoate	17331.50 (74.12%)	18395.00 (73.00%)	18331.50 (68.07%)	Sweet, fruity and fresh
Ethyl nonanoate	ND	3.00 (0.01%)	1.84 (<0.01%)	Cognac, fatty, oily
Ethyl decanoate	20.29 (0.09%)	66.73 (0.27%)	50.26 (0.19%)	Flowery, fruity
Isoamyl acetate	577.33 (2.47%)	525.33 (2.08%)	619.33 (2.30%)	Banana, pear
Diethyl succinate	24.71 (0.11%)	40.29 (0.16%)	31.57 (0.01%)	Light fruity
Methyl octanoate	30.65 (0.13%)	28.30 (0.11%)	30.65 (0.11%)	Intense citrus
Hexyl acetate	0.34 (<0.01%)	0.66 (<0.01%)	0.64 (<0.01%)	Sweet, perfume
2-Phenylethyl acetate	ND	10.00 (0.04%)	ND	Floral, rose, fruity, honey
Higher alcohols				
Isoamyl alcohol	2.52 (0.01%)	1.48 (<0.01%)	1.65 (<0.01%)	Solvent, sweet, nail polish
Isobutyl alcohol	ND	6.51 (0.03%)	-	Malty
3-Ethoxy-1-propanol	ND	6.40 (0.03%)	3.80 (0.01%)	Malty
3-Hexen-1-ol	2.05 (<0.01%)	1.25 (<0.01%)	1.40 (<0.01%)	Green, floral
1-Heptanol	1.70 (<0.01%)	2.19 (<0.01%)	1.77 (<0.01%)	Grape, sweet
1-Octanol	19.33 (0.08%)	15.67 (0.06%)	17.33 (0.06%)	Intense citrus, roses
1-Nonanol	ND	ND	12.07 (0.04%)	
Fatty acids				
Hexanoic acid	4.13 (0.02%)	3.6 (0.01%)	2.9 (0.01%)	Cheese, rancid, fatty, fruity
Octanoic Acid	4.18 (0.02%)	0.44 (<0.01%)	3.68 (0.01%)	Rancid, fatty acid, dairy
Terpene				
Linalool	84.4 (0.36%)	95.60 (0.38%)	129.20 (0.48%)	Fruity, citric
Sulphur compound				
Thiazole	5.26 (0.02%)	ND	ND	Popcorn, peanut

Note: C = tomato wine before ageing; C10 and C15 = tomato wine aged at 10^{o} and 15^{o} respectively. Values in brackets indicate ROC values.

CONCLUSIONS

The volatile profiles of tomato wine before and after storage have been investigated. Ethyl octanoate, ethyl hexanoate and isoamyl acetate, which are characterised by fruity notes, are the main contributors to the tomato wine aroma, both before and after storage. While the concentrations of most odour compounds which have desirable flavour descriptors are observed to increase during storage, those with less desirable flavour characteristics tend to drop.

ACKNOWLEDGEMENT

This project was funded by the Priority Academic Programme Development (PAPD) of Jiangsu Higher Education Institutions, Republic of China.

REFERENCES

1. C. Ortega, R. Lopez, J. Cacho and V. Ferreira, "Fast analysis of important wine volatile compounds: Development and validation of a new method based on gas chromatographic-flame ionization detection analysis of dichloromethane microextracts", *J. Chromatogr. A.*, **2001**, *923*, 205-214.
2. M. P. Marti, M. Mestres, C. Sala, O. Busto and J. Guasche, "Solid phase microextraction and gas chromatography olfactometry analysis of successively diluted samples: A new approach of the aroma extract dilution analysis applied to the characterization of wine aroma", *J. Agric. Food Chem.*, **2003**, *51*, 7861-7865.
3. P. Satora, P. Sroka, A. Duda-Chodak, T. Tarko and T. Tuszyński, "The profile of volatile compounds and polyphenols in wines produced from dessert varieties of apples", *Food Chem.*, **2008**, *111,* 513-519.
4. J. A. Alves, L. C. de Oliveira Lima, C. A. Nunes, D. R. Dias and R. F. Schwan, "Chemical, physico-chemical, and sensory characteristics of lychee (*Litchi chinensis* Sonn.) wines", *J. Food Sci.*, **2011**, *76*, 330-336.
5. H. Erten, H. Tanguler, T. Cabaroglu and A. Canbas, "The influence of inoculum level on fermentation and flavour compounds of white wines made from cv. *Emir.*", *J. Inst. Brew.*, **2006**, *112*, 232-236.
6. G. H. Fleet and G. M. Heard, "Yeasts-growth during fermentation", in "Wine Microbiology and Biotechnology" (Ed. G. H. Fleet), Harwood Academic Publishers, Chur (Switzerland), **1993**, pp.27-54.
7. B. Fernández de Simón, E. Cadahía, M. Sanz, P. Poveda, S. Perez-Magariño, M. Ortega-Heras and C. González-Huerta, "Volatile compounds and sensorial characterization of wines from four Spanish denominations of origin, aged in Spanish Rebollo (*Quercus pyrenaica* Willd.) oak wood barrels", *J. Agric. Food Chem.*, **2008**, *56,* 9046-9055.
8. E. J. Bartowsky and I. S. Pretorius, "Microbial formation and modification of flavor and off-flavor compounds in wine", in "Biology of Microorganisms on Grapes, in Must and Wine" (Ed. H. König, G. Unden and J. Fröhlich), Springer-Verlag, New York, **2009**, pp.209-231.
9. FAOSTAT, "Total world production quantity of tomatoes", **2012**, http://faostat.fao.org/site/567/DesktopDefault.aspx?pageID=567#ancor (Accessed: June 2012).

10. P. Juroszek, H. M. Lumpkin, R. Y. Yang, D. R. Ledesma and C. H. Ma, "Fruit quality and bioactive compounds with antioxidant activity of tomatoes grown on-farm: Comparison of organic and conventional management systems", *J. Agric. Food Chem.*, **2009**, *57*, 1188-1194.
11. R. Davidovich-Rikanati, Y. Azulay, Y. Sitrit, Y. Tadmor and E. Lewinsohn, "Tomato aroma: Biochemistry and biotechnology", in "Biotechnology in Flavour Production" (Ed. D. Havkin-Frenkel and F. C. Belanger), Blackwell Publishing Ltd, London, **2009,** pp.118-129.
12. R. G. Buttery, R. M. Seifert, D. G. Guadagni and L. C. Ling, "Characterization of additional volatile components of tomato", *J. Agric. Food Chem.*, **1971**, *19*, 524-529.
13. M. Petro-Turza, "Flavour of tomato and tomato products", *Food Rev. Int.*, **1987**, 2, 309-351.
14. J. S. Smith and Y. H. Hui, "Food Processing: Principles and Applications", Blackwell Publishing Professional, New York, **2004**, pp.481-486.
15. B. Jiang and Z. Zhang, "Volatile compounds of young wines from cabernet sauvignon, cabernet gernischet and chardonnay varieties grown in the loess plateau region of China", *Molecules*, **2010**, *15*, 9184-9196.
16. S. Samappito and L. Butkhup, "Effect of skin contact treatments on the aroma profile and chemical components of mulberry (*Morus alba* Linn.) wines", *Afr. J. Food Sci.*, **2010**, *4*, 052-061.
17. P.-R. Lee, Y.-L. Ong, B. Yu, P. Curran and S.-Q. Liu, "Profile of volatile compounds during papaya juice fermentation by a mixed culture of *Saccharomyces cerevisiae* and *Williopsis saturnus*", *Food Microbiol.*, **2010**, *27*, 853-861.
18. J. A. Pino and O. Queris, "Analysis of volatile compounds of pineapple wine using solid-phase microextraction techniques", *Food Chem.*, **2010**, *122*, 1241-1246.
19. F. Boukobza, P. J. Dunphy and A. J. Taylor, "Measurement of lipid oxidation-derived volatiles in fresh tomatoes", *Postharv. Biol. Technol.*, **2001**, *23*, 117-131.
20. K. Viljanen, M. Lille, R.-L. Heiniö and J. Buchert, "Effect of high-pressure processing on volatile composition and odour of cherry tomato pureé", *Food Chem.*, **2011**, *129,* 1759-1765.
21. J. K. Kraus, R. Scoop and S. L. Chen, "Effect of rehydration on dry yeast activity", *Am. J. Enol. Vitic.*, **1981**, *32,* 132-134.
22. R. S. Jackson, "Wine Science: Principles and Applications", Elsevier Inc., London, **2008**, pp. 270-320.
23. M. R. Brown, C. S. Ough, "A comparison of activity and effects of two commercial pectic enzyme preparations on white grape musts and wines", *Am. J. Enol. Vitic.*, **1981**, *32*, 272-276.
24. K. C. Fugelsang and C. G. Edwards, "Wine Microbiology: Practical Applications and Procedures", Springer Science + Business Media, LLC, New York, **2007**, pp.115-138.
25. W. Horwitz (Ed.), "Official Methods of Analysis of AOAC International", 17th ed., AOAC International, Baltimore (MD), **2000**.
26. P. Ribéreau-Gayon, Y. Glories, A. Maujean and D. Dubourdieu, "Handbook of Enology Volume 2: The Chemistry of Wine, Stabilization and Treatments", John Wiley and Sons Ltd, Chichester, **2006**, pp.72-207.
27. S. Williams, "Official Methods of Analysis of the AOAC", 14th ed., AOAC International, Washignton, D. C., **1984.**
28. G. D. Sadler and P. A. Murphy, "pH and titratable acidity", in "Food Analysis" (Ed. S. S. Nielsen), Springer Science + Business Media, LLC, New York, **2010**, Ch.13.
29. A. Jr. Caputi, M. Ueda and T. Brown, "Spectrophotometric determination of ethanol in wine", *Am. J. Enol. Vitic.*, **1968**, *19*, 160-165.

30. R. Márquez, R. Castro, R. Natera and C. García-Barroso, "Characterization of the volatile fraction of Andalusian sweet wines", *Eur. Food Res. Technol.*, **2008***, 226,* 1479-1484.
31. H. Guth, "Identification of character impact odorants of different white wine varieties", *J. Agric. Food Chem.*, **1997**, *45*, 3022-3036.
32. M. Cliff, D. Yuksel, B. Girard and M. King, "Characterization of Canadian ice wines by sensory and compositional analyses", *Am. J. Enol. Vitic.*, **2002**, *53,* 46-53.
33. M. Ugliano and P. A. Henschke, "Yeasts and wine flavour", in "Wine Chemistry and Biochemistry" (Ed. M. V. Moreno-Arribas and M. C. Polo), Springer Science + Business Media, LLC, New York, **2009**, pp.313-392.
34. M. G. Lambrechts and I. S. Pretorius, "Yeast and its importance to wine aroma—A review", *South Afr. J. Enol. Vitic.*, **2000**, *21*, 97-129.
35. V. Gallo, R. Beltrán, F. J. Herodia, M. L. González-Miret and D. Hernanz, "Application of multivariate statistical analyses to the study of factors affecting white wine volatile composition", *J. Food Qual.*, **2011**, *34*, 40-50.
36. J. H. Swiegers and I. S. Pretorius, "Yeast modulation of wine flavor", *Adv. Appl. Microbiol.*, **2005**, *57*, 131-175.
37. M. Czerny, M. Christlbauer, M. Christlbauer, A. Fischer, M. Granvogl, M. Hammer, C. Hartl, N. M. Hernandez and P. Schieberle, "Re-investigation on odour thresholds of key food aroma compounds and development of an aroma language based on odour qualities of defined aqueous odorant solutions", *Eur. Food Res. Technol.*, **2008**, *228,* 265-273.
38. M. Vilanova, Z. Genisheva, A. Masa and J. M. Oliveira, "Correlation between volatile composition and sensory properties in Spanish Albariño wines", *Microchem. J.*, **2010***, 95*, 240-246.
39. A. A. Apostolopoulou, A. I. Flouros, P. G. Demertzis and K. Akrida-Demertzi, "Differences in concentration of principal volatile constituents in traditional Greek distillates", *Food Control*, **2005**, *16,* 157-164.
40. S. Selli, T. Cabaroglu, A. Canbas, H. Erten and C. Nurgel, "Effect of skin contact on the aroma composition of the musts of *Vitis vinifera* L. cv. Muscat of Bornova and Narince grown in Turkey", *Food Chem.*, **2003**, *81*, 341-347.
41. R. G. Buttery, R. Teranishi, L. C. Ling, R. A. Flath and D. J. Stern, " Quantitative studies on origins of fresh tomato aroma volatiles", *J. Agric. Food Chem*., **1988**, *36*, 1247-1250.
42. R. Dharmalingam and P. Nazni, "'Phytochemical evaluation of *Coriandrum* L flowers", *Int. J. Food Nutr. Sci.*, **2013**, *2*, 34-39.
43. S. Selli, A. Canbas, T. Cabaroglu, H. Erten, J.-P. Lepoutre and Z. Gunata, "Effect of skin contact on the free and bound aroma compounds of the white wine of *Vitis vinifera* L. cv Narince", *Food Control*, **2006**, *17*, 75-82.
44. H. Smyth, D. Cozzolino, M. J. Herderich, M. A. Sefton and I. L. Francis, "Relating volatile composition to wine aroma: Identification of key aroma compounds in Australian white wines", Proceedings of 12th Australian Wine Industry Technical Conference, **2005**, Melbourne, Australia, pp.31-33.
45. P. Dubois, "Les arômes des vins et leurs defauts" *Rev. Franç. Oenol.*, **1993**, *33*, 63-72.
46. J. M. Eglinton, S. J. McWilliam, M. W. Fogarty, I. L. Francis, M. J. Kwiatkowski, P. B. Hoj and P. Henschke, "The effect of *Saccharomyces bayanus*-mediated fermentation on the chemical composition and aroma profile of Chardonnay wine", *Aust. J. Grape Wine Res.*, **2000**, *6*, 190-196.

47. E. Valero, L. Moyano, M. C. Millan, M. Medina and J. M. Ortega, "Higher alcohols and esters production by *Saccharomyces cerevisiae*: Influence of the initial oxygenation of the grape must", *Food Chem.*, **2002**, *78*, 57-61.
48. W. F. Duarte, D. R. Dias, J. M. Oliveira, M. Vilanova, J. A. Teixeira, J. B. A. e Silva and R. F. Schwan, "Raspberry (*Rubus idaeus* L.) wine: Yeast selection, sensory evaluation and instrumental analysis of volatile and other compounds", *Food Res. Int.*, **2010**, *43*, 2303-2314.
49. J. J. Mateo and M. Jimenez, "Monoterpenes in grape juice and wines", *J. Chromatogr. A*. **2000,** *881*, 557-567.
50. R. A. Peinado, J. Moreno, J. E. Bueno, J. A. Moreno and J. C. Mauricio, "Comparative study of aromatic compounds in two young white wines subjected to pre-fermentative cryomaceration", *Food Chem.*, **2004**, *84***,** 585-590.
51. I. L. Francis and J. L. Newton, "Determining wine aroma from compositional data", *Aust. J. Grape Wine Res.*, **2005**, *11*, 114-126.

Maejo Int. J. Sci. Technol. **2014**, *8*(02), 143-160

Maejo International Journal of Science and Technology

ISSN 1905-7873
Available online at www.mijst.mju.ac.th

Review

Merging the fields of swarm robotics and new media: Perceiving swarm robotics as new media

Monika O. Ivanova [1, *], Micael S. Couceiro [2, 3] and Fernando M. L. Martins [4, 5]

[1] School of Computing, Edinburgh Napier University, EH10 5DT, United Kingdom
[2] Artificial Perception for Intelligent Systems and Robotics (AP4ISR), Institute of Systems and Robotics (ISR), University of Coimbra, 3030-290, Coimbra, Portugal
[3] Ingeniarius, Lda., Rua da Vacariça, n.37, 3050-381, Mealhada, Portugal
[4] Institute of Telecommunications (IT), Convento Santo António, Covilhã, 6201-001, Portugal
[5] Polytechnic Institute of Coimbra, ESEC, DE, Rua Dom João III, Solum, 3030-329 Coimbra, Portugal
[*]Corresponding author, e-mail: monikaoivanova@gmail.com

Received: 23 August 2013 / Accepted: 16 June 2014/ Published: 17 June 2014

Abstract: The aim of this paper is to provide evidence that swarm robotic systems can be perceived as new media objects. A thorough description of the five principles of new media proposed by Lev Manovich in "The Language of New Media" is presented. This is complemented by a state of the art on swarm robotics with an in-depth comparison of the characteristics of both fields. Also presented are examples of swarm robotics used in new media installations in order to illustrate the cutting-edge applications of robotics and artificial intelligence achieved through the unity of both fields. The hypothesis of this research is that a novel point of view would be introduced by examining the field of swarm robotics through the scope of new media, which would benefit the work of both new media and swarm robotic researchers.

Keywords: new media object, swarm robotics, principles of Manovich

INTRODUCTION

There have been many debates on the nature of *new media*. However, there is a famous notion saying that 'medium is the message' and it is only natural that this expression emerges from a pioneering study of new media theory by Marshall McLuhan in his revolutionary work, "Understanding Media: The Extensions of Man" [1]. Just like the book, the current paper focuses on the media itself and not the content it carries. To observe *swarm robotics* from a media point of view would be indeed a very curious case and a supplement to robotics researchers [2]. Moreover, the notion that swarm robotics can be perceived as new media objects significantly increases the field's potential for application. For example, swarm robotics could be used as an artistic tool for the creation of interactive installations. The importance of this is that the increase of applicability

raises new challenges to the scientists and designers, the solution to which could be found in more scientific scenarios such as search and rescue missions.

Undoubtedly, media in its most basic form is created to be an extension of man [1]. Although swarm robotic systems do not have content like the one found in newspapers or television, they are a strong medium with significant sociological influence [3]. In their basics, swarm robotic systems are designed to be an extension of man, enabling him to explore areas that would be inaccessible to a human being. In addition to that, swarm robotic systems also assist or replace people in search and rescue scenarios that would be too hard or too dangerous to be executed by humans alone.

According to McLuhan, any medium 'amplifies or accelerates existing processes' and introduces 'a change of scale or pace or shape or pattern into human association, affairs and action', resulting in 'psychic and social consequences' [1]. With the rapid advances and the pioneering research done in the field of swarm robotics such as enabling an unanimated robot to possess processes embedded in the nature of living beings (i.e. self-regeneration and self-replication), swarm robotics amplify the existing processes of creating machines at a human concept level. This significantly accelerates the scientific advances and brings humanity to a new level of human-machine interaction [4]. Supporting this, one of the main beliefs of McLuhan about the role of media is that it continually shapes and reshapes the way in which individuals, societies and cultures perceive and understand the world [1]. This complies with advances in the field of swarm robotics that continually shape and reshape the way individuals, societies and cultures perceive the notion of robotics and their capabilities [5].

Having stated that, there can be no doubt that swarm robotic systems comply with the definition of media objects as presented by McLuhan [1]. Furthermore, it turns out that there are also a variety of principles describing the nature of new media that also hold true when it comes to swarm robotic systems. This paper presents the five main principles of new media introduced by Lev Manovich in "The Language of New Media" [6] that also apply to swarm robotics, thus proving that swarm robotic systems can be perceived as new media objects and building the bridge between the two fields of new media and swarm robotics. The hypothesis of this research is that through the analysis of swarm robotics as new media objects, a novel point of view for both roboticists and media designers can be achieved. Hence a collaboration could be formed leading to the development of more advanced technology both in the fields of new media and robotics.

SWARM ROBOTICS AS NEW MEDIA

This section reviews the current state of the art on swarm robotics while providing a close analogy to new media objects according to the five principles of Manovich [6].

Numerical Representation

The first and most distinctive characteristic of a *new media object* is that it is a numerical representation or, in other words, it is composed of a binary code. This brings up two key consequences. First of all, it makes the new media object *programmable*; that is to say, it can be formally (mathematically) described and is subject to algorithmic manipulation. In other words, the behaviour of the object is defined by mathematical functions in binary code. Secondly, unlike the continuous nature of analogue media, new media is *digitised*; that is to say, it is composed of discrete samples. The process of digitisation is divided into two parts. The first is called sampling. It

describes the division of a new media object into separate measurements which are made according to a specific procedure [6]. The second is called quantisation. Each sample is then quantified, i.e. assigned a specific value from a predefined range. In addition, because a new media object is constructed from autonomous samples, new media is developed towards an individual customisation rather than mass standardisation. All of the aforementioned information holds true when it comes to swarm robotics.

The driving force behind the behaviour of any robot, either the most advanced industrial models or the simplistic ones used in swarm applications, is controlled by digital code. Although coding has become more accessible and visual due to the ever-increasing robotics community and the user-friendly graphical user interfaces [7], those are compiled in executable machine codes, i.e. sequences of zeros and ones. For instance, some robotic agents with a certain degree of autonomy, related also to the 2nd law of modularity and the 3rd law of automation in new media by Manovich [6], are able to self-reconfigure or self-repair by executing a set of mathematical models defined by code [8]. Therefore, the behaviour and, in certain cases, the creation of a robotic agent may be formally (i.e. mathematically) defined. This makes it possible to describe the task to be executed the way it is supposed to be executed and also the further conditions related to it (Figure 1).

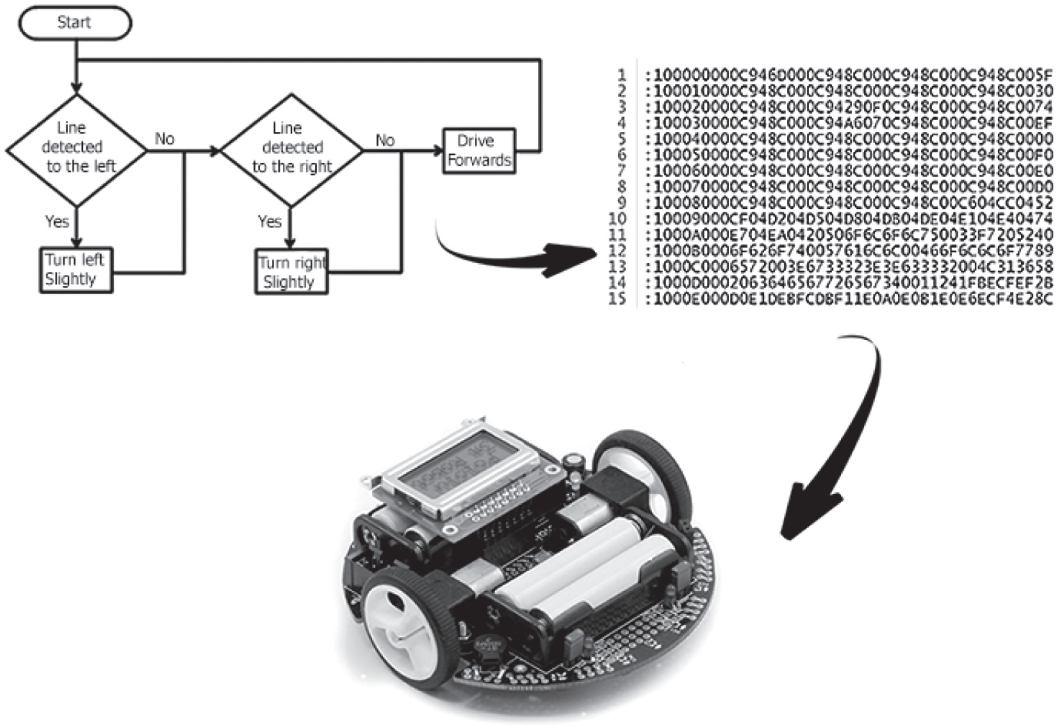

Figure 1. Numerical representation principle: visual representation of the behaviour of a 3pi robot in a simple line-following task, illustrating the algorithm, its compiled form and the 3pi robot itself [9-11]

As a natural consequence, the behaviour of one robotic agent or even the multi-robot system (e.g. swarm of robots) is subject to algorithmic manipulation. In other words, each robot's actions depend on the implemented processes that usually follow a given flow. Although the adaptive behaviour towards contextual information has been successfully implemented in most of the recent robotic applications [12], robots continue to follow a certain set of programmed rules, either deterministic or stochastic, algorithmically translated through coding [13].

The individual agents of a system are defined as *nodes* and can be perceived as the 'samples' constructing a new media object, given that the object itself is represented as the swarm. It is only natural that they also need to be 'quantified' with a specific identification, which would ease the communication between different agents and help to define the individual contribution to the collective behaviour of the entire swarm [14].

In short, similar to the creation of a new media object, a swarm of robots is comprised of discrete samples that are represented by autonomous agents, quantified according to their identification, whose behaviour is formally (i.e. mathematically) described and subject to algorithmic manipulation.

Modularity

The second principle of new media, according to Manovich, describes the structure of a new media object [6]. Modularity, or the so-called *fractal-structure* of new media, describes the specific alignment of identic elements with different scalability constructing a new media object. In other words, a new media object consists of collections of discrete samples, which can then be assembled into larger-scale ones, although they would still retain their separate identities. Again, the newly founded objects can be combined to create even larger objects without losing their autonomy. Since each object retains its independence and identity, it can be accessed and modified at any time without affecting the structure of the entire larger-scale object. Furthermore, if a specific module in the system is modified or removed, this would not jeopardise its existence as a whole. In short, a new media object consists of small and self-sufficient modules which, in turn, consist of even smaller and self-sufficient modules, thus providing the possibility of modifying one module without affecting the structure of the entire object as a whole.

This is a recurrent principle observed in swarm robotics. At the lowest level, each swarm robot comprises of multiple electronic circuits. As the work of Dorigo et al. [15] depicts, the notion of electronic modularity may be applied at that level. This is obtained by partitioning the required functionality of each module to make them as autonomous as possible.

Moving up in the hierarchy, a swarm of mobile robots consists of small, self-sufficient mobile agents that correspond to the concept of discrete samples in new media as previously mentioned. This means that each swarm and, in turn, each separate agent can be easily taken apart and reassembled into different configurations corresponding to the specific tasks of each mission. In swarm robotics, the modular structure allows for better flexibility in construction and data flow. In addition, the modular structure of the agents forming a swarm makes it possible to have different types of specialised robots in the system, thus making it more cost efficient and also increasing the separation of identity of the agents in it. A robotic swarm system usually consists of relatively few homogenous groups of robots [3]. This improves the fault-tolerance of the system; should one agent experience a failure, the execution of the task would not be severely jeopardised. Similarly, in new media if some of the samples constructing the object are damaged or missing (e.g. pixels in a digital image), the structure of the object would still be recognisable.

On a larger scale, modularity can be perceived in one more specific case of swarm robotics. This is the case where a swarm consists of several other swarms, each in turn consisting of different types of specialised agents. For example, the work of Navarro-Serment et al. [16] illustrates a use of this particular case with their example of creating a swarm combining several other swarms, each separately consisting of large all-terrain vehicles, medium-sized tank-like robots, and centimeter-scale *Millibots*. All of the swarms are designed to execute a specific task (i.e. the all-terrain vehicles

being used to deploy medium-sized tank-like robots and the Milibots) and by being individual, self-sufficient parts of a swarm entity, they perfectly illustrate the modularity principle in new media. This concept is also supported in the work of Alunni et al. [14], where the author presented the idea that groups of nearby robots could self-organise to form collective agents. The hierarchy is created by the expansion of those groups of collective agents to eventually consist of the entire swarm. Similarly, Couceiro et al. [17] proposed an algorithm denoted as robotic Darwinian particle swarm optimisation, in which each swarm of robots competes to strive for a better solution while robots within each swarm co-operate. With this co-opetitive (i.e. co-operative and competitive) behaviour associated with the Darwinian principles of survival of the fittest, the swarms that are able to improve proliferate over the others and at some point all robots form a unique swarm (Figure 2a).

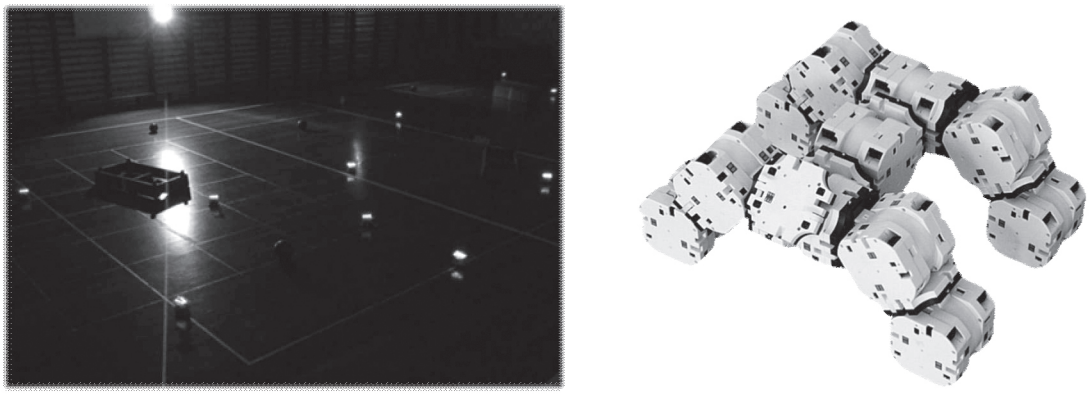

a) b)

Figure 2. Modularity principle: a) co-opetitive behaviour with different colours representing different swarms of robots that evolve based on survival-of-the-fittest principles [17]; b) swarm of self-assembly modular robots that can reshape into a larger collective system [18]

At a higher level, the work of Wei et al. [18] (Figure 2b) discusses the use of self-assembly modular robots as a new concept in swarm robotics co-operation. As a swarm of robots use numerous simple robots to achieve the desired task through co-operation, self-reconfigurable modular robots rely on the same concept by connecting and disconnecting autonomous agents in a bigger system that can reshape, without human intervention, to adjust to the demands of the environment and the task at hand. In this case the modules relating to the idea of discrete samples are the autonomous agents while the object itself is the swarm robotic structure.

In short, the modularity design of swarm robotic systems allows for the creation of specialised robots with particular modular configuration. The combination of those simple agents forming a swarm increases its possibilities while still maintaining energy efficiency, small cost and size [16].

Automation

Automation is a concept inherent to both new media and swarm robotics. In new media automation is a process in the creation or modification of a certain object, which removes, at least partially, the need for human intervention. This concept becomes possible because of the existence of the aforementioned principles of numerical coding (the first principle of new media) and modularity (the second principle of new media), and it allows for parts of the modification, creation

and access processes to be done without human intervention [6]. The process of automation in new media is divided into two sub-categories: low-level automation and high-level automation. The difference between the two categories is that while low-level automation processes allow the user to create new media objects using templates or simple repetitive algorithmic computations, high-level automation requires a computer to understand to an extent the semantics behind the generated objects [6].

It is in the process of high-level automation that new media most significantly resembles robotics since high-level automation is one of the approaches of artificial intelligence engines and an inseparable part of both new media and swarm robotics used to simulate bio-inspired intelligence. Ismail [19] described the latest projects in the field of swarm robotics as the so-called *Symbrion* and *Replicator* projects. Both of them were inspired by swarm intelligence based on natural examples and focused on enabling the agents in the swarm to autonomously manage their software and hardware mechanisms. This is believed to configure the robotic organism in a way that would make it self-healing, self-optimising and self-protecting against software and hardware failure. Hence a swarm would be created of exceptionally adaptive agents that would also have enhanced scalability and ability to evolve. Furthermore, it is believed that the robots forming the swarm would also have the ability to reprogramme themselves, which would significantly increase the degree of automation.

High-level automation is also considered to be related to the degree of evolvability inherent to a swarm. Similar to high-level automation in new media, in this case the swarm is required to 'think' or, in other words, to have a certain understanding of the configurations it could autonomously reshape so as to, for instance, overcome obstacles (Figure 3b). This example is thoroughly illustrated by Kernbach et al. [20]: in order to overcome an obstacle and reach the recharge station, a swarm has to 'grow legs' by forming a collective organism of a quadruped robot which would enable it to 'step over' the obstacle (Figure 3a).

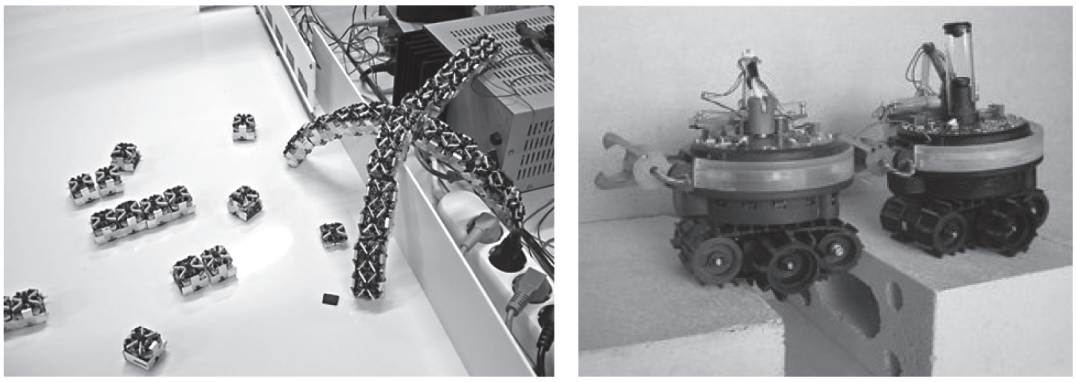

a) b)

Figure 3. Automation principle: a) Replicator and Symbrion project agents forming a four-legged robotic structure in order to overcome the barrier to the charging doc [20]; b) similar situation in which two foot-bots dock together to overcome the lack of bridge between the two surfaces [15].

Alternatively, the work of Dai et al. [21] discusses a prototype for a self-healing and self-reproducing swarm robotic system. Their goal is to create, by using Autonomic Computing, which mimics the autonomic nervous system present in most bio-organisms, a virtual neuron which would be in charge of the monitoring of the hardware and software systems of the agent. In addition to that, it would have certain *prescriptions* embedded in its code that would take care of the analysis

and reparation of possible system failure. Moreover, due to the virtual neuron, the agents in a swarm would be able to mutually heal one another or in the case of complete failure of an agent, another agent would be able to collect the good 'organs'. If a sufficient stack of organs is gathered, a third robot could autonomously combine those to make a new agent. The latter process is called *self-reproduction.* Other means of self-reproduction may involve the creation of a robot from the spare parts of other robots. The time and execution of this process is dictated by the virtual neuron and happens without human intervention, thus presenting this work as being an extreme case of high-level automation in swarm robotics.

However, low-level automation in the form of simple repetitive actions is also observed in swarm robotics. For example, the work of Melhuish et al. [22] shows how, by following four simple programmed rules (principle of numerical representation), a swarm of robots are able to perform a complicated task like carrying and sorting out several different types of objects. Such complicated patch sorting task can be achieved using a simple mechanism and without any sort of explicit communication between robots, thus making this approach highly scalable. Most of the control architectures in swarm robotics have included a low-level automation layer. For instance, many swarm robotic behaviours are programmed without considering obstacle avoidance or the kinematic or dynamic structure of robots [23]. The work of Pugh and Martinoli [24] was one of the first adapted versions of the particle swarm optimisation to handle real world constraints by using the *Braitenberg* obstacle avoidance algorithm [25]. Such low-level behaviours were subsequently programmed in swarm robots as a low-level control layer that receives the output commands of the main layer and translates those into low-level commands designed for a specific robotic system.

In short, high-level and low-level automation are present both in the field of new media and that of swarm robotics. Low-level automation is exhibited in the repetition of simple algorithmic computations used to describe the behaviour or the creation of an object while high-level automation requires a certain degree of understanding about the nature of the object that is being generated.

Variability

Variability in new media is closely related to the nature of new media as are numerical representation (first principle) and its modular structure (second principle). It means that a new media object can exist in different, potentially infinite, versions of itself [6]. What is specific to a new media object is that instead of simply having completely identical copies of itself, it enables the creation of many different versions. A necessary condition for the existence of variability in a new media object is the presence of modularity. The modular structure of a new media object, made of autonomous discrete samples, makes it possible to reassemble the separate modules in the object under the supervision of preprogrammed computations.

The concept of variability is also present in the field of swarm robotics. As previously mentioned, just like a new media object, a swarm has a modular structure consisting of a large number of autonomous agents which can be configured in accordance with the objectives of the task at hand [18]. The behaviour of the swarm is subject to algorithmic computations (numerical representation) and each swarm robotic system also possesses a certain degree of automation.

A specific case of the variability principle in new media is that the media elements are various and stored in a database from which they can be assembled beforehand or on demand. A similar case is illustrated in the field of swarm robotics. Calisi et al. [12] proposed that each robot of the created prototype swarm would have a certain amount of spare parts attached to its body. In the

case of self-reproduction dictated by the virtual neuron, a new robot could be autonomously assembled by the others to fit the requirements of the environment. This new robot would be a perfect example of the variability principle since it would be constructed from different modules present in the swarm 'database' and its construction would be subject to predefined computations.

In terms of software, the work of Waibel et al. [13] presents a novel approach to storing the shared memory of multiple robots into a database called RoboEarth. Unlike other methods in which the vast majority of data for robots is tightly dependant on the robots' hardware and difficult to reuse across platforms, RoboEarth collects, stores and shares information in a platform-independent way, thus making it widely effective throughout various configurations and scenarios. Also, the aim of the RoboEarth project is to enable the sharing and reuse of knowledge instead of using the collected data only to create algorithms to be used offline without connection to the original information. According to the authors, the benefit of this approach would be a better coordination and improved efficiency in missions requiring the robots to operate in complex, unstructured environments. The RoboEarth database is subject to constant update since at the end of each task the robot shares the acquired knowledge by uploading it to the distributed database. This is yet another link to the variability principle in new media, which defines a new media object to be subject to constant updates [6].

Another example of the variability principle in new media is termed *hypermedia*. Manovich defines hypermedia as systems that provide the user with the ability to create, manipulate and examine a network of information containing nodes connected by relational links [6]. Hyperlinking provides the connection (i.e. the wiring) between the different nodes in the network. This is of course possible due to the modular nature of new media and the principle of numerical representation. The hypermedia example can also be found in swarm robotics. From the definition, it can be deduced that hyperlinks represent the connecting wires in a decentralised network and are in charge of the control and navigation of the entire system.

The work of Dorigo et al. [15] illustrates this principle. The authors proposed an innovative swarm robotic system built from several swarms of three types of different autonomous agents (also supporting the modularity principle) called *Swarmanoid*. The Swarmanoid consists of a sub-swarm of small autonomous agents called *foot-bots*, which specialised in movement on both even and uneven terrains (Figure 4b), and which are also capable of self-assembling and transportation. There is also a sub-swarm of *hand-bots* (Figure 4a) which are capable of manipulating small objects and climbing vertical surfaces. Finally, the Swarmanoid system also consists of a sub-swarm of autonomous flying agents called *eye-bots*, which are capable of attaching themselves to indoor ceilings, analysing the environment and transporting both the foot-bots and the hand-bots. Supporting the concepts of modularity and automation, the agents of a particular type in the swarm system are directly interchangeable and also possess self-configurability. In this particular example, the eye-bots act as navigational agents between the foot-bots and hand-bots in a decentralised system, providing the wiring link between the two subsystems.

A system with a hyperlink typology also has a branching structure and an if-case application – a certain action is executed if a certain condition is fulfilled (Figure 5a). This also applies to the behaviour of the separate agents in the work of Dorigo et al. [15]. In the Swarmanoid system for search and retrieval scenarios the environment is scanned by the eye-bots. If they detected the desired object in the environment, the location would be passed down to the foot-bots, which should bring a hand-bot to the place (since hand-bots have no ability for locomotion on their own) (Figure 5b).

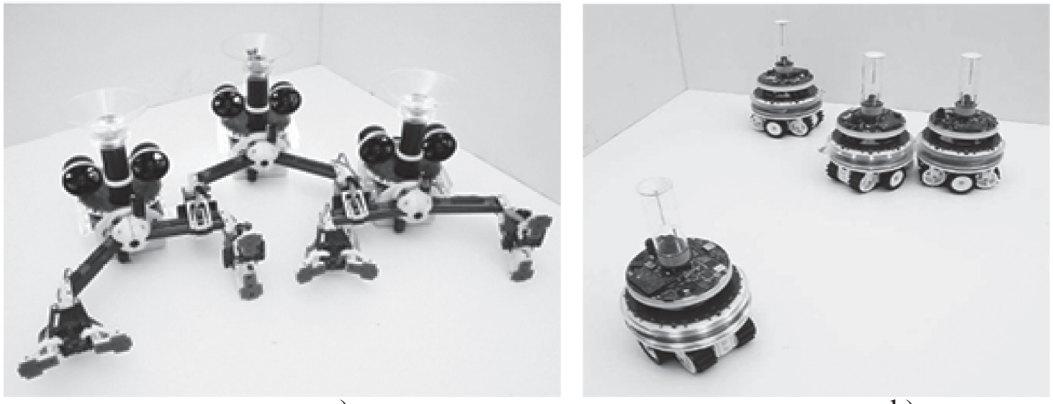

a) b)

Figure 4. Variability principle: a) Hand-bots, a sub-swarm of the Swarmanoid project, capable of climbing vertical surfaces and manipulating small objects [15]; b) Foot-bots, a sub-swarm of the Swarmanoid project, capable of self-assembling and transportation [15]

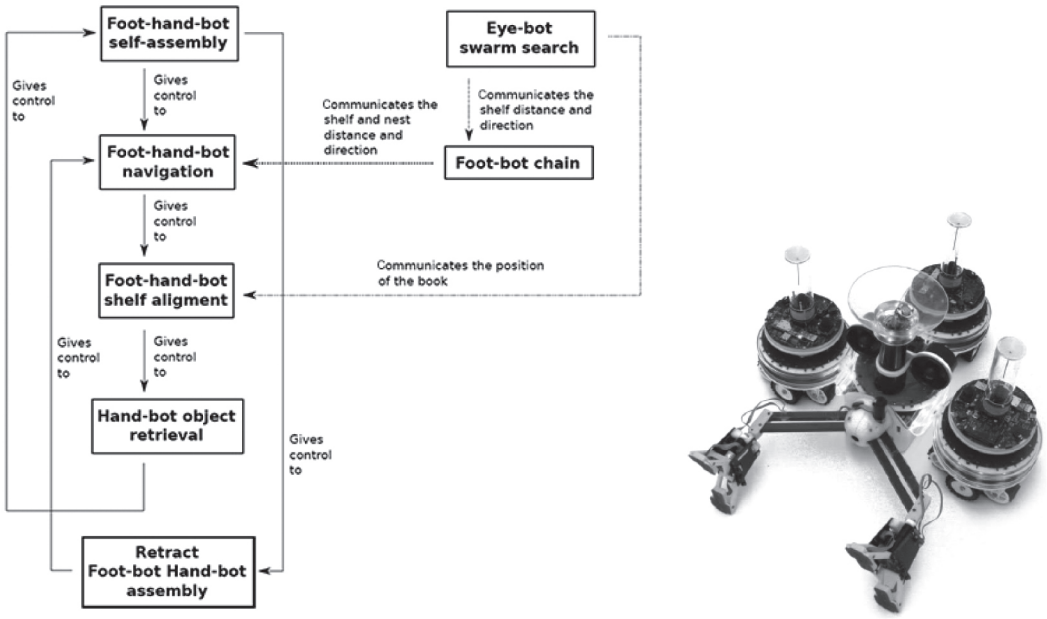

a) b)

Figure 5. Variability principle: a) a scheme representing the behavioural scenario and the interactions of the robots within the Swarmanoid [15]; b) foot-bots docked to a hand-bot in order to bring it to the desired location [15]

In the programming code defining the behaviour of a swarm robotic system, a branching topology can also be found [15]. The system is programmed to execute an action if a certain condition is true, thus creating a set of commands that aim at covering the actions for as many conditions as possible. This way it is also possible to obtain a higher degree of automation. For example, every time the swarm encounter an obstacle, they follow the predefined actions for that condition or, in other words, they execute only one version at a time from the pre-programmed code. The branching code topology defining the behaviour of a swarm robotic system serves as a definite example of how the principle of variability applies to swarm robotics.

Another sub-case of the variability principle in new media is termed *scalability*. Lev Manovich describes this principle as the ability to create versions of a media object which differ in their size or level of detail [6]. This nature of new media also allows for the creation of versions of a new media object which differ from each other in more substantial ways. In swarm robotics, Murata et al. [26] describe scalability to be a remarkable consequence of the modular structure of the agents in a swarm and the system itself. In this case the size of a swarm is changeable by the number of modules in it as this is vital in order to achieve the best configuration for the task at hand. Moreover, Rubenstein et al. [27] describe scalability as the condition that all of the operations of one robot should work on the collective as a whole without the need for human intervention or individual attention to the agent. If they do, the robot is called *scalable*. In the cited paper, several examples of scalable computations are presented. For instance, the authors present a collective programming of the behaviour in a swarm by using an infrared communication channel, which removes the need for each agent to be programmed separately. The authors also present another example of a scalable operation in regard to the power control of an agent, whereas in order to remove the need for human intervention, a charging dock is introduced for the swarm to recharge itself autonomously. Furthermore, Bjerknes et al. [28] argue about the application of the scalability principle in relation to the size of the swarm. They present arguments as to why the so-far-assumed-to-be-true concept that the swarm decision-making system based on local sensing and communication is only natural to lead to swarms scalable to large numbers of agents, is actually not true in several different cases. One of those shows that a large number of robots in a system would be less beneficial in the case of self-repair and self-configuration since it would increase the swarm's failure rate. They argue that at some point the swarm would 'die under its own weight', thus rendering the scalability principle not true in this particular case.

Just as new media is highly customisable to fit individual needs by creating different versions of one and the same object, the swarm robotic system can either be reconfigured to suit the personal demands (cost, functionality) when targeted to non-professional or everyday usage (e.g. simple cleaning tasks) [29], or it can be modularly reconfigured when it comes to the execution of specific tasks or missions (e.g. exploration of large unknown areas, surveillance, rescue, coordinated weight lifting).

In short, the variability principle is derived from the modular structure and the automation attribute of new media. This principle describes several qualities of the new media object that include its storage in a database, its branching type structure, its scalability and hypermedia. All of those concepts are also applicable in swarm robotics and again emerge from the modular structure and the level of automation in a swarm.

Transcoding

Transcoding is the fifth and final Manovich's principles of new media. It is the most evident result of the first principle of numerical representation and it represents the machine-readable information describing the interface of a new media object. It also depicts the new and distinct structure of new media as consisting of two autonomous and mutually influential layers: a *cultural layer* and a *computer layer* [6] (Figure 6). The cultural layer displays the information in a new media object in a way that is comprehensible (images, text, etc.) to the human user while the computer layer turns the same information into a machine-readable language (functions, variables, arrays, binary code, etc.). Since the two layers are strongly dependable on each other, they also become mutually influential. With the constant advance of the hardware and software specifications

of a computer system on which the computer layer depends, new opportunities arise for creating different or variant types of the cultural layer of the same object. This interconnectivity defines the creation of a new computer culture where the new media object is a blend of meanings for human and computer. Hypermedia is also a particular case of the variability principle previously described in this paper and is in fact also a distinct example of the transcoding principle since the data and navigation characteristics of its structure exist separately. Another case in point of the transcoding principle is the modular structure of a new media object. The analogy with a computer programme supports this statement as, similar to a new media object, a programme consists of small, autonomous modules which in turn consist of even smaller, autonomous objects. It can be said that the most general definition of transcoding is the translation of something from one format into another [6].

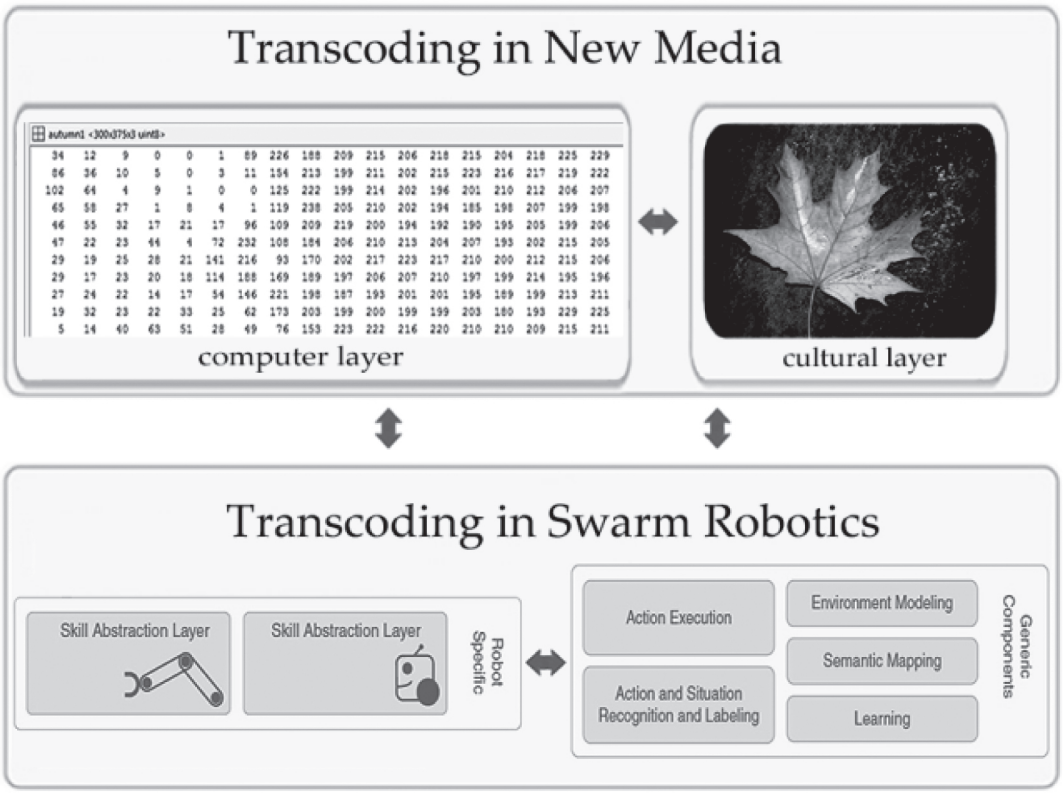

Figure 6. Transcoding principle: a visual representation of the analogy between the different layers constituting the fields of new media and those of swarm robotics [13]

However, in order to understand how the transcoding principle works in swarm robotics, it is necessary to explain the structure of the agents building the system. Each swarm agent's hardware is made of different layers. The first layer deals with the information gathered from the sensors and the second layer translates it into a machine-readable language. However, in swarm robotics it is also possible to have a third layer which is responsible for the robot's self-assessment. The work of Kunze et al. [30] illustrates the principle of layered topology. It describes a way to connect high-level action instructions with low-level robot descriptions in the structure of a robot's manipulators. By doing this, the researchers tried to input in the robot's system a certain amount of knowledge about itself that would enable it to assess whether it would be able to perform the required action.

Apart from being a necessity for an object to be defined as a new media object, the layered structure of a swarm agent is also an addition to the branched topology of the code defining the behaviour of the agent. As previously discussed, the code defining the behaviour of a robot is structured around context-driven choices. For instance, when the swarm agent encounters an obstacle, the information about its surrounding is gathered by the sensors and translated into numerical data, which further enables the robot to search into its predefined database of actions in order to decide what to do next regarding the environmental context. However, in order to use the predefined database of actions, the robot should possess certain knowledge about its existence. One of the ways to achieve this is with the so-called *Semantic Web*, which organises the available data, hence enabling an agent to create knowledge about itself without the need of a large-scale artificial intelligence [31].

Similarly, the work of Waibel et al. [13] describes the RoboEarth database as having a three-layered architecture. The first core layer is a server storing the RoboEarth database comprising global world model, reusable information of objects, and environments and actions linked to semantic information. In addition, the semantic information also provides Web services enabling the robot to conduct basic reasoning. The second layer of the database is comprised of generic components which are a part of the robot's local control software whose main function is to allow the agent to interpret the action recipes embedded in the distributed database. This layer also extends and enhances several of the robot's capabilities including sensing, modelling, reasoning and learning. The third layer implements skills and uses a skill abstraction layer to provide an interface to the robot's specific hardware-dependent functions (Figure 6). In addition to that, the information in RoboEarth is linked on several levels. For example, the semantic description of an object, its properties, its relation to other objects and instructions for manipulation can be linked to the three dimensional model of the object. This provides not only the wiring between the different levels of the robot's architecture involved in the recognition of an object and the execution of the task at hand, but also the connection between the robot's layered architecture and the layered structure of the distributed database.

The work of Juarez [31] illustrates the use of *Semantic Mediawiki* to associate wiki pages with the agent itself and each of its components. Also, the paper argues about the efficiency of such a system and the demands it poses on its users. Furthermore, the author proposes an improved model called *RoboDB*, a system for creating knowledge about robots and their capabilities. This can be achieved mainly by using *ontologies*, which are at the core of knowledge generation in the Semantic Web. Ontologies are used to formally describe a group of objects linked together and the vocabularies used to embed knowledge in this domain. They are also means of representing semantics of documents as well as structuring and defining the metadata terms collected by RoboDB. Ontologies are closely related to the concept of transcoding in new media since they describe different layers of the robotic entity, the relationship between those layers and the properties or attributes that the layered topology may have. Moreover, the use of ontologies enables the performance of semi-automated reasoning. This is important as it increases the level of automation possessed by an agent and hence its ability to perform tasks in a more intelligent and accurate way at a human concept level. On a more profound layer, the protocol behind reasoning with ontologies is called *Description Logic*, which represents a variety of formal knowledge representation languages which describe the concept and techniques of computing the relationships between the different layers in an agent.

Furthermore, Juarez [31] also describes a concept in robotics called *motor schemas* as every action or behaviour the robot exhibits. The motor schemas comply with several different levels of abstraction such as *sensory schemas*, which deal with the low-level input from the robot's sensors and the actuator output, and *perceptory schemas*, which work at high-level abstraction in order to process the information gathered from the sensory schemas. The work of Tang and Parker [32] takes this concept one step further by introducing a variation of its application to swarm robotics in the context of task planning and execution. They extend the capabilities of the old system and create various level schematics dealing with different sensors and communicators within the swarm. Moreover, they also propose a way of labelling the capabilities of the agents within the swarm and then use this to match them within the system in order to construct a task execution plan.

One more example of the layered structure of a robot is described by Sablatnog et al. [33]. The introduced middleware platform Miro there uses three levels of abstraction in order to describe a robot's capabilities: device layer, service layer and class framework layer. The device layer extracts information gathered by the robot's sensors and actuators, the surface layer deals with the robot's interface and the class framework layer deals with the processing algorithms.

However, the previously discussed layered topology can also be applied to a swarm of robots as a whole as shown by Alunni et al [14]. The author describes a certain type of topology where a swarm consists of three levels of communication, two of which are administrative and one is responsible for object detection. The top level of the swarm is called level zero and is addressed as 'the queen'. Its function is to govern and direct the entire swarm and more specifically the second level, which is called 'the worker' (or level one) and is directly under the queen's control. It has the basic functionalities of level zero but is only in charge of a sub-section of the map. The third level (or level two) is called 'the scout' and represents the physical interface of the swarm and the surrounding environment. It is also the only level equipped with sensors for scanning the external world. Each agent is only able to communicate to its 'parent' or 'child' level. The major advantage of using this typology is the increase in scalability of the system. This topology model also simplifies communication in the swarm in case new agents should be added as they would be presented as new layers and would not affect the connections throughout the swarm as a whole.

This shows that the concept of layered architecture of an agent and using contextual information, ontologies and semantics in order to translate the data gathered by different layers in a way that would be understandable throughout the entire system are common practice in robotics and are also applicable to swarm robotics.

EXPECTATIONS

A direct consequence of the new media structure of a swarm robotic system is that it broadens the application areas of robotics. For example, a swarm of robots not only have the structure of a new media object, but it may also be used to create new media interactive installations. The UMwelt-VIRUtopia [34] uses swarm robotics in an interactive installation which is specifically designed to create a dialogue involving space, sound, light and the audience. Its purpose is to bring up questions concerning the way people perceive the combination of robots and sensing stimuli – whether or not the swarm architecture and patterns can be changed through interaction, and overall, if those approaches can be used to reprogramme space and behaviour or even a new experience and a new world. Another possibility would be to use swarm robotic systems as new tools for expression for new media artists and designers, or new ways to build upon work

that has already been created in the field. For instance, an interactive installation and a research project in human robot interaction called *Swarming Heads* is based and built upon Stelarc's project 'Prosthetic head' [35]. In the Swarming Heads installation the robots were capable of detecting humans and certain gestures to which the robots were programmed to respond. However, each robot was designed as an individual and so it happens that, at times, it could behave quite unexpectedly due to the external stimuli it received [36]. Another example of an interactive installation is that of Michael Theodore and Nikolaus Correll called *Swarm Wall* [37]. It was designed to respond to human presence in an interactive way. Moreover, when it 'thinks' it is being ignored, it would try harder to catch the audience's attention. The people behind this installation have also created an active lab where students from various disciplines in engineering and arts collaborate in order to create cutting-edge applications of robotics and artificial intelligence. Their motivation behind this project is that even though the difference between art and science is very significant, the goal of both fields is to discover new things. Furthermore, artistic exploration can help engineers ask questions they would not have otherwise asked [37]. An example of this is Albin's research on musical swarm robot simulation strategies [38]. One of the goals of his work is to determine the legibility of the motion to musical mapping. However, the solutions to the simultaneous localisation and mapping problems encountered in this study may also be used in other scenarios such as search and rescue or exploration tasks [39]. It is highly possible that the problems faced in the study of the robots' motion to music would be different than the ones faced in other more scientifically oriented scenarios. However, implementing those solutions in different missions may significantly enhance the robots' overall performance. This is an example of how the new media structure of a swarm robotic system can widen its range of application possibilities, which is a cause of the emergence of new types of problems whose solutions improve the overall performance of the robotic teams.

Besides their use in music, the work of Bornhofen et al. [40] discusses the use of swarm robotics in the creation of art. An example is Disney's project called *Display Swarm* [41]. It introduces the concept of an innovative display design comprised of a mobile robot swarm of agents called *Pixelbots*. Each agent of the swarm acts as an individual pixel with controllable colour in a dynamic image or animation made entirely by robots (Figure 7a). In addition, the authors have also developed an app for iPad allowing the users to create a drawing and the robots will shift accordingly so as to recreate it. During the development of this project the authors also significantly contributed to the research on collision avoidance [42] and pattern formation in swarm robotics [41]. Another similar example is the work of Kronemann and Hafner [29] discussing *Lumibots* – a swarm of small autonomous robots with high sensitivity and reaction to light. Their purpose is to create images that are ever changing due to the UV-LED at their tail (Figure 7b). Yet again, those are very simple robots programmed to follow the trail of each other. Nevertheless, observing such processes can raise questions that may help enhancing the robots' performance in more diverse applications in formation control, coverage and flocking [43].

In sum, the use of swarm robotics in the field of new media presents the swarm robotic system as a novice tool for the new media artists and designers to express themselves, convey a certain message or build upon famous works of previous authors in the field. However, the new media structure of a swarm robotic system not only expands the application possibilities for a swarm robotic system, but also presents a different environment with different situations, thus significantly enhancing the performance of the system in various types of applications.

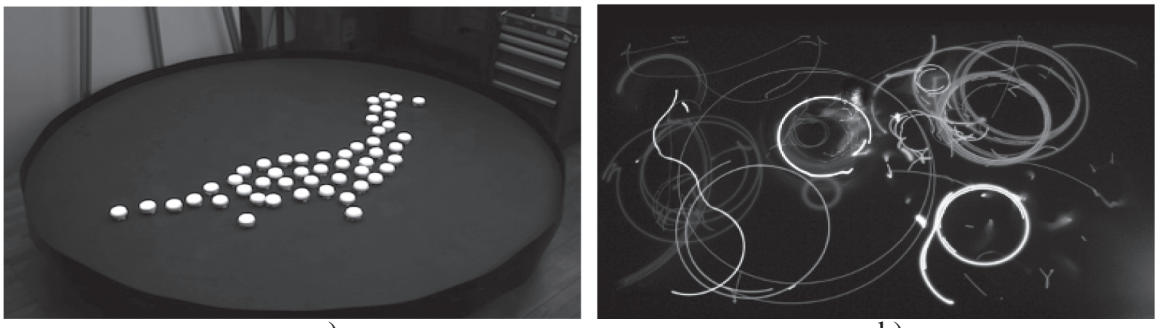

a) b)

Figure 7. The use of swarms in interactive installations: a) Disney's *Display Swarm* [41]; b) Lumibots [29]

CONCLUSIONS

Not only can swarm robotic systems be perceived as new media objects, but also the collaboration between the fields of new media and swarm robotics can be mutually beneficial. A novel approach to perceiving the field of swarm robotics by comparing it to the current vastly expanding field of new media has been presented. The authors of this paper support the notion that through collaboration between swarm robotics engineers and new media artists, novice, cutting-edge applications for both fields can be achieved. While the fields of new media and swarm robotics are generally considered to be relatively different, the aim of this paper is to bridge them and prove their resemblance. With the fulfilment of such concept, the authors believe that the connection between new media and swarm robotics can prove useful and enhance future projects and research into both fields.

ACKNOWLEDGEMENTS

This research is financed by a PhD scholarship (SFRH/BD/73382/2010) from the Portuguese Foundation for Science and Technology, the Institute of Systems and Robotics (ISR-Coimbra) and the Institute of Telecommunications (IT-Covilhã). The authors thank Tom Flint and Emilia Sobolewska for their cooperation and advice.

REFERENCES

1. M. McLuhan, "Understanding Media: The Extensions of Man", McGraw-Hill, London, **1964**.
2. G. Beni, "From swarm intelligence to swarm robotics", Proceedings of the Swarm Robotics Workshop, **2004**, Heidelberg, Germany, pp.1-9.
3. E. Sahin, "Swarm robotics: From sources of inspiration to domains of application" in "Swarm Robotics" (Ed. E. Şahin and W. M. Spears), Springer Berlin Heidelberg, Berlin, **2005**, pp.10-20.
4. A. M. Naghsh, J. Gancet, A. Tanoto and C. Roast, "Analysis and design of human-robot swarm interaction in firefighting", Proceedings of 17th IEEE International Symposium on Robot and Human-Interactive Communication, **2008**, Munich, Germany, pp.255-260.
5. J. M. Hereford and M. A. Siebold, "Bio-inspired search strategies for robot swarms", in "Swarm Robotics, from Biology to Robotics" (Ed. E. M. Martinez), InTech, Rijeka (Croatia), **2010**, Ch. 1.
6. L. Manovich, "The Language of New Media", MIT Press, Cambridge, **2001**.

7. M. Quigley, B. Gerkey, K. Conley, J. Faust, T. Foote, J. Leibs, E. Berger, R. Wheeler and A. Ng, "ROS: An open-source robot operating system", Proceedings of International Conference on Robotics and Automation, **2009**, Kobe, Japan, pp.1-6.
8. Q. Wu, S. Liu, G. Cao and Y. Fei, "Mechatronics design of a modular self-reconfigurable and self-repair robot", Proceedings of IEEE International Conference on Control and Automation, **2007**, Guangzhou, China, pp.2243-2247.
9. Pololu Robotics and Electronics, "Pololu 3pi Robot", **2011,** http://www.pololu.com/catalog/product/975 (Accessed: May 2014).
10. Imperial College Robotics Society, **2011,** http://www.icrobotics.co.uk/wiki/images/thumb/a/a9/Line_follow_simple_flow_chart.png/600px-Line_follow_simple_flow_chart.png (Accessed: May 2014).
11. Pi-robot, "Line-follower.hex", **2010**, http://code.google.com/p/pi-robot/source/browse/trunk/pi-robot/line-follower/line-follower/default/line-follower.hex?r=3 (Accessed: May 2014).
12. D. Calisi, L. Locchi, D. Nardi, G. Randelli and V. A. Ziparo, "Improving search and rescue using contextual information", *Adv. Robot.*, **2009**, *23*, 1199-1216.
13. M. Waibel, M. Beetz, J. Civera, R. D'Andrea, J. Elfring, D. Galvez-Lopez, K. Haussermann, R. Janssen, J. M. M. Montiel, A. Perzylo, B. Schiessle, M. Tenorth, O. Zweigle and R. van de Molengraft, "RoboEarth", *IEEE Robot. Automat.Magaz.*, **2011**, *18*, 69-82.
14. N. Alunni, R. Goloski, A. Haggerty and E. Jones, "Hierarchical Swarm Robotics", Project Report No. GSF113, **2011**, Worcester Polytechnic Institute, Worcester, Great Britain.
15. M. Dorigo, D. Floreano, L. M. Gambardella, F. Mondada, S. Nolfi, T. Baaboura, M. Birattari, M. Bonani, M. Brambilla, A. Brutschy, D. Burnier, A. Campo, A. L. Christensen, A. Decugniere, G. D. Caro, F. Ducatelle, E. Ferrante, A. Foster, J. M. Gonzales, J. Guzzi, V. Longchamp, S. Magnenat, N. Mathews, M. M. de Oca, R. O'Grady, C. Pinciroli, G. Pini, P. Retornaz, J. Roberts, V. Sperati, T. Stirling, A. Stranieri, T. Stutzle, V. Trianni, E. Tuci, A. E. Turgut and F. Vaussard, "Swarmanoid: A novel concept for the study of heterogeneous robotic swarms", *IEEE Robot. Automat. Magaz.*, **2013**, *20*, 60-71.
16. L. E. Navarro-Serment, R. Grabowski, C. J. Paredis and P. K. Khosla, "Modularity in small distributed robots", Proceedings of SPIE Conference on Sensor Fusion and Decentralized Control in Robotic Systems II, **1999**, Boston (MA), USA, pp.297-306.
17. M. S. Couceiro, J. A. T. Machado, R. P. Rocha and N. M. F. Ferreira, "A fuzzified systematic adjustment of the robotic Darwinian PSO", *Robot. Autonomous Syst.*, **2012**, *60*, 1625-1639.
18. H. Wei, Y. Cai, H. Li, D. Li and T. Wang, "Sambot: A self-assembly modular robot for swarm robot", Proceedings of IEEE International Conference on Robotics and Automation, **2010**, Anchorage (AK), USA, pp.66-71.
19. A. R. Ismail, "Immune-inspired self-healing swarm robotic systems," *PhD Thesis*, **2011**, University of York, United Kingdom.
20. S. Kernbach, E. Meister, F. Schlachter, K. Jebens, M. Szymanski, J. Liedke, D. Laneri, L. Winkler, T. Schmick, R. Thenius, P. Corradi and L. Ricotti, "Symbiotic robot organisms: Replicator and Symbrion projects", Proceedings of 8th Workshop on Performance Metrics for Intelligent Systems, **2008**, Gaithersburg (MD), USA, pp.62-69.
21. Y.-S. Dai, M. Hinchey, M. Madhusoodan, J. L. Rash and X. Zou, "A prototype model for self-healing and self-reproduction in swarm robotics system", Proceedings of 2nd IEEE International Symposium on Dependable, Autonomic and Secure Computing, **2006**, Indianapolis (IN), USA, pp.3-10.

22. C. Melhuish, M. Wilso and A. Sendova-Franks, "Patch sorting: Multi-object clustering using minimalist robots" in "Advances in Artificial Life" (Ed. J. Kelemen and P. Sosík), Springer Berlin Heidelberg, Berlin, **2001**, pp.543-552.
23. G. Antonelli, F. Arrichiello and S. Chiaverini, "The NSB control: A behavior-based approach for multi-robot systems", *PALADYN J. Behav. Robot.*, **2010**, *1*, 48-56.
24. J. Pugh and A. Martinoli, "Inspiring and modeling multi-robot search with particle swarm optimization", Proceedings of IEEE Swarm Intelligence Symposium, **2007**, Honolulu (HI), USA, pp.332-339.
25. V. Braitenberg, "Vehicles: Experiments in Synthetic Psychology", MIT Press, Cambridge, **1984**.
26. S. Murata, K. Kakomura and H. Kurokawa, "Toward a scalable modular robotic system: Navigation, docking, and integration of M-TRAN", *IEEE Robot. Automat. Magaz.*, **2007**, *14*, 56-63.
27. M. Rubenstein, C. Ahler and R. Nagpal, "Kilobot: A low cost scalable robot system for collective behaviors", Proceedings of IEEE International Conference on Robotics and Automation, **2012**, St. Paul (MN), USA, pp.3293-3298.
28. J. D. Bjerknes and A. F. T. Winfield, "On fault tolerance and scalability of swarm robotic systems", in "Distributed Autonomous Robotic Systems" (Ed. Martinoli et al.), Springer Berlin Heidelberg, Berlin, **2013**, pp.431-444.
29. M. L. Kronemann and V. V. Hafner, "Lumi-bots: Making emergence graspable in a swarm of robots", Proceedings of 8th ACM Conference on Designing Interactive Systems, **2010**, Aarhus, Denmark, pp.408-411.
30. L. Kunze, T. Roehm and M. Beetz, "Towards semantic robot description languages", Proceedings of IEEE International Conference on Robotics and Automation, **2011**, Shanghai, China, pp.5589-5595.
31. A. Juarez, "Semantic web for robots: Applying semantic web technologies for interoperability between virtual worlds and real robots", *PhD Thesis*, **2012**, Eindhoven University of Technology, Netherlands.
32. F. Tang and L. E. Parker, "A complete methodology for generating multi-robot task solutions using ASyMTRe-D and market-based task allocation", Proceedings of IEEE International Conference on Robotics and Automation, **2007**, Rome, Italy, pp.3351-3358.
33. H. Utz, S. Sablatnog, S. Enderle and G. Kraetzschmar, "Miro — middleware for mobile robot applications", *IEEE Trans. Robot. Automat.*, **2002**, *18*, 493-497.
34. F. D. Wilde, M. Szymanski and A. Kettler, "UMwelt-VIRUtopia: A swarm robotics interactive installation", **2011**, http://frederik-de-wilde.com/projects/umwelt_virutopia/ (Accessed: May 2014).
35. Stelarc, "Prosthetic head", **2003**, http://stelarc.org/?catID=20241 (Accessed: May 2014).
36. D. C. Herath, C. Kroos and Stelarc, "Encounters: From talking heads to swarming heads", Proceedings of 7th ACM/IEEE International Conference on Human-Robot Interaction, **2012**, Boston (MA), USA, p.415.
37. M. Theodore, N. Correll and C. Rowe, "Robotic 'swarm wall' at CU-boulder created through intersection of art and technology", **2012**, http://www.colorado.edu/news/releases/2012/05/30/robotic-%E2%80%98swarm-wall%E2%80%99-cu-boulder-created-through-intersection-art-and (Accessed: May 2014).

38. A. T. Albin, "Musical swarm robot simulation strategies," *MS Thesis*, **2011**, Georgia Institute of Technology, USA.
39. M. W. M. G. Dissanayake, P. Newman, S. Clark, H. F. Durrant-Whyte and M. Csorba, "A solution to the simultaneous localization and map building (SLAM) problem", *IEEE Trans. Robot. Automat.*, **2001**, *17*, 229-241.
40. S. Bornhofen, V. Gardeux and A. Machizaud, "From swarm art toward ecosystem art", *Int. J. Swarm Intelligence Res.*, **2012**, *3*, 1-18.
41. J. Alonso-Mora, A. Breitenmoser, M. Rufli, R. Siegwart and P. Beardsley, "Multi-robot system for artistic pattern formation", Proceedings of IEEE International Conference on Robotics and Automation, **2011**, Shanghai, China, pp.4512-4517.
42. J. Alonso-Mora, A. Breitenmoser, P. Beardsley and R. Siegwart., "Reciprocal collision avoidance for multiple car-like robots", Proceedings of IEEE International Conference on Robotics and Automation, **2012**, St. Paul (MN), USA, pp.360-366.
43. H. Çelikkanat and E. Sahin, "Steering self-organized robot flocks through externally guided individuals", *Neural Comput. Appl.*, **2010**, *19*, 849-865.

Maejo Int. J. Sci. Technol. **2014**, *8*(02), 161-164

Maejo International Journal of Science and Technology

ISSN 1905-7873
Available online at www.mijst.mju.ac.th

Short Communication

Chemical constituents of essential oil of *Senecio bombayensis* flower

Rajesh K. Joshi

Department of Phytochemistry, Regional Medical Research Centre (Indian Council of Medical Research), Belgaum, Karnataka-590 010, India

E-mail: joshirk_natprod@yahoo.com

Received: 27 July 2013 / Accepted: 23 June 2014 / Published: 26 June 2014

Abstract: The essential oil composition of the flower of *Senecio bombayensis* was analysed by gas chromatography and gas chromatography/mass spectrometry. Forty-six compounds representing 98.2% of the total oil were identified. The main constituents are linalool (26.3%), *β*-cedrene (14.5%), *E*-*β*-farnesene (10.8%), 2,5-dimethoxy-p-cymene (7.0%), *E*-*β*-ocimene (5.9%), terpinen-4-ol (5.1%) and *Z*-*β*-ocimene (4.7%). The oil is rich in sesquiterpene hydrocarbons (38.1%), followed by oxygenated monoterpenes (32.3%), monoterpene hydrocarbons (17.7%), oxygenated sesquiterpenes (6.0%) and others (4.1%).

Keywords: *Senecio bombayensis*, Asteraceae, essential oil, terpenes, terpenoids

INTRODUCTION

Senecio bombayensis Balakr. Syn. *S. grahamii* of the family Asteraceae is an erect, herbaceous, much branched herb distributed in the Western Peninsula and Rajputana of India [1] and commonly found amidst of the grasses [2]. The essential oil compositions of endemic species of the genus *Senecio* from this region have been reported. The major components from the essential oil of aerial parts of *S. bombayensis* were reported, with thymol, methyl ether, terpin-4-ol, *α*-copaene, cis-thujone and α-humulene as major constituents [3]. For oil of *S. belgaumensis* (aerial parts), 1-undecanol, *β*-caryophyllene, *p*-cymene, *α*-humulene and *cis*-ocimene were reported as major constituents [4] while from the flower, 1-undecanol, *β*-caryophyllene, caryophyllene oxide and *γ*-terpinene were reported as major constituents [5]. The aim of this study is to investigate the terpenoid profile of the essential oil of the flower of *S. bombayensis*.

MATERIALS AND METHODS

The flowers of *S. bombayensis* were collected at Amboli (c800-m elevation), Maharashtra, India in November 2012. The plant was identified by Dr Harsha Hegde, Scientist of Regional Medical Research Centre, Belgaum (voucher specimen no. RMRC-908). The fresh plant material (200 g) was hydro-distilled for 3 hr using a Clevenger-type apparatus. The oil was dried over anhydrous Na_2SO_4 and stored at -4°C until analysis. The yield of the oil was 0.2% (v/w).

The analysis of the oil was carried out on a Varian 450 gas chromatograph equipped with flame ionisation detector and stationary phase CP Sil-8-CB (30 m × 0.25 mm i.d., 0.25- µm film thickness) under the experimental conditions reported earlier [6, 7]. Nitrogen was used as the carrier gas at a flow rate of 1.0 mL/min. Temperature programming was 60-220° at 3°/min for injector and detector temperatures were 230° and 250°. The injection volume was 1.0 µL of 1% solution in *n*-hexane (split ratio = 1: 50).

The analysis of the oil by gas chromatography-mass spectrometry was carried out on Thermo Scientific Trace Ultra gas chromatograph interfaced with Thermo Scientific ITQ 1100 mass spectrometer. A column fitted with TG-5 (30 m × 0.25 mm i.d., 0.25-µm film thickness) was used and the oven temperature was programmed between 60-220° at 3°/min. using helium as a carrier gas at 1.0 mL/min. The injector temperature was 230° and injection volume was 0.1 µL of 1% solution in *n*-hexane (split ratio = 1:50). The mass spectra were taken at 70 eV with a mass scan range of 40-450 amu. The mass spectrometric parameters were those reported earlier [8, 9].

Identification of constituents were done on the basis of retention indices (determined with reference to homologous series of *n*-alkanes C_8-C_{28}, under identical experimental condition), mass spectra library search (NIST 08 MS Library version 2.0 f and WILEY MS 9th Edition), and by comparison with mass spectra literature data [10]. The relative amounts of individual components were calculated based on gas chromatographic peak area (flame ionisation detector response) without using correction factor.

RESULTS AND DISCUSSION

Forty-six compounds comprising 98.2% of the total oil constituents were characterised and identified according to their mass spectra and their relative retention indices determined on a non-polar stationary phase capillary column. The identified compounds are listed in Table 1 in elution order from the TG-5 column, along with the per cent composition of each component and its retention index. Sesquiterpene hydrocarbons as a major class of components constitute 38.1%, followed by oxygenated monoterpenes (32.3%), monoterpene hydrocarbons (17.7%), oxygenated sesquiterpenes (6.0%) and others (4.1%). The major constituents are linalool (26.3%), *β*-cedrene (14.5%), *E*-*β*-farnesene (10.8%), 2,5-dimethoxy-p-cymene (7.0%), *E*-*β*-ocimene (5.9%), terpinen-4-ol (5.1%) and *Z*-*β*-ocimene (4.7%).

The essential oil profile reported [3] from the aerial parts of *S. bombayensis* in terms of major compounds is somewhat similar to that found this study, although the relative amounts of the components are different. The oxygenated monoterpene and sesquiterpene hydrocarbon contents are greater in flower oil while amounts of monoterpene hydrocarbons, oxygenated sesquiterpenes and other type of compounds are not as great as compared to those present in the oil from the aerial parts. Moreover, the compounds thuja-2,4(10)-diene, 1,3,8-*p*-menthatriene, 4-oxoisophorone, *n*-decanol, *α*-cubebene, *β*-elemene, *γ*-muurolene, 6,11-oxido-acor-4-ene, *α*-acorenol, *α*-muurolol and 7-epi-*α*-eudesmol are not present in the aerial part oil. Further, tricyclene, *α*-phellandrene, *α*-

Table 1. Chemical composition of essential oil of *S. bombayensis* flower

Compound	RI	%	Identification
α-Thujene	906	0.1	RI, MS
α-Pinene	907	0.2	RI, MS
Fenchene	919	0.4	RI, MS
Thuja-2,4 (10)-diene	923	0.8	RI, MS
Sabinene	936	0.2	RI, MS
β-Pinene	939	0.6	RI, MS
Myrcene	949	0.5	RI, MS
p-Cymene	980	0.9	RI, MS
Limonene	984	3.1	RI, MS
Z-*β*-Ocimene	991	4.7	RI, MS
E-*β*-Ocimene	1001	5.9	RI, MS
Linalool	1056	26.3	RI, MS
cis-Thujone	1060	t	RI, MS
1,3,8-*p*-Menthatriene	1080	0.3	RI, MS
4-Oxoisophorone	1107	1.5	RI, MS
Terpinen-4-ol	1144	5.1	RI, MS
α-Terpineol	1161	0.8	RI, MS
trans-Dihydrocarvone	1177	0.1	RI, MS
Thymol, methyl ether	1213	0.7	RI, MS
Carvacrol, methyl ether	1223	1.9	RI, MS
n-Decanol	1279	t	RI, MS
α-Cubebene	1350	t	RI, MS
α-Copaene	1381	t	RI, MS
β-Cubebene	1399	0.3	RI, MS
β-Elemene	1402	0.1	RI, MS
α-Cedrene	1424	0.2	RI, MS
β-Cedrene	1434	14.5	RI, MS
2,5-dimethoxy-*p*-cymene	1441	7.0	RI, MS
α-Humulene	1474	0.1	RI, MS
E-*β*-Farnesene	1478	10.8	RI, MS
γ-Muurolene	1498	1.0	RI, MS
γ-Curcumene	1504	2.7	RI, MS
cis-*β*-Guaiene	1520	0.2	RI, MS
α-Zingiberene	1523	0.3	RI, MS
α-Muurolene	1529	0.2	RI, MS
E,*E*-*α*-Farnesene	1538	0.3	RI, MS
δ-Cadinene	1555	0.4	RI, MS
6,11-oxido-acor-4-ene	1568	0.6	RI, MS
α-Calacorene	1577	0.3	RI, MS
cis-Dihydro occidentalol	1642	1.1	RI, MS
β-Oplopenone	1652	0.6	RI, MS
1,10-di-*epi*-cubenol	1656	1.7	RI, MS
1-*epi*-*γ*-Eudesmol	1669	0.3	RI, MS
α-Acorenol	1673	0.3	RI, MS
α-Muurolol	1688	0.7	RI, MS
7-*epi*-*α*-Eudesmol	1701	0.4	RI, MS
Total identified		98.2	
Monoterpene hydrocarbons		17.7	
Oxygenated monoterpenes		32.3	
Sesquiterpene hydrocarbons		38.1	
Oxygenated sesquiterpenes		6.0	
Others		4.1	

Note: RI = retention index relative to C_8-C_{25} *n*-alkanes on TG-5 column; MS = mass spectrum from NIST and Wiley library and the literature; t = trace (< 0.1%)

terpinene, *γ*-terpinene, naphthalene, *trans*-pulegol, isobornyl acetate, methyl acetate, isomenthyl acetate, eugenol, neryl acetate, *β*-maaliene, *ar*-curcumene, *E*-*β*-ionone, *trans*-*β*-guaiene and caryophyllene oxide are present in the aerial part oil of *S. bombayensis* [3] but not detected in flowers oil. As expected, apart from the phytochemical group of substances typical for a taxon, its chemical profile also depends on the plant part as well as the stage of plant development. The qualitative and quantitative changes in individual or groups of substances, in addition to the disappearance or appearance of some compounds as new constituents, are a common occurrence [11].

ACKNOWLEDGEMENTS

The author is grateful to the Indian Council of Medical Research, New Delhi for providing the necessary facilities. Mr. Mahesh B. Wagarwadi is also thanked for processing the plant material and extracting the oil.

REFERENCES

1. T. Cooke, "The Flora of the Presidency of Bombay", Botanical Survey of India: Sree Saraswaty Press Ltd, Calcutta, **1967**, p.110.
2. S. R. Yadav and M. M. Sardesai, "Flora of Kolhapur District", Rajhuns Printing Press, Kolhapur, **2002**, p.254.
3. R. K. Joshi, "Essential oil of *Senecio bombayensis* from Western Ghats region of India", *Chem. Nat. Compd.*, **2014**, *50*, 382-383.
4. R. K. Joshi, "Chemical composition of *Senecio belgaumensis* from India", *Chem. Nat. Compd.*, **2012**, *47*, 1010-1011.
5. R. K. Joshi, "GC/MS analysis of the essential oil of *Senecio belgaumensis* flowers", *Nat. Prod. Commun.*, **2011**, *6*, 1145-1146.
6. R. K. Joshi, "Chemical constituents and antibacterial property of the essential oil of the roots of *Cyathocline purpurea*", *J. Ethnopharmacol*., **2013**, *145*, 621-625.
7. R. K. Joshi, "Essential oil of flowers of *Anaphalis contorta*, an aromatic and medicinal plant from India", *Nat. Prod. Commun.*, **2013**, *8*, 225-226.
8. R. K. Joshi, "Volatile composition and antimicrobial activity of the essential oil of *Artemisia absinthium* growing in Western Ghats region of North West Karnataka, India", *Pharm. Biol.,* **2013**, *51*, 888-892.
9. R. K. Joshi, "Chemical composition of the essential oil of *Croton bonplandianus* from India", *Nat. Prod. Commun.*, **2014**, *9*, 269-270.
10. R. P. Adams, "Identification of Essential Oil Components by Gas Chromatography/Mass Spectroscopy", Allured Publishing Corporation, Carol Stream (IL), **2007**.
11. C. Franz and J. Novak, "Sources of essential oils", in "Handbook of Essential Oils: Science, Technology, and Applications" (Ed. K. H. C. Baser and G. Buchbauer), CRC Press, New York, **2010**, pp.39-81.

Maejo Int. J. Sci. Technol. **2014**, *8*(02), 165-180

Maejo International Journal of Science and Technology

ISSN 1905-7873
Available online at www.mijst.mju.ac.th

Full Paper

Spring-based tactile array for assistive robotic surgical applications

Safar Pourabbas [1] and Sunita Chauhan [2, *]

[1] Department of Industrial Design, Applied Art School, Tabriz Islamic Art University, Iran
[2] School of Mechanical and Aerospace Engineering, Monash University, Australia

* Corresponding author, e-mail: sunita.chauhan@monash.edu

Received: 27 May 2013 / Accepted: 16 June 2014 / Published: 27 June 2014

Abstract: Tactile sensing is highly desirable for robotic surgery, more specifically minimally invasive surgery, during tissue/organ manipulation. For safe handling and safe grasping of tissues, the two most important aspects are the monitoring and controlling of force and the stiffness information that exists at the sensor-tissue interface. In this study, a spring-based tactile sensing system is used to measure both the interacting forces and stiffness in surgical assistive applications. A differential analysis is performed to obtain the stiffness of a compliant object whilst individual elements of the proposed sensing array experience different deflections when they come in contact with the object. A lumped model formulation for tactile array performance shows that larger differences in stiffness between the force sensing elements provide higher sensitivity in evaluating the object stiffness. For benchmarking of our sensing principle, a macro tactile-sensor array is designed and tested. Different stiffness combinations of the sensing elements show an inverse linear relationship between the stiffness of the object and the output signal magnitude of the stiffness sensing unit. The proposed tactile array based on spring-based stiffness sensing has high potential for safe grasping/handling of the tissues when integrated into the jaws of a surgical grasper during the minimally invasive robotic procedures.

Keywords: tactile sensor, minimally invasive surgery, force sensing, stiffness sensing

INTRODUCTION

Tactile sensing is highly desirable for minimally invasive surgery (MIS) in order to overcome severe reduction in the surgeons' sensory perception during organ/tissue manipulation. Thus, the integration of tactile sensors into surgical instruments has drawn researchers' attention [1, 2]. The

application of a tactile sensing system to the MIS can be categorised as either diagnostic or assistive. Diagnostic tactile systems involve examining dynamically changing tissue characteristics, such as hardness/softness and elasticity, to evaluate abnormal structures and diseased areas. Most of the studies conducted in diagnostic tactile sensing originate from a single sensing principle of resonant vibrations [3-8]. A resonant vibrating sensor consists of two lead zirconate titanate elements, one as a transducer and the other for vibration pickup. Normally, a rod that comes in contact with the tissue is used as a 'feeler' that vibrates at the resonance frequency of the sensor. As a result, the resonance frequency of the sensor-tissue pair changes to a new value and is detected by a phase-shift circuit to be interpreted as a measure of tissue stiffness. Thus, in general, the diagnostic tactile sensing systems using the resonant vibration sensing principle are based on a non-force approach.

An assistive tactile sensing, on the other hand, is aimed for safe grasping and handling of tissues during surgical interventions. Thus, the sensing of grasping and pulling forces during tissue manipulation plays a key role in fulfilling such an objective, and the measured force may be regarded as the most important parameter in the assistive tactile systems for MIS. Initial attempts on assistive tactile feedback were based on the integration of the force sensing elements into the forceps of surgical grasping instruments [9,10]. While measurement of the forces present at the grasper-tissue interface is necessary, it is not sufficient to secure the safe handling of tissues. In this aspect, stiffness sensing can be considered the most favourable parameter since it can represent the firmness of grasping at the tissue-grasper interface. Integrating force and stiffness together would thus result in the safe grasping and handling of tissues.

Attempts on simultaneous sensing of force and stiffness can be categorised as active and passive procedures. Takao et al. [11] developed a multifunctional tactile imager using active sensing approach. For elasticity detection of object, they applied a vibration component to assess the swelling pressure of the sensor skin. Shikida et al. [12] developed a piezo-resistive tactile sensor equipped with a chamber for pneumatic actuation. In these active procedures, besides signal read-out wiring, it was also necessary to supply pressurised air into the sensing site. This requirement adds to the space restriction problem while integrating the tactile sensing arrays into the surgery graspers.

A passive spring-based stiffness sensing approach employs two force sensing elements with different stiffness values in a parallel fashion. When these elements come in contact with a compliant object, they experience different deflections which can be formulated to obtain the stiffness of the object. By making use of such a force-based approach, both the stiffness and forces present at the grasper-tissue interface can be measured simultaneously. Engel et al. [13, 14] developed a multimodal polymer-based sensor skin of which stiffness sensing, as one of the sensing modes, takes benefit of the spring-based principle. The study mainly focused on the multimodality of the sensor skin and had not concentrated in exploring the effectiveness of this principle in accurate evaluation of object stiffness and its applicability to different engineering fields, especially in MIS. Peng et al. [16] developed a spring-based stiffness sensor using micro-electro-mechanical systems (MEMS) technology. They reported measurement results for three different polymers while emphasising only on the fabrication aspects of MEMS capacitive sensors. Dargahi et al. [15] used the stiffness sensing principle for tissue softness measurement. In their study, they made use of polyvinylidene difluoride (which is only suited for dynamic response) instead of strain gauges as the sensing element. However, static and quasi-static responses are equally important as dynamic ones. Thus, for evaluating the effectiveness of assistive tactile sensing based on spring-based stiffness sensing, it is

favourable to use strain gauges as sensing elements. In short, the application of spring-based stiffness sensing to tactile sensing needs a further focused study for targeted MIS applications.

The next important criterion is the optimum positioning of sensors on desired surgical instruments. They can be placed or integrated at various possible locations on a surgical manipulator, such as near the actuation mechanism, on the manipulator shaft and into the grasper. Integrating the sensing elements into the grasper of a surgical manipulator provides the most direct measurement of forces. This is because friction and other disturbances generated from any moving mechanisms do not affect the measurement of sensed data while it could happen at other locations within a surgical system. However, the jaws of the grasper have severe space limitation, which makes the integration very challenging [1]. This requires some micro-fabrication technology for high-resolution sensing arrays while maintaining the magnitude and sensitivity of the desired data. There have been several attempts on the fabrication of force and pressure sensing arrays using MEMS fabrication techniques for applications other than in MIS. For instance, piezo-resistive sensor arrays comprising three axial force sensors with sub-millimetre resolution can be realised [17-20]. Further studies were conducted on understanding the issues of miniaturisation of the sensing arrays as well as various technologies and transduction methods used to improve the tactile sensing capabilities [21, 22]. Such high resolution micro-sensors are desirable for MIS as they can be integrated into a surgical grasper. However, prior to miniaturising, it is necessary to investigate and validate the sensing concept and its effectiveness in evaluating the stiffness of biological objects, along with other determining factors for a specified performance.

In this paper, a spring-based stiffness sensor array for simultaneous sensing of both the grasping force and the object stiffness is investigated. A lumped model is used for the formulation and description of the sensing concept. By making use of a macro tactile array as benchmark, the experimental validation of the sensor design is reported. Also, a detailed analysis of the tactile array fabrication technique and its performance is presented.

SENSOR DESIGN CONCEPT AND FORMULATION

The spring-based stiffness sensing concept is illustrated in Figure 1(a), in which each stiffness sensing unit is represented by a pair of force sensing elements (with different stiffness). These force sensing elements are named as measuring sensing element and reference sensing element with K_m and K_r as their stiffness values respectively. The measured stiffness, K_m, is designed to be smaller than the reference stiffness, K_r, and hence the measuring sensing element experiences higher deflections as compared to the reference element. K_{obj} represents the stiffness of a compliant object to be measured. When a stiffness sensing unit (comprising a pair of measuring and reference sensing elements) is driven either manually or by motor, against an object with stiffness K_{obj}, the measuring and reference sensing elements experience different deflections, represented as Δ-δ_m and Δ-δ_r respectively. The value of the ratio, $R = \Delta\text{-}\delta_m/\Delta\text{-}\delta_r$, is considered to be proportional to the stiffness of the object, K_{obj} [13,14]. This means that when a stiffness sensing unit with a given pair of K_m and K_r values comes in contact with objects with different stiffness, it should record different values for R. Thereby, a correlation between R and K_{obj} can be established and in this way the governing principle not only provides a possibility of measuring tactile forces, but also measures the stiffness of compliant objects. In this study a linear spring model is used to simulate the sensor-tissue interaction and simplify the sensing principle. However, the viscoelastic properties of tissues are not considered at this stage. Our

assumption is supported by an experimental study of Rentschler et al. [23], who studied liver tissue stiffness and considered both the linear model and viscoelastic model in simulating the tissue behaviour. Their study suggests that a linear force-deflection relationship for liver tissue is adequate.

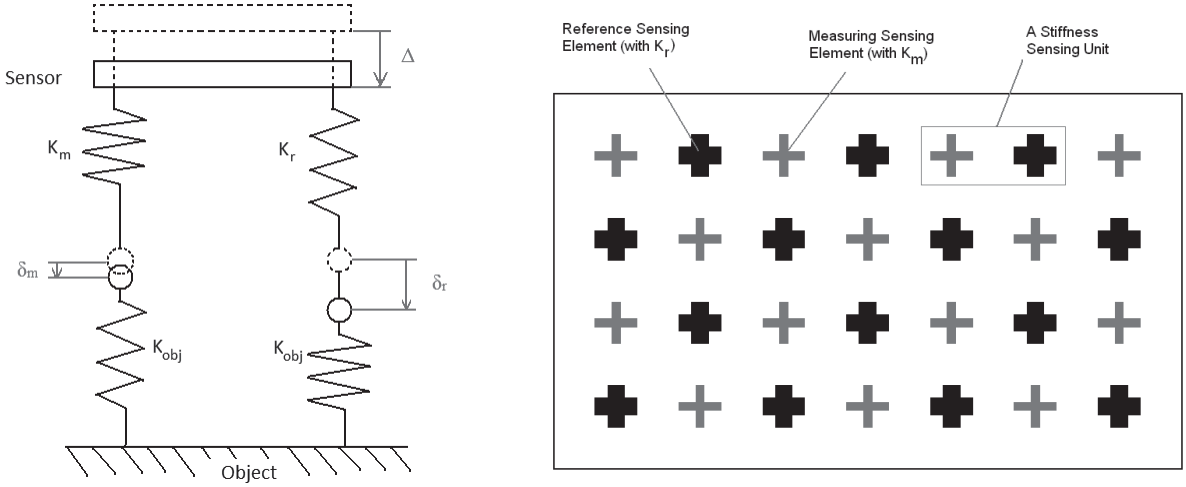

(a) (b)

Figure1. Sensor design concept: (a) a lumped model description of the interaction between a spring-based stiffness sensor and the object; (b) schematic presentation of the proposed force and stiffness tactile sensor array

The sensor prototype can be realised as an array of the force sensing elements with two different stiffness values which are arranged alternately as shown in Figure 1(b). In this Figure, the '+' patterns represent either the measuring or the reference force sensing element while a pair of one measuring and one reference sensing element is considered as a stiffness sensing unit. The force sensing elements, in general, measure the tri-axial forces. Such a sensing system can provide three components of forces as well as the contact stiffness, thereby rendering a four-component vector as its output. For formulating the performance of the proposed sensing array, the lumped model in Figure 1(a) is considered. When the sensor is given a displacement of Δ against the object, the interface between the sensing elements and object will experience δ_m and δ_r displacements for the measuring and reference sensing elements respectively. Thus, the deflections at the measuring and reference sensing elements can be expressed as Δ-δ_m and Δ-δ_r respectively. Based on the force equilibrium in the vertical direction, we can formulate the following relationship:

$$K_{obj}\delta_m = K_m(\Delta - \delta_m) \Rightarrow \quad \delta_m = \frac{K_m}{K_{obj} + K_m}\Delta$$
$$K_{obj}\delta_r = K_r(\Delta - \delta_r) \Rightarrow \quad \delta_r = \frac{K_r}{K_{obj} + K_r}\Delta \qquad (1)$$

Following (1), the ratio of data read by the measuring sensing element to that of the reference sensing element, $R = (\Delta-\delta_m)/(\Delta-\delta_r)$, can be related to the stiffness of sensing elements and object (stiffness-sensing-unit output) as follows:

$$R = \frac{\Delta - \delta_m}{\Delta - \delta_r} = \frac{K_r + K_{obj}}{K_m + K_{obj}} \quad (2)$$

Thus, R is a function of stiffness of the object, K_{obj}, and also stiffness of the force sensing elements, K_m and K_r. Equation (2) can be rearranged in a way that K_{obj} can be explicitly expressed as a function of R while K_m and K_r are constant for a given sensor array:

$$K_{obj} = \frac{K_r - RK_m}{R - 1} \quad (3)$$

Further explanation and finite element method (FEM) analysis of the concept were reported in our earlier work [24], according to which sensor arrays with higher K_r/K_m ratios provide higher sensitivity. Also, it was concluded that a stiffness sensing unit with K_r and K_m higher than the object stiffness, K_{obj}, is required in order to obtain a higher sensitivity for object stiffness.

VALIDATION: MACRO-TACTILE SENSING ARRAY AS A BENCHMARK

This section concentrates on the experimental validation of sensor design concept including both the force measurement and the stiffness evaluation. For this purpose, a macro-tactile array was designed, fabricated, calibrated and tested.

Design of Macro-Tactile Array

The main element of this macro-tactile array is a flexural element as shown in Figure 2(a). In this design, strain gauges are installed at the flexing point of each sensing element. Following the application of an upward force at the tip of a given sensing element (contact area), the tip gets deflected, which is measured as a change in voltage across the poles of the corresponding strain gauge. For pairs of sensing elements with different stiffness, with each pair representing a stiffness sensing unit, the sensing elements are set to have different measuring arm lengths (i.e. $a1 \neq a2$ in Figure 2(a)). As a result, even though such design can only measure one component of the general force vector (the normal component), it can also sense the required stiffness. The macro-tactile array as shown in Figure 2(a), was designed as 2×5 array of sensing elements with a resolution of 4 mm. Sensing elements with longer arms are more compliant as compared to ones with shorter arms. This design was analysed using ANSYS®. Figure 2(b) illustrates an example of the meshed model for sensing elements. The model includes the applied force to the sensing element tip and boundary condition. A 2 N force was applied at the tip upwards while the thickness of the flexing point was made to vary from 0.15 mm to 0.4 mm. The sensor material was made of aluminum, with elastic modulus of 69000 MPa and poison ratio of 0.33. Planar stress condition with a model thickness of 3 mm was assumed. The flexing point arm length was varied from 4 mm to 8 mm. The deflection of the sensor tip and strain at the surface of the flexing point were obtained for all possible combinations. Based on the results, the sensing element with a flexing point of 0.25 mm in thickness was chosen for the sensor fabrication. In such sensing elements fabricated from an aluminum sheet of 3-mm thickness, the strain values for different arm lengths (as stated above) varied between 0.2711-0.6316%. Since the strain gauges are very sensitive devices, such a large range of strain is a considerable value to be measured.

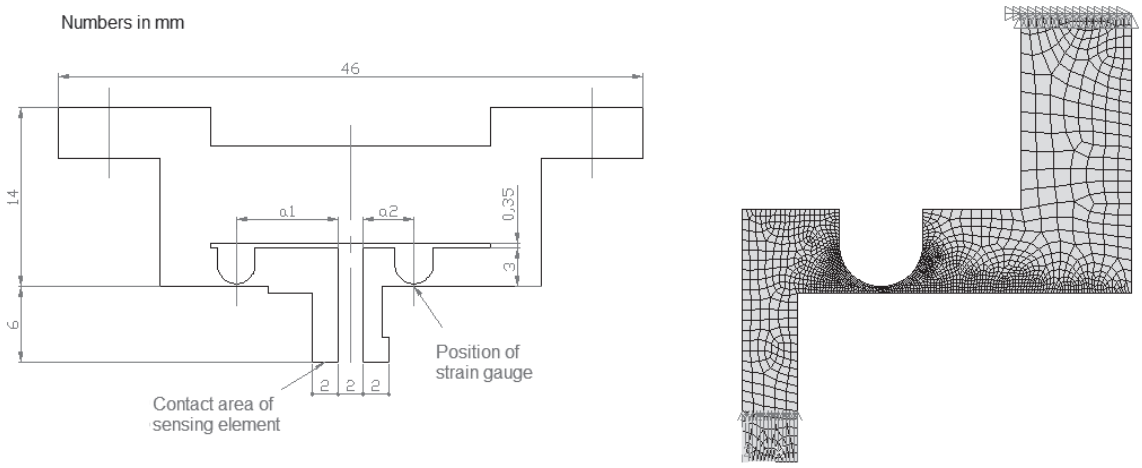

(a) (b)

Figure 2. Design of macro-tactile sensor: (a) side view of a pair of sensing elements with different measuring arms; (b) example of FEM modelling for the macro sensing element

Fabrication of Macro-Tactile Array

Following the FEM analysis of sensing elements, the detailed design of mechanical parts for the macro-tactile set-up was performed. The whole set-up as shown in Figure 3 consists of the sensing elements, along with the holding and clamping parts to fix them in an array. Each sensing element, Figure 3(a), was fabricated by a wire-cut process, resulting in a negligibly small cutting force and the cutting of flexing point in the sensing element being conducted easily. Figure 3(b) shows the overall assembled tactile set-up. It also shows the translational axes of the set-up which were used during the calibration of the sensing elements. Figure 3(c) depicts the completed macro-tactile sensing set-up following the bonding of strain gauges on the sensing elements, along with soldered electrical connections to the measuring circuit.

The amplification and read-out circuitry for the signals from individual sensing elements in the array is presented schematically in Figure 3(c). Each sensing element in the tactile array was set up in the form of a quarter-bridge configuration. Strain gauges of 120 Ω each were bonded on each sensing element beside three other reference strain gauges to form a Wheatstone bridge. A single MOSFET device was used to isolate the connection between the zero line of the power source and the ground. In this way the current flow into the strain gauges prior to read-out signals was prevented. Only at the read-out moment did a signal from a digital output of the DAQ device activate the MOSFET and the current flow into the zero line. The output voltages of the bridges were amplified by AD621 instrumentation amplifier and were acquired by the DAQ device (NI USB 6258) through Lab-View programme. For each of the sensing elements in the tactile array, the programme was set to take 10 samples in every measurement and provide their average as the representative value for that particular measurement.

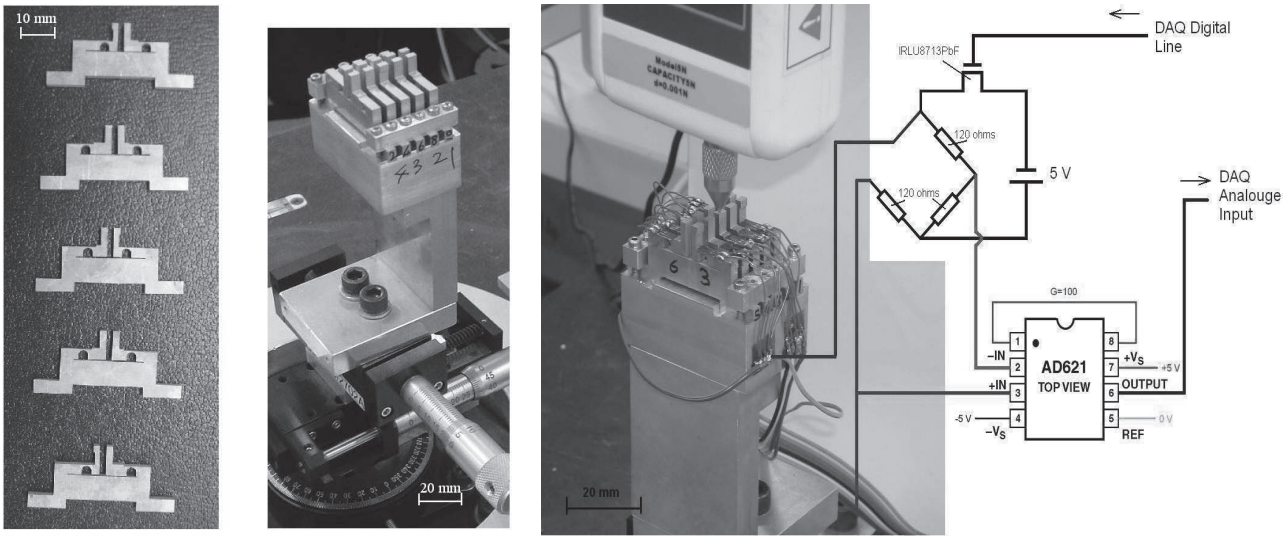

(a) (b) (c)

Figure 3. (a) Tactile sensing elements fabricated by wire-cut process; (b) The whole mechanical set-up after its fabrication and assembly; (c) Macro-tactile set-up after bonding of strain gauges on sensing elements and soldering of connection wires, together with schematic presentation of read-out circuit

Calibration of Macro-Tactile Array

A mechanical set-up using micro-stages for carrying the macro-tactile array was developed for calibration of the sensing elements (whose horizontal axes can be seen in Figure 3(b)). Each sensing element was positioned accurately below the commercial Sauter FH5 force sensor tip (Figure 3(c)). This force sensor itself was installed on the Z-axis and pointed downward. A differential Opto Sigma micro-meter head was installed on the Z-axis to give a 0.5-µm vertical resolution. The commercial force sensor had a maximum 5-N loading capacity and a 0.001-N resolution for measuring the forces. The calibration process was aimed to get both the force deflection relationship and the signal deflection relationship for each sensing element. The Z-axis carrying the commercial force sensor was displaced in increments of 25 µm to a total displacement of 150 µm. This was repeated for all the sensing elements. As the commercial force sensor utilises a stiffness-based load-cell with stiffness of 57.04 N/mm, a part of the applied 150-µm displacement was absorbed by the force sensor itself. By considering the commercial force sensor and the macro-sensing element as two springs in series, the deflection of each sensing element was offset by deducing the commercial force sensor deflection.

Figure 4 shows the calibration graphs for a typical sensing element. For a given sensing element, every measurement was conducted in triplicate and the collected data were averaged to obtain a representative graph. Figure 4(a) shows the applied force (N) versus sensing element deflection (µm). Hence the slope of the graph represents the stiffness of the sensing element, which amounts to 40.1 N/mm in this case. Figure 4(b) depicts a relationship between signal (V) and deflection (µm). As it can be seen, both force deflection and signal deflection exhibit a linear relationship. The resolution of the force measurement was equal to or above 0.01 N and the linearity error was in the range of 1.15-2.32 %.

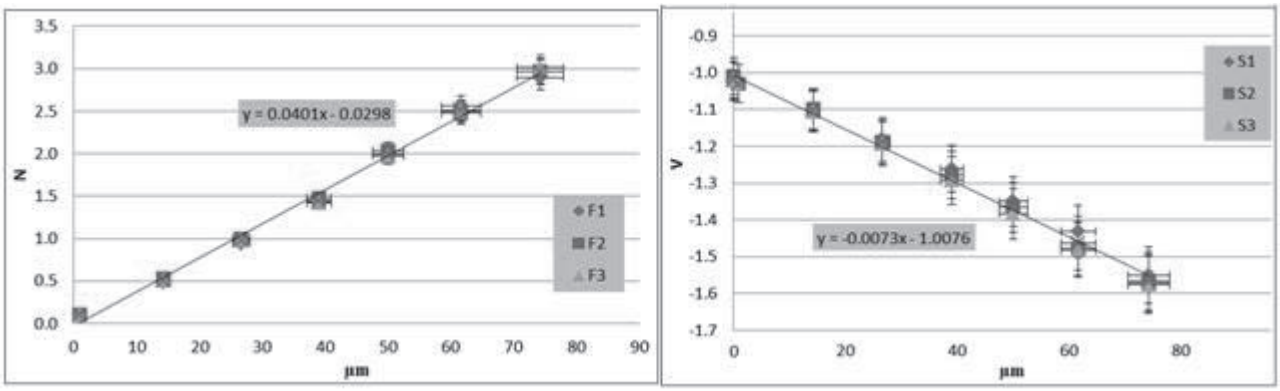

(a) (b)

Figure 4. Example of calibration graphs for sensing elements: (a) force (N) vs deflection (µm); (b) voltage change (V) vs deflection (µm)

Table 1 summarises the calibration results for all sensing elements (element no. 5 not functioning). From this Table, the deflection in each sensing element, Δ, can be calculated as:

$$\Delta = (1/K_v)*(V-V_0) \quad (4)$$

where K_v is the slope of the data represented in Figure 4(b) for any given sensing element, V_0 is the initial signal (zero deflection) and V is the measured signal in volts. Next, by computing the value for Δ, the force applied to the sensing element can be obtained as:

$$F = K* \Delta \quad (5)$$

where K is the stiffness of the corresponding sensing element (the slope of data in Figure 4(a)). Hence by substituting (4) into (5), the force can be calculated as:

$$F = (K/K_v)*(V-V_0) \quad (6)$$

Table 1. Calibration results for all sensing elements

Sensor	*K (N/mm)*	*Maximum deflection (µm)*	*Max. support force (N)*	*Maximum signal change (V)*	*K_v (V/mm)*	*K_v/K (V/N)*	*V_0 (V)*	*Flexing arm length(mm)*
1	40.12	74.3	2.96	0.55	-7.3	-0.182	-1.01	4
2	11.57	118.9	1.41	0.59	-4.9	-0.425	0.08	7
3	14.91	103.7	1.55	0.37	-3.6	-0.239	-0.08	6
4	5.78	143.1	0.85	0.53	-3.8	-0.652	-2.14	8
6	7.35	135.2	1.04	0.63	-4.6	-0.623	0.10	8
7	15.25	108.7	1.78	0.40	-3.7	-0.241	-1.47	5
8	80.38	50.6	4.33	0.47	-9.0	-0.112	0.20	4
9	15.05	105.3	1.64	0.63	-6.0	-0.401	0.05	5
10	9.05	123.5	1.20	0.45	-3.7	-0.408	-0.33	7

The stiffness provided by the sensing elements (*K* column in Table 1) shows a stiffness ratio of 13.9 between the stiffest sensing element (element 8) and the softest (element 4). This was measured while the arm length of the sensing elements was varied from 4 to 8 mm for the stiffest and softest elements respectively. Thus, by changing the length of measuring arm, the stiffness of the sensing elements could be easily tuned. Three of the nine functioning sensing elements (elements 3, 7 and 9) had very close stiffness values within 2.3%. To avoid redundancy in results, one of them was picked to represent the others, making a total of 7 distinct sensing elements. As the maximum deflection (column 3) shows, most of the sensing elements experienced deflections of more than 100 µm. It was assumed that such level of deflection should be sufficient in calibrating the sensing elements. The maximum changes in signal for all the sensing elements, irrespective of the applied deflection and force, showed readings of the same order.

The sensitivity of the sensing elements is one of the key factors for their performance. In this study two different sensitivity parameters are considered: sensitivity of signal output of the sensing elements with respect to force and to deflection. The K_v (V/mm) column in Table 1 lists the former and the K_v/K (V/N) column, the latter. The highest sensitivity of signal to deflection belongs to the stiffest element(s) and the lowest sensitivity, to the softest element(s). During the grasping of tissues, the pressure in the tissue-grasper interface is directly translated as the force applied to the sensing elements. So the sensitivity of signal to applied force is more crucial for the overall performance of the tactile sensors (column K_v/K). Comparing the K_v/K ratio of different sensing elements, it can be observed that the softer sensing element has a higher signal-to-force sensitivity than does the stiffer elements. For example, the softest sensing element's sensitivity of -0.652 V/N was recorded while for the stiffest sensing element it was -0.112 V/N. Contrary to this trend, the K_v sensitivity parameter decreases while moving from the stiffest sensing element to the softest one.

Tissue Phantom Test: Specimen and Test Set-up

Our search for suitable test samples for tissue phantom as applicable to the present study was mainly based upon two criteria: 1) the elasticity/stiffness needs to be demonstrated over a wide range in order to evaluate the stiffness sensing, and 2) the material should be continuum compliant so that multiple-measurement data can be obtained for discerning generic trends over a relevant range of forces and resilience. Various gel-based, soft tissue phantoms were tried initially for their suitability. However, the soft gels tended to break under multi-point force application as desired in this study (within the force/stiffness range as deduced from the literature). Further experiments were carried out using animal tissues acquired directly from wet markets. The large variation of the data observed among different samples as well as sections of the same sample, however, precluded their use as standard test samples at this stage, when the emphasis was more on testing the desired parametric characteristics of the fabricated sensors. The high variation in the test environment could lead to inconclusive outcomes on sensing feasibility over the desired stiffness range. Thus, rubber samples were chosen to resemble a continuum-compliant medium with the main emphasis on their stiffness characteristics that can provide a reasonably acceptable range for the present application. Thereby, a range of commercially available rubber samples with varied stiffness values were used for simulating biological samples. The stiffness tests on these samples were conducted in the laboratory and those with stiffness values comparable to those of the softer sensing elements in Table 1 were selected for validation purpose. However, we understand that the magnitude of stiffness for rubber samples is higher than that for biological tissues.

A mechanical set-up as shown in Figure 5 was arranged for obtaining the stiffness of rubber samples. The individual samples were positioned in the clamping area of a wheeled cart as shown. Vacuum clamping created by a vacuum pump and pneumatic hose was used to hold the sample on the cart. The cart itself was situated on the base plate through four ball-bearings. In this manner, no horizontal force could be created at the interface between the macro-tactile array and rubber sample. Only vertical forces were then applied at the interface of the force sensor and rubber sample. The force sensor was displaced towards the rubber sample in increments of 50 μm and to a maximum distance of 300 μm. For a given sensor's contact area of the size adopted in this study, such magnitude was considered to be sufficient [23]. The contact force was then measured at each step, thereby generating the force-deflection relationship for all the samples. The measuring apparatus and the sensing elements had the same contact area of 2×3 mm^2.

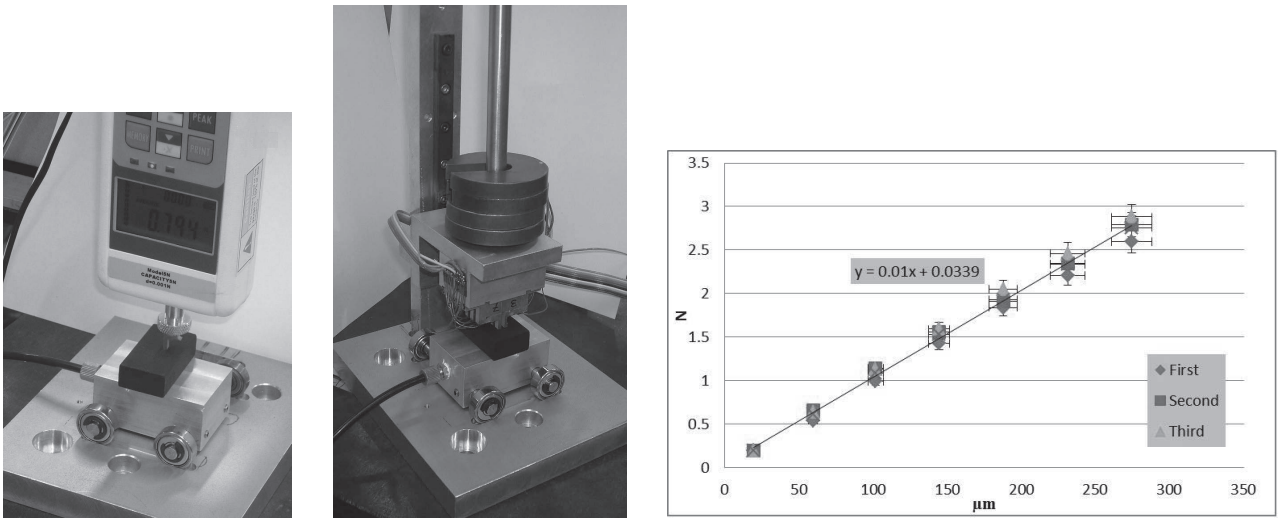

(a) (b) (c)

Figure 5. (a) Mechanical set-up for measuring the stiffness of rubber samples; (b) Evaluating stiffness of rubber samples by macro-tactile array; (c) Force-deflection relationship for one of the rubber samples

Fifteen test samples were used and measurement of the force-deflection relationship for each sample under a quasi-static condition as described above was repeated three times and the averaged readings were plotted to study the force-deflection relationship as shown in Figure 5(c). It was found that the samples have a linear force-deflection relationship and their linearity error varies in the range of 0.72-1.9%. Eight out of fifteen samples were found to have distinct stiffness values. The sample stiffness varies in the range of 2.34-10.01 N/mm, resulting in the stiffness ratio of the stiffest sample to the softest one being ~4.28. This ratio provides an acceptable range of variation in stiffness value of the samples.

Stiffness Evaluation Using Macro-Tactile Array

In Table 1 the stiffness of the tactile sensing elements varies between 5.78-80.384 N/mm. Comparing this range with the one provided by the rubber samples shows that the ratio of stiffness for the stiffest sensing element (highest K_m) when in contact with the softest rubber sample is 40.12/2.34=17.14, while the same ratio for the softest sensing element to the stiffest rubber sample is 5.78/10.01= 0.577. This wide range of ratios of 0.577-17.14 from combinations of the sensing

elements and rubber samples exhibits a stiffness range sufficient for all biological tissues, thus verifying the validity of the sensing concept proposed in this study.

The stiffness of rubber samples was evaluated by the macro-tactile array and was compared with the measurements obtained using a commercial force sensor. For this purpose another mechanical set-up was designed and fabricated as shown in Figure 5(b), where the macro-tactile array was fixed on a linear axis that could be displaced vertically while the rubber sample was fixed on a wheeled cart. Standard weights of 100 g each were used to implement the vertical grasping force in the macro-tactile array and rubber sample interface. These weights were pre-calibrated with a standard commercial force sensor. Each of the eight samples was tested by placing them on the central part of the cart's top surface and was clamped firmly by suction power of the vacuum pump. Next, the macro-tactile probe, installed on the vertical axis, was gently brought in contact with the rubber sample.

The first value of the grasping force between the macro-sensor array and the rubber sample was equal to the weight of the vertical axis itself. This weight included that of the linear carrier, the vertical bar and the macro-tactile array, which all together added up to 3.235 N. At first, the data were collected when there was no loading between the macro-tactile array and rubber sample, i.e. under zero grasping force. In the next loading steps, 100-g weights were added one at a time. The data acquisition programme in the Lab-View was set to collect 10 data samples for every measurement step. The average value, as representative for each measurement attempt, was calculated and saved. Figure 6 shows a typical set of graphs which illustrate the data collected for eight rubber samples during the loading of reference sample with a stiffness of 3.85 N/mm.

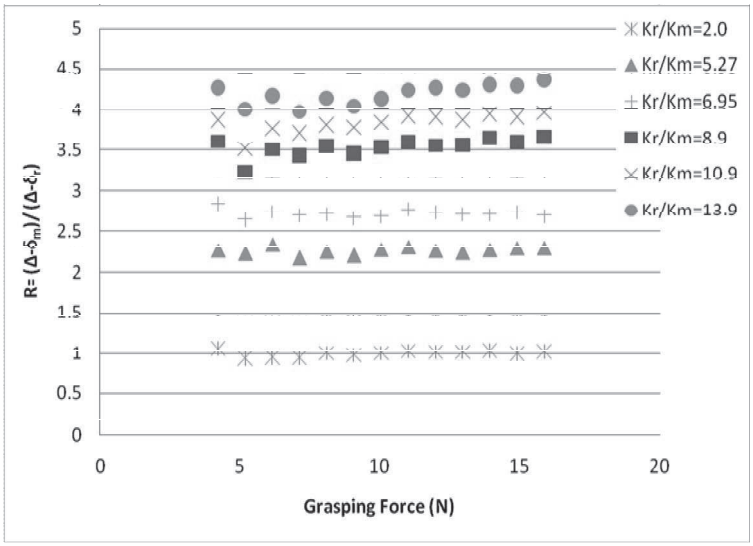

Figure 6. The measuring element deflection (Δ-δ_m) to reference element deflection (Δ-δ_r) ratio, R, for different stiffness combinations of K_r/K_m in the case of rubber sample with 3.85 N/mm of stiffness

The deflection readings of all sensing elements, excluding the stiffest one, were divided by the deflection of the stiffest sensing element to obtain these graphs. In our formulation, K_r is used to represent the stiffness of the stiffest element (the reference element) and K_m is used to represent the stiffness of the rest of the elements (the measuring element). Thus, Figure 6 is an illustration of the ratio of deflection of the measuring elements, Δ-δ_m, to the deflection of the stiffest element, Δ-δ_r. The

horizontal axis is the applied grasping force in Newton and the vertical axis represents the deflection ratio, $R = (\Delta - \delta_m)/(\Delta - \delta_r)$. Since K_r is greater than K_m, the ratio R is always larger than 1.0. As Figure 6 shows, in the case of all K_r/K_m combinations, the R ratio for different values of grasping force mostly remains constant, which implies that the deflection ratio of the tactile sensor array, R, is independent of the change in the grasping force present at the interface of the macro-tactile sensor and the rubber sample.

Validation and Overall Performance of Tactile Array

As eight rubber samples with different stiffness values were chosen to mimic biological tissues with different stiffness, eight different graphs were obtained, of which Figure 6 is a member. A more detailed (discrete points) and conclusive information can be presented in a tabular form as represented in Table 2. Based on such experimental information, the performance of the macro-tactile array in sensing object stiffness not only can be evaluated, but it can also be used to validate the sensing concept itself. As the ratio R mainly remains constant for different values of grasping force, each of these graphs can be viewed as six average values for R. By sorting R values for the softest rubber sample to the stiffest one, a generic trend for variability in R can be obtained.

Table 2. The readings of macro-tactile sensors during the grasping of rubber samples with different stiffness (K_r= 80.38 N/mm)

K_m (N/mm)	K_r/K_m		K_{obj} (N/mm)							
			10.01	7.26	6.28	5.41	4.51	3.85	3.57	2.34
40.12	2.004	K_m/K_{obj}	4.083	5.541	6.470	7.412	9.008	10.610	11.226	17.085
		R	0.977	0.840	0.830	0.822	1.002	1.004	0.942	1.416
15.25	5.270	K_m/K_{obj}	1.552	2.107	2.460	2.818	3.425	4.033	4.268	6.495
		R	1.729	1.816	2.001	2.002	2.174	2.283	2.186	2.461
11.57	6.950	K_m/K_{obj}	1.177	1.597	1.865	2.137	2.597	3.059	3.236	4.926
		R	2.134	2.402	2.410	2.320	2.787	2.757	2.852	3.770
9.05	8.884	K_m/K_{obj}	0.921	1.249	1.459	1.672	2.0312	2.393	2.532	3.853
		R	2.938	3.002	2.993	3.253	3.601	3.536	3.828	4.523
7.35	10.933	K_m/K_{obj}	0.748	1.015	1.186	1.358	1.651	1.944	2.057	3.131
		R	2.827	3.119	3.257	3.407	3.729	4.064	4.225	4.779
5.78	13.905	K_m/K_{obj}	0.588	0.798	0.932	1.068	1.298	1.529	1.617	2.462
		R	3.142	3.324	3.480	3.534	3.994	4.186	4.293	5.451

As the stiffest sensing element in the macro-sensor array was the element no. 8 with 80.38 N/mm of stiffness (Table1), this sensing element was considered as the reference sensing element and the other eight elements softer than this were considered the measuring sensors. As stated earlier, the stiffness of the reference sensing element was represented by K_r and the stiffness of the measuring

elements, by K_m. The values of K_m are listed as the first column in Table 2 and the second column shows all the available combinations of reference versus measuring sensors as K_r/K_m ratios in ascending order. Eight possible combinations for K_r and K_m were expected as there were nine functioning sensors in the sensing array. However, as mentioned earlier, the sensing elements no. 3, 7 and 9 having almost the same stiffness, element no. 7 was chosen to represent others. In this way the total number of K_r/K_m ratios was reduced to six.

The R values versus K_m/K_{obj} variation are listed in Table 2 for a given K_r/K_m combination of the reference element and the measuring element. Thus, this Table can be used for performance analysis of the macro-tactile array. Figure 7 represents K_m/K_{obj} with respect to the corresponding R ratio and each of the six trend lines belongs to one of the K_r/K_m values in Table 2. It can be seen that any increase in K_m/K_{obj} (moving from stiffer samples to softer ones) leads to an increase in R for all the given K_r/K_m combinations in the tactile array. Smaller K_r/K_m ratios (in the vicinity of 2.0) were ignored since they would have insignificant stiffness sensitivity in the evaluation of object stiffness. For K_r/K_m= 5.27 and larger, this sensitivity improves remarkably.

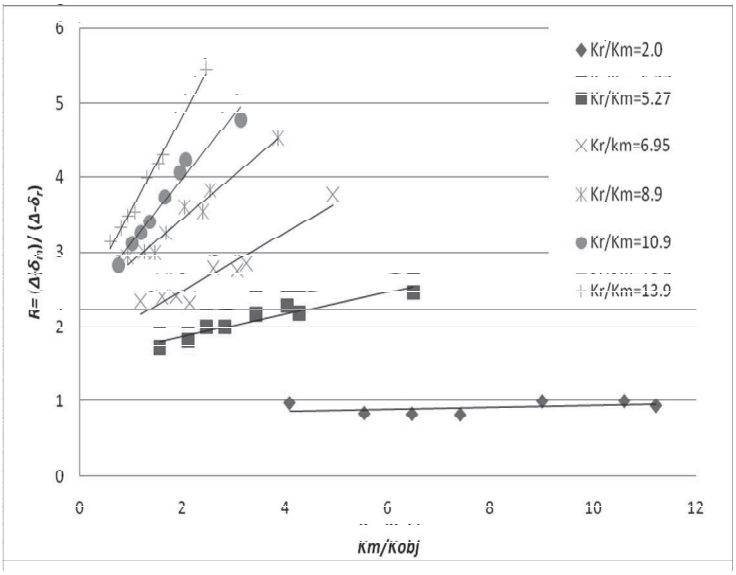

Figure 7. Performance of macro-tactile sensor in grasping rubber samples with different stiffness

For further performance evaluation, both the deflection range and the output signal range in the reference element were monitored. The reference element, being the stiffest, was expected to undergo the lowest deflection among all the sensing elements. Furthermore, the reference element showed the lowest value for K_v/K ratio (Table 1), the sensitivity of signal with respect to the force applied in the sensing element. The maximum signal change for the reference element in grasping the rubber sample was in the range of 0.06-0.14 V, which indicated a deflection range of 28.6-37.2 μm in the reference element. A signal change of up to 0.61V and a deflection of 141.9 μm were experienced in some of the softer elements.

CONCLUSIONS

In an attempt towards the safe handling and grasping of tissues during MIS, a spring-based stiffness sensor is proposed in this paper. The sensor is an array of force sensors made up of two sets of force sensing elements with different stiffness. As a result, both stiffness and force can be

measured simultaneously. A lumped model is used to describe the sensor performance. This model includes the stiffness of two force sensing elements: K_r for the reference and K_m for the measuring force sensing elements. The stiffness, K_{obj}, refers to the object with which the sensing elements come in contact. The ratio of deflection of the measuring sensing element to that of the reference sensing element is defined as the output for the stiffness sensing unit. A lumped model correlates this ratio (K_r and K_m) with K_{obj}. It was found that a higher stiffness difference between the force sensing elements (i.e. higher K_r/K_m) provides a higher sensitivity for the evaluation of object stiffness. Furthermore, larger K_m/K_{obj} values can help to improve the sensitivity of sensing the object stiffness.

A macro-sensor array is fabricated as a benchmark to validate the sensor design concept. Sensing elements with different stiffness are realised by providing different measuring arms in a flexural sensing mechanism. Rubber samples were used to mimic biological tissues during the experiments with stiffness in the range of 2.34-10.01 N/mm. As a result, a wide range of sensor-rubber stiffness combinations was available during the experiments. Such a wide range makes it possible to validate the sensing concept. It was shown that the deflection ratio of the tactile sensor array, R, is independent of changes in the grasping force but when the same K_r/K_m comes in contact with rubber samples with different stiffness and K_m/K_{obj} is subjected to change, the R ratio varies linearly. Thus, it can be concluded that the proposed design concept is capable of evaluating the stiffness of objects. The experimental results suggest that it is favourable to have a high K_r/K_m to improve the sensitivity of the stiffness evaluation while sufficient signal readings and deflection of the reference sensing elements are secured. Otherwise, the results regarding the evaluation of object stiffness might be misleading. So the ratio of K_r/K_m for fabrication of the MEMS should be optimised, which is proposed to be ~10 based on the results of our experiments.

REFERENCES

1. P. Puangmali, K. Althoefer, L. D. Seneviratne, D. Murphy and P. Dasgupta, "State-of-the-art in force and tactile sensing for minimally invasive surgery", *IEEE Sensors J.*, **2008**, *8*, 371-381.
2. P. Valdastri, K. Harada, A. Menciassi, L. Beccai, C. Stefanini, M. Fujie and P. Dario, "Integration of a miniaturised triaxial force sensor in a minimally invasive surgical tool", *IEEE Trans. Biomed. Eng.*, **2006**, *53*, 2397-2400.
3. S. Omata and Y. Terunuma, "New tactile sensor like the human hand and its applications", *Sensors Actuat. A: Phys.*, **1992**, *35*, 9-15.
4. Y. Murayama, C. E. Constantinou and S. Omata, "Development of tactile mapping system for the stiffness characterization of tissue slice using novel tactile sensing technology", *Sensors Actuat. A: Phys.*, **2005**, *120*, 543-549.
5. Y. Murayama, M. Haruta, Y. Hatakeyama, T. Shiina, H. Sakuma, S. Takenoshita, S. Omata and C. E. Constantinou, "Development of a new instrument for examination of stiffness in the breast using haptic sensor technology", *Sensors Actuat. A: Phys.*, **2008**, *143*, 430-438.
6. T. Hemsel, R. Stroop, D. Oliva Uribe and J. Wallaschek, "Resonant vibrating sensors for tactile tissue differentiation", *J. Sound Vibrat.*, **2007**, *308*, 441-446.
7. N. Sakai, M. Tatsuta, H. Yano, H. Iishi and S. Ishiguro, "Diagnosis of the extent of gastric cancers by a new endoscopic ultrasonic tactile sensor", *Gastrointest. Endosc.*, **2000**, *51*, 69-73.

8. S. Omata, Y. Murayama and C. E. Constantinou, "Real time robotic tactile sensor system for the determination of the physical properties of biomaterials", *Sensors Actuat. A: Phys.*, **2004**, *112*, 278-285.
9. N. Kattavenos, B. Lawrenson, T. G. Frank, M. S. Pridham, R. P. Keatch and A. Cuschieri, "Force-sensitive tactile sensor for minimal access surgery", *Minim. Invasive Ther. Allied Technol.*, **2004**, *13*, 42-46.
10. S. Schostek, C. N. Ho, D. Kalanovic and M. O. Schurr, "Artificial tactile sensing in minimally invasive surgery – a new technical approach", *Minim. Invasive Ther. Allied Technol.*, **2006**, *15*, 296-304.
11. H. Takao, M. Yawata, K. Sawada and M. Ishida, "A multifunctional integrated silicon tactile imager with arrays of strain and temperature sensors on single crystal silicon diaphragm", *Sensors Actuat. A: Phys.*, **2010**, *160*, 69-77.
12. M. Shikida, T. Shimizu, K. Sato and K. Itoigawa, "Active tactile sensor for detecting contact force and hardness of an object", *Sensors Actuat. A: Phys.*, **2003**, *103*, 213-218.
13. J. Engel, J. Chen, Z. Fan and C. Liu, "Polymer micromachined multimodal tactile sensors", *Sensors Actuat. A: Phys.*, **2005**, *117*, 50-61.
14. J. Engel, J. Chen and C. Liu, "Development of polyimide flexible tactile sensor skin", *J. Micromech. Microeng.*, **2003**, *13*, 359-366.
15. J. Dargahi, S. Najarian and B. Liu, "Sensitivity analysis of a novel tactile probe for measurement of tissue softness with applications in biomedical robotics", *J. Mater. Process. Technol.*, **2007**, *183*, 176-182.
16. P. Peng, A. S. Sezen, R. Rajamani and A. G. Erdman, "Novel MEMS stiffness sensor for force and elasticity measurements", *Sensors Actuat. A: Phys.*, **2010**, *158*, 10-17.
17. W. L. Jin and C. D. Mote Jr, "Development and calibration of a sub-millimeter three-component force sensor", *Sensors Actuat. A: Phys.*, **1998**, *65*, 89-94.
18. M. Adam, T. Mohacsy, P. Jonas, C. Dücso, E. Vazsonyi and I. Barsony, "CMOS integrated tactile sensor array by porous Si bulk micromachining", *Sensors Actuat. A: Phys.*, **2008**, *142*, 192-195.
19. M. Adam, E. Vazsonyi, I. Barsony, G. Vesarhelyi and C. Dücso, "Three dimensional single crystalline force sensor by porous Si micromachining", *Proc. IEEE Sensors*, **2004**, *1*, 501-504.
20. G. Vasarhelyi, M. Adam, E. Vazsonyi, Z. Vizvary, A. Kis, I. Barsony and C. Dücso, "Characterization of an integrable single-crystalline 3-D tactile sensor", *IEEE Sensors J.*, **2006**, *6*, 928-934.
21. R. S. Dahiya, G. Metta, M. Valle and G. Sandini, "Tactile sensing—from humans to humanoids", *IEEE Trans. Robotics*, **2010**, *26*, 1-20.
22. R. S. Dahiya, D. Cattin, A. Adami, C. Collini, L. Barboni, M. Valle, L. Lorenzelli, R. Oboe, G. Metta and F. Brunetti, "Towards tactile sensing system on chip for robotic applications", *IEEE Sensors J.*, **2011**, *11*, 3216-3226.
23. M. E. Rentschler, J. Dumpert, S. R. Platt, K. Iagnemma, D. Oleynikov and S. M. Farritor, "Modeling, analysis, and experimental study of in vivo wheeled robotic mobility", *IEEE Trans. Robotics*, **2006**, *22*, 308-321.

24. S. P. Abbas, S. Chauhan, S. J. Phee and G. K. Lau, "Real-time, non-vision sensory feedback during minimally invasive surgery", Proceedings of IEEE Region 10 Conference (Tencon 2009), **2009**, Singapore, pp.1-6.

Maejo Int. J. Sci. Technol. **2014**, *8*(02), 181-189

Maejo International Journal of Science and Technology

ISSN 1905-7873
Available online at www.mijst.mju.ac.th

Full Paper

Synthesis of 3-indolylacetamide derivatives and evaluation of their plant growth regulator activity

Weerachai Phutdhawong [1], Chanakan Winyakul [2] and Waya S. Phutdhawong [2,*]

[1] Department of Chemistry, Faculty of Liberal Arts and Science, Kasetsart University, Kampeang Sean Campus, Nakhon Pathom, 73140, Thailand
[2] Department of Chemistry, Faculty of Science, Silpakorn University, Nakhon Pathom, 73000, Thailand
[*] Corresponding author, email: sengwaya@su.ac.th; tel.: +66-34-255797; fax: +66-34-271365

Received: 4 May 2013 / Accepted: 1 July 2014 / Published: 15 July 2014

Abstract: Some 3-indolylacetamide derivatives were synthesised via the coupling of indole-3-acetic acid (IAA) with aminobenzene derivatives and were screened for their plant growth regulator activities on rice seedling. The results show that some of the compounds synthesised possess considerable growth promoting activities in the concentration range of 1.7-0.17 ppm compared to IAA.

Keywords: 3-indolylacetamides, indole-3-acetic acid, plant growth regulator, rice seedling

INTRODUCTION

Plant growth regulators comprise a large number of structurally diverse compounds capable of regulating many biological processes including cell division, differentiation and enlargement, chloroplast development, and senescence. Their wide use in agriculture and plant biotechnology gives them a relevant role in science and technology. Among them, auxins play an important role in plant growth regulation, especially the ability to promote cell division, hasten root initiation, and increase the number and quality of roots [1-4]. The most widely occurring natural auxin, indole-3-acetic acid (IAA), is found in both the free form and the covalently bound via its carboxyl group to yield esters, glycosides and/or peptides of surprising structural diversity [5-6]. Other compounds such as derivatives of indole, naphthalenes, phenoxyacetic acids and some benzoic acids are known as synthetic growth regulators that elicit auxin-type responses in cell growth and cell division [7]. A halogen substituted on the benzene ring of benzoic acid was reported to increase the growth regulator activity quite markedly [8]. In order to access compounds with improved growth regulating properties in comparison to the original auxin and also to establish their structure-activity relationship, the search for potential plant growth regulators is of particular interest. Indoleacetic

acid incorporated with aminobenzene derivatives via an amide link have been brought to our attention since both moieties possess plant growth promoting properties. Thus, they might reinforce the plant growth regulating properties of the resulting compounds. In this study some of such compounds, 3-indolylacetamide derivatives, obtained from indole-3-acetic acid conjugated with aminobenzene derivatives are reported and their plant growth regulator activities on rice seedling are investigated.

SYNTHESIS OF 3-INDOLYLACETAMIDE DERIVATIVES

Discussion

The indole derivatives (**3a-b**, **4a-c**) were synthesised via the coupling of indole-3-acetic acid (**1**) and phenols or aromatic amines at room temperature (Scheme 1). The benzene derivatives (**2a** and **2b**) were prepared [9] for use as starting materials. Reductive amination [10] of *o*-bromoaniline (**2c**) using formaldehyde or benzaldehyde with sodium cyanoborohydride rapidly afforded the corresponding *N*-substituted-*o*-bromoanilines (**2d** and **2e**) in moderate yields. The benzene derivatives were then acylated by indole-3-acetic acid (**1**) at room temperature in the presence of DCC in dichloromethane to give **3a-b** and **4a-c** (Scheme 1). The structures of these synthesised compounds were characterised by their spectral data.

In order to study the structure-activity relationship of the synthesised compounds, *N*-alkylation on the indole ring of compounds **4a-c** was performed using alkyl halides in the presence of potassium hydroxide to give compounds **5a-d** in moderate to high yields (Scheme 2).

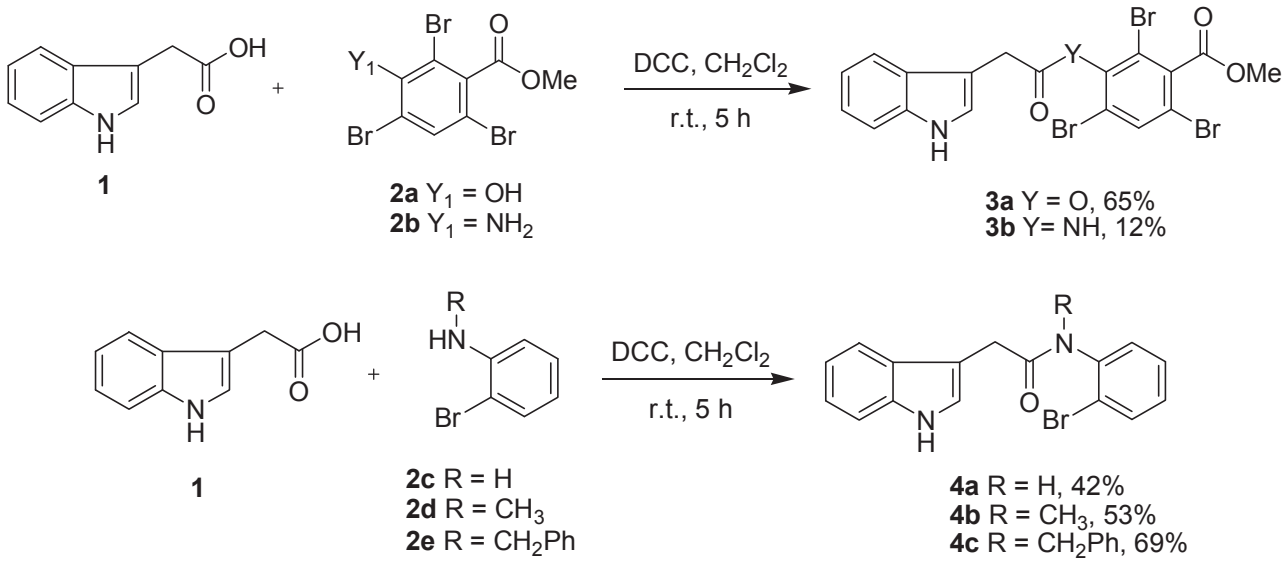

Scheme 1. Preparation of methyl 3-(2-(1*H*-indol-3-yl)acetoxy)-2,4,6-tribromobenzoate (3a) and some 3- indolylacetamides (3b, 4a-c)

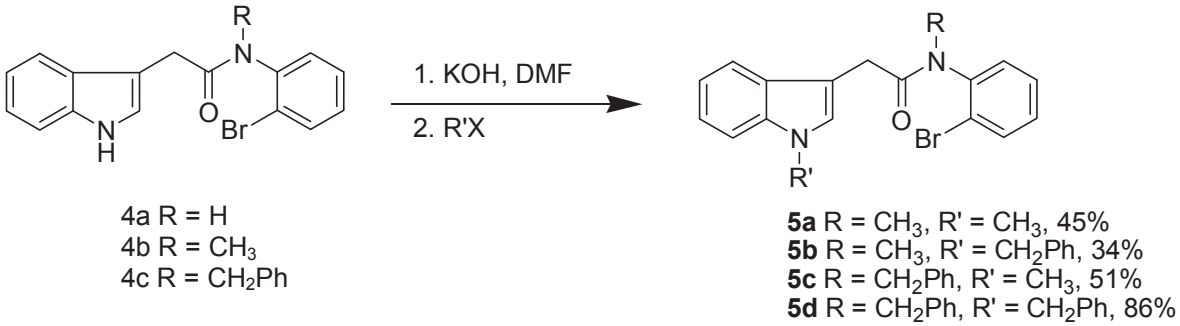

Scheme 2. *N*-alkylation on the indole ring of 3-indolylacetamides (4a-c)

Experimental

Melting points were determined on a Stuart Scientific SMP 2 melting point apparatus and were uncorrected. Infrared spectra were recorded as CH_2Cl_2-film with a Perkin-Elmer GX FT-IR spectrophotometer. 1H- and 13C-NMR spectra were recorded in $CDCl_3$ at 300 MHz for ^1H and 75 MHz for ^{13}C with a Bruker Avance 300 spectrometer. TMS was used as internal standard. Mass spectra were recorded on a Polaris Q or Hewlett Packard 5973 mass spectrometer. Reagents were purchased from Sigma-Aldrich or Fluka and were used as received. All solvents used were of analytical reagent grade except dichloromethane, which was distilled over CaH_2 under nitrogen prior to use.

*Methyl 3-(2-(1H-indol-3-yl)acetoxy)-2,4,6-tribromobenzoate (**3a**)*

N,N'-dicyclohexylcarbodiimide (DCC) (0.10 g, 0.48 mmol) was added to a stirred solution of 3-indolyl acetic acid (0.07 g, 0.40 mmol) and methyl 2,4,6-tribromo-3-hydroxybenzoate (**2a**) (0.20 g, 0.53 mmol) in dry CH_2Cl_2 (5.0 mL) at 0^o under argon atmosphere. The reaction mixture was stirred at room temperature for 24 hr. The precipitate was filtered and washed with CH_2Cl_2. The filtrate was evaporated to give a crude product which was purified by column chromatography (silica gel; hexane: EtOAc = 4:1) to give a yellow oil (0.14 g, 65%): IR 1079, 1095, 1152, 1222, 1271, 1570, 1739, 3407 cm^{-1}; ^1H-NMR δ 3.94 (s, 3H), 4.13 (s, 2H), 7.11-7.22 (m, 3H), 7.33 (d, *J*=7.8 Hz, 1H), 7.66 (d, *J*=7.5 Hz, 1H), 7.76 (s, 1H), 8.20 (br s, 1H, NH) ppm; ^{13}C-NMR δ 30.7, 53.2, 106.6, 111.2, 116.0, 118.8, 119.3, 119.8, 122.3, 123.7, 127.1, 135.5, 136.0, 138.1, 146.2, 165.4, 167.7 ppm; HRES-MS m/z calulated for $[M+H]^+$ $C_{18}H_{12}Br_3NO_4$= 565.8214, found 565.8214.

*General Procedure for Preparation of N,N-Disubstituted-2-(1H-indol-3-yl)acetamides (**3b**, **4a-c**) [11]*

To a solution of 3-indolylacetic acid (1 eq.) and methyl 2,4,6-tribromo-3-aminobenzoate or 2-bromoaniline derivative (1 eq.) in dry CH_2Cl_2 was added *N,N'*-dicyclohexyl carbodiimide (DCC) (1 eq.). The reaction mixture was stirred for 5 hr at room temperature under argon atmosphere. The reaction mixture was then filtered and the filtrate was evaporated *in vacuo* to give the crude product which was purified by column chromatography (silica gel; hexane: EtOAc= 4:1) to afford a pure *N*-(substituted phenyl)-2-(1*H*-indol-3-yl)acetamide**.**

*Methyl 3-(2-(1H-indol-3-yl)acetamido)-2,4,6-tribromobenzoate (**3b**)*

According to the general procedure, treatment of 3-indolylacetic acid (0.090 g, 0.52 mmol) and 2,4,6-tribromo-3-amino benzoate (**2b**) (0.20 g, 0.52 mmol) in dry CH_2Cl_2 (26.0 mL) with DCC (0.10 g, 0.52 mmol) under argon atmosphere gave **3b** as yellow oil (0.034 g, 12%): IR 1010, 1095, 1163, 1624, 1730, 2850, 2925, 3057, 3047 cm^{-1}; ^{1}H-NMR δ 3.69 (s, 3H), 3.78 (s, 2H), 7.10-7.21 (m, 3H), 7.24 (s, 1H), 7.33 (d, *J*=7.5 Hz, 1H), 7.60 (d, *J*=7.8 Hz, 1H), 8.14 (br s, 1H, NH) ppm; ^{13}C-NMR δ 31.1, 51.9, 108.4, 111.2, 111.3, 118.6, 119.7, 119.8, 120.1, 122.1, 122.2, 122.5, 123.0, 123.4, 127.2, 136.1, 172.5 ppm; HRES-MS m/z calculated for $[M+H]^+$ $C_{18}H_{13}Br_3N_2O_3$= 564.8374, found 564.8304.

*N-(2-Bromophenyl)-2-(1H-indol-3-yl)acetamide (**4a**) [11]*

According to the general procedure, treatment of 3-indolylacetic acid (0.10 g, 0.57 mmol) and 2-bromoaniline (**2c**) (0.10 g, 0.58 mmol) in dry CH_2Cl_2 (25.0 mL) with DCC (0.24 g, 1.16 mmol) under argon atmosphere gave **4a** as a yellow solid (0.078 g, 42%), mp. 95.9-104.5^o: IR 1023, 1302, 1434, 1520, 1589, 1672, 3332 cm^{-1}; ^{1}H-NMR δ 3.94 (s, 2H), 6.88 (td, *J*=1,2 Hz, 6.0 Hz, 1H), 7.16 (td, *J*=0.9 Hz, 6.9 Hz, 1H), 7.22-7.28 (m, 3H), 7.35 (dd, *J*=1.2 Hz, 8.1 Hz, 1H), 7.37 (d, *J*=8.1 Hz, 1H), 7.62 (d, *J*=7.8 Hz, 1H), 8.03 (br s, 1H, NH), 8.37 (dd, *J*=1.2 Hz, 8.4 Hz, 1H), 8.51 (br s, 1H, NH) ppm; ^{13}C-NMR δ 34.66, 108.36, 111.39, 113.17, 118.82, 120.31, 121.34, 122.90, 124.01, 124.97, 126.95, 128.22, 132.09, 135.58, 136.45, 169.81 ppm.

*N-(2-Bromophenyl)-N-methyl-2-(1H-indol-3-yl)acetamide (**4b**)*

According to the general procedure, treatment of 3-indolylacetic acid (0.082 g, 0.47 mmol) and *N*-methyl-2-bromoaniline (**2d**) (0.085 g, 0.45 mmol) in dry CH_2Cl_2 (23.0 mL) with DCC (0.10 g, 0.48 mmol) under argon atmosphere gave **4b** as a pale yellow solid (0.083 g, 53%), mp. 152.0-154.5^o: IR 564, 1383, 1432, 1582, 1651, 2882, 3301 cm^{-1}; ^{1}H-NMR δ 3.22 (s, 3H), 3.51 (br s, 1H), 3.52 (br s, 1H), 6.95 (s, 1H), 7.03 (t, *J*=6.9 Hz, 1H), 7.11-7.37 (m, 6H), 7.69 (d, *J*=8.1 Hz, 1H), 8.03 (s, 1H, NH) ppm; ^{13}C-NMR δ 31.1, 36.1, 109.3, 110.9, 119.4, 121.9, 123.0, 124.0, 127.5, 128.8, 129.7, 130.1, 133.8, 135.9, 142.6 ppm; HRES-MS m/z calculated for $[M+H]^+$ $C_{17}H_{16}BrN_2O$= 365.0265, found 365.0260.

*N-(2-Bromophenyl)-N-benzyl-2-(1H-indol-3-yl)acetamide (**4c**)*

According to the general procedure, treatment of 3-indolylacetic acid (0.18 g, 1.01 mmol) and *N*-benzyl-2-bromoaniline (**2e**) (0.27 g, 1.0 mmol) in dry CH_2Cl_2 (50.0 mL) with DCC (0.20 g, 1.0 mmol) under argon atmosphere gave **4c** as a pale yellow solid (0.293 g, 69%), mp. 146.3-148.3^o: IR 699, 1030, 1583, 1654, 2850, 2928, 3059, 3313 cm^{-1}; ^{1}H-NMR δ 3.51 (br s, 1H), 3.52 (br s, 1H), 4.06 (d, *J*=14.4 Hz, 1H), 5.66 (d, *J*=14.4 Hz, 1H), 6.67 (dd, *J*=1.5 Hz, 9.0 Hz, 1H), 6.94 (s, 1H), 7.00-7.37 (m, 11H), 7.68 (dd, *J*=1.5 Hz, 9.0 Hz, 1H), 8.08 (br s, 1H, NH) ppm; ^{13}C-NMR δ 31.3, 51.7, 109.1, 109.6, 110.9, 118.8, 119.3, 121.9, 123.1, 124.0, 127.4, 128.1, 128.2, 128.3, 129.3, 129.7, 131.7, 133.8, 134.136.0, 137.0, 140.8, 171.1 ppm; HRES-MS m/z calculated for $[M+H]^+$ $C_{23}H_{19}BrN_2O$= 441.0578, found 441.0578.

General Procedure for Preparation of N,N-Disubstituted-2-(1-substituted-1H-indol-3-yl)acetamides (5a-d)

A solution of *N,N*-disubstituted-2-(1*H*-indol-3-yl)acetamide (1 eq.) and KOH (1.5 eq.) in DMSO or DMF was stirred for 10-20 min. at room temperature under argon atmosphere. Benzyl chloride or methyl iodide (2 eq.) was then added at 0^o. The reaction mixture was stirred at room temperature for 2-3 hr and then added to ice water and diluted with EtOAc or Et_2O. The organic layer was washed with saturated NaCl solution, dried with anhydrous Na_2SO_4 and concentrated *in vacuo* to give the crude product which was purified by column chromatography (silica gel; hexane: EtOAc = 4:1) to afford a pure *N,N*-disubstituted-2-(1-substituted-1*H*-indol-3-yl)acetamide.

*N-(2-Bromophenyl)-N-methyl-2-(1-methyl-1H-indol-3-yl)acetamide (**5a**)*

According to the general procedure, treatment of *N*-(2-bromophenyl)-2-(1*H*-indol-3-yl)acetamide (**4a**) (0.088 g, 0.27 mmol) and KOH (0.090 g, 1.6 mmol) in DMSO (4.0 mL) with methyl iodide (0.20 g, 1.5 mmol) under argon atmosphere gave (**5a**) [11] as a colourless oil (0.033 g, 45%): IR 129, 740, 1373, 1476, 1583, 1651, 1666, 3024, 3054 cm^{-1}; ^{1}H-NMR δ 3.21 (s, 3H), 3.49 (br s, 1H), 3.50 (br s, 1H), 3.70 (s, 3H), 6.84 (s, 1H), 6.99 (d, J=1.2 Hz, 1H), 7.01 (t, J=1.2 Hz, 1H), 7.14-7.33 (m, 5H), 7.68 (dd, J=1.2 Hz, 7.8 Hz, 1H) ppm; ^{13}C-NMR δ 30.85, 32.57, 36.10, 107.50, 108.96, 118.79, 118.88, 121.39, 123.58, 127.78, 128.78, 129.63, 130.14, 133.80, 136.80, 142.92, 166.10 ppm; HRES-MS m/z calculated for $[M+H]^+$ $C_{18}H_{17}BrN_2O$= 356.0524, found 356.0524.

*N-(2-Bromophenyl)-N-methyl-2-(1-benzyl-1H-indol-3-yl)acetamide (**5b**)*

According to the general procedure, treatment of *N*-(2-bromophenyl)-*N*-methyl-2-(1*H*-indol-3-yl)acetamide (**4b**) (0.24 g, 0.69 mmol) and KOH (0.090 g, 1.6 mmol) in DMF (7.0 mL) with benzyl chloride (0.20 mL, 1.73 mmol) under argon atmosphere gave **5b** as a pale yellow oil (0.10 g, 34%): IR 1464, 1664, 2923 cm^{-1}; ^{1}H-NMR δ 3.21 (s, 3H), 3.51 (br s, 1H), 3.52 (br s, 1H), 5.22 (s, 2H), 6.83 (s, 1H), 7.01 (t, J=0.8 Hz, 1H), 7.02 (d, J=0.8 Hz, 1H), 7.12 (td, J=2.3 Hz, 7.8 Hz, 4H), 7.17-7.27 (m, 5H), 7.39 (d, J=7.8 Hz, 1H), 7.62-7.66 (m, 1H) ppm; ^{13}C-NMR δ 31.2, 36.1, 49.9, 77.2, 108.3, 109.4, 119.1, 119.2, 121.6, 123.6, 126.9, 127.1, 127.5, 128.0, 128.6, 128.7, 129.6, 130.2, 133.8, 136.4, 137.6, 142.8, 171.1 ppm; HRES-MS m/z calculated for $[M+H]^+$ $C_{24}H_{21}BrN_2O$ = 455.0735, found 455.0732.

*N-Benzyl-N-(2-bromophenyl)-2-(1-methyl-1H-indol-3-yl)acetamide (**5c**)*

According to the general procedure, treatment of *N*-(2-bromophenyl)-*N*-benzyl-2-(1*H*-indol-3-yl)acetamide (**4c**) (0.29 g, 0.69 mmol) and KOH (0.10 g, 1.78 mmol) in DMSO (6.0 mL) with methyl iodide (0.10 mL, 1.60 mmol) under argon atmosphere gave **5c** as a yellow oil (0.15 g, 51%): IR 561, 1474, 1583, 1661, 2925, 3058 cm^{-1}; ^{1}H-NMR δ 3.51 (br s, 1H), 3.52 (br s, 1H), 3.70 (s, 3H), 4.05 (d, J=14.4 Hz, 1H), 5.68 (dd, J=1,2 Hz, 7.2 Hz, 1H), 6.85 (S, 1H), 7.01 (t, J=7.2 Hz, 1H), 7.10 (tt, J=1.2 Hz, 1H), 7.16-7.32 (m, 9H), 7.68 (d, J=7.8 Hz, 1H) ppm; ^{13}C-NMR δ 31.2, 32.6, 51.7, 107.4, 107.9, 118.8, 118.9, 121.4, 124.0, 124.9, 127.4, 127.8, 127.9, 128.9, 128.1, 128.3, 129.3, 129.4, 129.6, 133.7, 133.8, 137.0, 140.8, 171.1 ppm; HRES-MS m/z calculated for $[M+H]^+$ $C_24H_{21}BrN_2O$= 455.0735, found 455.0748.

*N-(2-Bromophenyl)-N-benzyl-2-(1-benzyl-1H-indol-3-yl)acetamide (**5d**)*

According to the general procedure, treatment of *N*-(2-bromophenyl)-*N*-benzyl-2-(1*H*-indol-3-yl)acetamide (**4c**) (0.10 g, 0.24 mmol) and KOH (0.020 g, 0.36 mmol) in DMF (2.4 mL) with benzyl chloride (0.060 g, 0.48 mmol) under argon atmosphere gave **5d** as a pale yellow oil (0.10 g, 86%): IR 698, 1585, 1613, 1660, 2849, 2917, 3060 cm^{-1}; ^{1}H-NMR δ 3.51 (br s, 1H), 3.52 (br s, 1H), 4.04 (d, J=14.4 Hz, 1H), 5.22 (s, 2H), 5.64 (d, J=14.4 Hz, 1H), 6.62 (dd, J=1.5 Hz, 7.8 Hz, 1H), 6.86 (s, 1H), 6.98-7.27 (m, 15H), 7.37 (d, J=8.1 Hz, 1H), 7.63 (dd, J=1.2 Hz, 7.8 Hz, 1H) ppm; ^{13}C-NMR δ 31.5, 49.9, 51.6, 108.2, 109.4, 119.1, 121.7, 124.0, 126.9, 127.1, 127.4, 127.5, 128.0, 128.3, 128.6, 129.3, 129.6, 131.7, 133.7, 136.4, 137.0, 137.6, 140.8, 171.0 ppm; HRES-MS m/z calculated for $[M+H]^+$ $C_{30}H_{25}BrN_2O$= 531.1048, found 531.1053.

PLANT GROWTH PROMOTING ACTIVITIES

Methods

The methods of Vargas et al. [12] and Fulbright et al. [13] were employed. Solutions of the synthesised compounds or IAA in 1.7, 0.17, 0.017 and 0.0017 ppm concentrations were prepared in H_2O-MeOH (H_2O: MeOH = 99.95: 0.05). Rice (*Oryza sativa*) seeds were surface disinfected by 70% ethanol for 1 min., followed by 1% sodium hypochlorite for 10 min. They were then washed five times with sterile distilled water. The sterilised seeds were immersed in sterile distilled water overnight. Sterilised Petri dishes (9.0-cm diameter), each containing 20 seeds, were used for germination experiments. Each dish contained two sheets of filter paper which were moistened with 4.0 mL of water or a solution of a test compound. The Petri dishes were placed under artificial light for 24 hr at 30º. The shoot growth and root growth were determined on day 5. Each experiment was done in triplicate.

Results and Discussion

Plant growth regulator activities of the selected compounds (**3a-b, 4a, 4c, 5a-b and 5d**) are shown in Table 1 and Figures 1-2 in comparison to the commercial plant growth regulator (IAA). Compounds **3b** and **5b** exhibit higher activities than IAA on both shoot and root growth in the concentration range of 1.7-0.017 ppm, while compounds **3b**, **5b** and **5d** exhibit better activities than IAA on root growth in the same range of concentration. Maximum shoot growth was observed in the presence of **4a** at the concentration of 1.7 ppm and maximum root growth was observed in the presence of **5b** at the same concentration.

From Table 1, it can be seen that the methyl ester group and a number of bromine atoms on the benzene ring have no effect on the growth promoting activities. Compounds **3a** and **3b** show slight difference in activities on both root and shoot while the substituents on the nitrogens of acetamide and indole affect the activities. Compound **4a**, which has no *N*-substituents, shows better growth promoting activities at low concentration than compound **4c,** which carries a benzyl group at the amide nitrogen. However, compound **4c** can stimulate the root growth at high concentration (1.7 ppm). The benzyl substituent on the indole nitrogen (**5d**) shows fluctuation in activities compared to compound **4c**. The methyl substituent on the acetamide nitrogen (**5a**) imparts better growth promoting activities on both shoot and root than the benzyl substituent (**5b**) in the concentration range of 1.7-0.17 ppm while the reverse is the case in the concentration range of 0.017-0.0017 ppm.

Table 1. Effect of 3-indolylacetamide derivatives on the shoot growth and root growth of *O. sativa* seedlings

Compound	% Germination	1.7 ppm		0.17 ppm		0.017 ppm		0.0017 ppm	
		SL	RL	SL	RL	SL	RL	SL	RL
H_2O	100	3.51±0.57	1.69±0.99	3.51±0.57	1.69±0.99	3.51±0.57	1.69±0.99	3.51±0.57	1.69±0.99
IAA	100	4.09±0.95	6.03±1.69	3.87±0.79	3.07±1.75	2.80±0.69	2.45±0.75	4.14±0.53	3.64±1.89
3a	100	4.27±0.48	6.84±2.72	3.24±0.81	2.52±1.14	4.12±1.15	2.17±1.07	3.67±0.40	3.98±1.29
3b	100	4.19±0.48	6.42±2.29	4.20±0.65	3.73±1.22	3.70±0.71	3.40±1.66	4.07±0.61	3.55±1.03
4a	100	4.38±0.53	4.63±2.17	3.77±0.57	4.04±1.48	3.90±0.75	3.52±1.62	3.93±0.70	4.0±1.45
4c	100	3.64±0.71	6.89±1.15	3.64±0.71	2.60±1.55	3.78±0.74	3.12±0.96	3.59±0.60	2.97±1.24
5a	100	4.12±1.15	5.49±2.19	3.52±0.71	2.69±1.17	4.28±0.48	3.66±1.32	3.85±0.66	3.25±1.11
5b	100	4.16±0.48	7.15±2.32	4.10±0.61	3.82±1.24	4.16±0.48	2.70±1.64	3.86±0.97	3.20±1.68
5d	100	4.07±0.61	6.71±1.84	3.95±0.50	3.79±2.04	4.04±0.95	2.61±1.60	3.49±0.94	2.71±1.59

Note: SL = shoot length in cm; RL = root length in cm

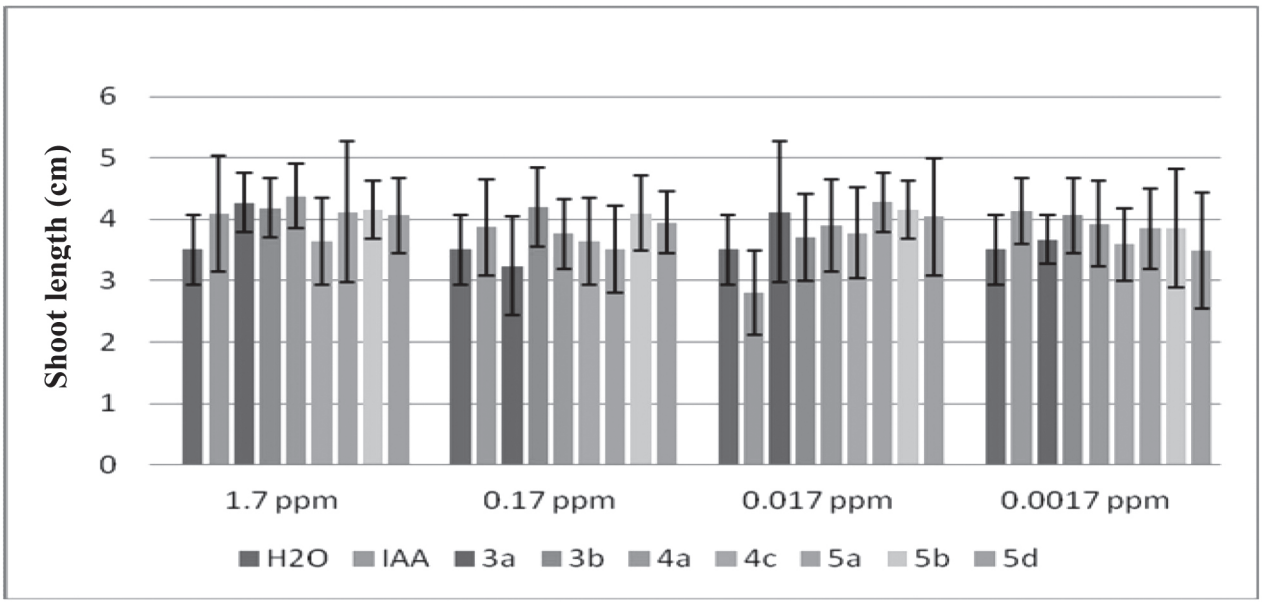

Figure 1. Comparative effects of IAA and 3-indolylacetamide derivatives on shoot growth of rice seedling

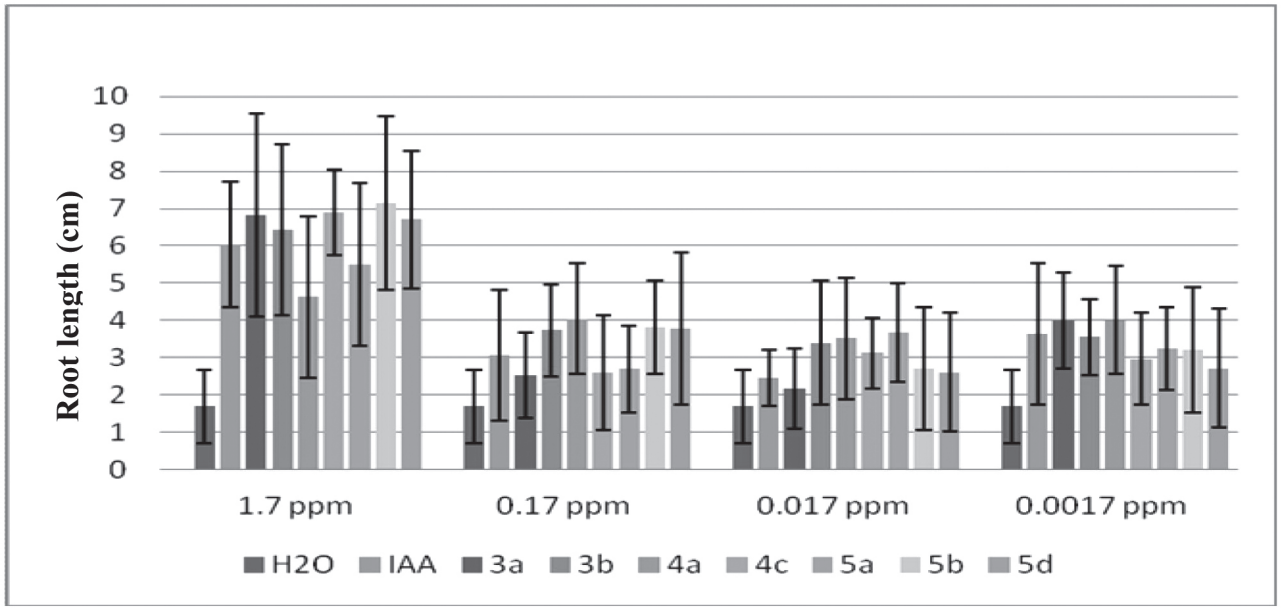

Figure 2. Comparative effects of IAA and 3-indolylacetamide derivatives on root growth of rice seedling

CONCLUSIONS

Although the plant growth regulator activities of some of the synthesised 3-indolylacetamide derivatives are higher than those of IAA in the concentration range of 1.7-0.017 ppm, the overall activities of the derivatives are considered comparable to those of IAA.

ACKNOWLEDGEMENTS

We are grateful to the Department of Chemistry, Faculty of Science, Silpakorn University and the Thailand Toray Science Foundation for financial support. We also thank Kasetsart University Research and Development Institute and the National Research Council of Thailand for financial support to W.P.

REFERENCES

1. K. V. Thimann and J. B. Koepfli, "Identity of the growth-promoting and root-forming substances of plants", *Nature*, **1935**, *135*, 101-102.
2. B. E. Haissig, T. D. Davis, "A historical evaluation of adventitious rooting research to 1993", in "Biology of Adventitious Root Formation" (Ed. T. D. Davis and B. E. Haissig), Plenum Press, New York, **1994**, pp.275-331.
3. H. T. Hartmann, D. E. Kestar, F. T. Davies and R. L. Geneve, "Plant Propagation: Principles and Practices", 6th Edn., Prentice Hall, Englewood Cliffs (N.J.), **1996**, p.770.
4. D. W. Armstrong, Y. S. Liu, L. He, K. H. Ekborg-Ott, C. L. Barnes and C. F. Hammer, "Potent enantioselective auxin: Indole-3-succinic acid", *J. Agric. Food Chem*., **2002**, *50*, 473-476.
5. M. Šoškić, B. Klaić, V. Magnus and A. Sabljić, "Quantitative structure-activity relationships for *N*-(indol-3-ylacetyl)amino acids used as sources of auxin in plant tissue culture", *Plant Growth Reg*., **1995**, *16*, 141-152.
6. S. Jiang, J. Gao and L. Han, "Synthesis and biological activity of *N*-acyl-*O*-Indolylalkyl ethanolamines", *Biosci. Biotechnol. Biochem*., **2011**, *75*, 768-770.
7. L. M. Srivastava, "Plant Growth and Development: Hormones and Environment", Academic Press, Oxford, **2002**.
8. C. E. Minarik, D. Ready, A. G. Norman, H. E. Thomson and J. Fred Owings, Jr., "New growth-regulating compounds II. Substituted benzoic acids", *Bot. Gazette*, **1951**, *113*, 135-147.
9. A. I. Vogel, A. R. Tatchell, B. S. Furnis, A. J. Hanaford and P. N. G. Smith, "Vogel's Textbook of Practical Organic Chemistry", 5th Edn., Longman Scientific and Technical, Essex, **1989**.
10. R. F. Borch, M. D. Bernstein and H. D. Durst, "Cyanohydridoborate anion as a selective reducing agent", *J. Amer. Chem. Soc.*, **1971**, *93*, 2897-2904.
11. J. G. Avila-Zárraga, A. Lujan-Montelongo, A. Covarrubias-Zúniga and M. Romero- Ortega, "New Heck coupling strategies for the synthesis of paullone and dimethyl paullone" *Tetrahedron Lett.*, **2006**, *47*, 7987-7989.
12. L. K. Vargas, B. B. Lisboa, G. Schlindwein, C. E. Granada, A. Giongo, A. Beneduzi and L. M. P. Passaglia, "Occurrence of plant growth-promoting traits in clover-modulating rhizobia strains isolated from different soils in Rio Grande do Sul State", *Rev. Bras. Ci. Solo*, **2009,** *33*, 1227-1235.
13. T. E. Fulbright, K. S. Flenniken and G. L. Waggerman, "Methods of enhancing germination of Anacua seeds", *J. Range Manage.*, **1986**, *39*, 450-453.

Maejo Int. J. Sci. Technol. **2014**, *8*(02), 190-197

Maejo International Journal of Science and Technology

ISSN 1905-7873
Available online at www.mijst.mju.ac.th

Full Paper

Suitable criteria for drought-tolerant peach rootstocks grown in northern Thailand

Siriwan Boonanunt [1, 3], Krisana Krisanapook [1, 3, *], Unaroj Boonprakob [1, 3], Aussanee Pichakum [2] and Lop Phavaphutanon [1, 3]

[1] Department of Horticulture, Faculty of Agriculture at Kamphaeng Saen, Kasetsart University, Kamphaeng Saen Campus, Nakhon Pathom, Thailand

[2] Department of Plant Science, Faculty of Science, Mahidol University, Bangkok, Thailand

[3] Centre for Advanced Agriculture and Food Research, Kasetsart University, Bangkok, Thailand

* Corresponding author, e-mail: krisana.k@ku.ac.th

Received: 15 October 2013 / Accepted: 15 July 2014 / Published: 28 July 2014

Abstract: Peach growing in rainfed areas in the highlands of northern Thailand is suffering from drought conditions, which are becoming increasingly severe every year. Drought tolerant rootstocks provide one option to alleviate this problem. Thus, this study aims to find some guides for selecting drought-tolerant peach rootstocks. The local peach variety 'Red Angkhang' and 3 new hybrid cultivars '42047T1', '43060T1' and '43087T2' were used in this study. Two-year-old peach seedlings of each cultivar were grown in pots and divided into 2 groups. The first group consisted of well-watered plants (100% of evapotranspiration) and the second group consisted of water-deficit plants which received only 30% of evapotranspiration for 5 weeks. After that, the water-deficit peach seedlings were re-watered in the same manner as the well-watered plants for 2 weeks. Water stress led to a decrease in growth in all cultivars. The water-deficit tolerance of Red Angkhang was comparable to that of the new hybrid 42047T1, but the two cultivars used different mechanisms: Red Angkhang responded to water deficit by increasing only the root dry weight while hybrid 42047T1 also accumulated sorbitol. The 43060T1 and 43087T2 hybrids were less tolerant to water deficit and responded by decreasing the root dry weight with no sorbitol accumulation. From this study, we suggest that root dry weight and sorbitol concentration can be used to screen drought tolerant rootstocks in peach in northern Thailand.

Keywords: peach rootstock, *Prunus persica*, drought tolerance, root growth, sorbitol accumulation

INTRODUCTION

Peach (*Prunus persica* (L.) Batsch) has been grown in the highlands of northern Thailand for many decades and some varieties have adapted to the local environment. However, the highland areas are now encountering drought conditions which may become more severe in the near future. The accumulation of solutes as a result of osmotic adjustment is one line of plant response to water stress. In Rosaceae fruit trees such as apple, pear and peach, sorbitol is an important translocated sugar and several studies have reported the relationship between concentration of sorbitol and stress tolerance [1, 2]. In *Prunus* spp., sorbitol is the main solute reported to accumulate during stress periods [3]. Kanayama et al. [4] found that sorbitol accumulation in apple, peach, Japanese pear and European pear is enhanced by stress. Soluble sugars have also been reported to be involved in stress tolerance in maize and wheat [5]. In apple trees (*Malus domestica*) the water deficit affects the production of roots in varying degrees depending on the rootstocks and it was suggested that drought tolerance can be determined by root dry matter production [6]. In Thailand the breeding programme for drought-tolerant peach rootstocks commenced in 2002 [7] and there are currently some promising new hybrid cultivars. However, their mechanisms of drought tolerance are not well understood. Since sorbitol, soluble sugars and the production of roots have been reported to be involved in stress in Rosaceae fruit trees, this study aims to investigate whether these traits can be used as guides for screening drought-tolerant peach rootstocks grown in northern Thailand. The findings from this study may be useful for a peach breeding programme.

MATERIALS AND METHODS

Plant Materials and Experimental Design

This study was conducted at the Royal Angkhang Agricultural Station, Chiang Mai province (19°5'4.633"N, 99°0'2.537"E). The experiment was designed as a 2x4 factorial using a completely randomised design with 2 levels of irrigation and 4 peach cultivars, namely Red Angkhang (local cultivar) and there new hybrid cultivars from the rootstock breeding programme of the Royal Project Foundation, viz. '43060T1' (AK1-1-1-35 x Fla 84-18C), '42047T1' (open pollination of AK1-1-14-35) and '43087T2' (open pollination of AK 1-1-12-35). Two-year-old peach seedlings were planted in pots (15-inch diameter) with 2 replications (trees) per treatment and placed under a plastic roof. The field experiment started in April-May, 2011 (hot and dry season). The average temperature and relative humidity were 21º and 85% respectively. Before irrigation, the plants were weighed to determine the daily evapotranspiration for 2 weeks using a method modified from Rieger et al. [8]: the average daily evapotranspiration was found to be 1,100 mL/tree. Then the plants were divided into 2 groups. To each plant in the first group, the well-watered plants used as control group, 1,100 mL of water (100% of evapotranspiration) was applied daily, whereas each plant in the second group, the water-deficit plants, received a daily dose of only 330 mL (30% of evapotranspiration) for 5 weeks. After that, the water-deficit seedlings were watered everyday for 2 weeks with the same amount of water as the control seedlings.

Sampling, Shoot and Root Variables

Sampling was taken at 3 stages: the first day and the last day of water-deficit treatment and 2 weeks after full watering. Two leaf discs (1 cm^2) were punched out from the fourth or the fifth leaf from the tip for sugar concentration determination.

In each plant, 4 shoots, each measuring 20 cm in length, were tagged and their increased length was monitored on the first and last day of water deficit and 2 weeks after full watering. Each plant was then collected and separated into shoot and root. The shoot was weighed, then kept at 80º for 72 hr or until dry and the dry mass was determined. The roots were washed and separated into coarse roots (≥2 mm in diameter) and fine roots (<2 mm in diameter) before drying at 80º for 72 hr or until dry and the dry mass was determined.

Sugar Analysis

Fresh leaf samples were used for determination of soluble sugars (sucrose, glucose and fructose) and sorbitol. Briefly, 0.05 g of each sample was cooled in liquid nitrogen and finely crushed in a precooled eppendorf tube with a small pestle. Then 1 ml of nanopure water was added and the sample was sonicated for 15 min. After centrifugation at 12,000 rpm for 15 min., the supernatant was collected, filtered through a 0.45-μm filter and stored at -20^{o} for further analysis. The total sugars extracted from the sample were analysed by high-performance liquid chromatography using a Shimadzu chromatograph coupled with refractive index detector and a method modified from that of Karkacier et al. [10]. The analytical column was a CABOSep coregel-87C equipped with a guard column. The mobile phase was deionised water, the injection volume was 50 μL and the flow rate was 0.6 mL min^{-1}.

Statistical Analysis

Analysis of variance (ANOVA) was performed to test for statistical differences among rootstocks and water treatment regimes. Cluster analysis was performed in order to group these rootstocks based on their drought response.

RESULTS AND DISCUSSION

The shoot length, shoot fresh weight and shoot dry weight of water-deficit plants were less than those of the well-watered plants although the shoot dry weight shows no significant difference in all cultivars (Tables 1 and 2). Similar results were also reported for a *Eucalyptus* tree species [11] and Imperial Gala apple trees [12] when subjected to water stress.

At the end of week 5, water stress affected root growth in each cultivar, although in a different manner. The root dry weight of the water-deficit plants decreased in cultivars 43060T1 and 43087T2, whereas it increased in Red Angkhang and 42047T1. The coarse root weight in the well-watered plants increased slightly in Red Angkhang and 42047T1 while the fine root weight of 42047T1 and Red Angkhang increased by 50.20% and 1.89% respectively (Figure 1 and Table 2).

The study on drought tolerance of rootstocks has focused on the root system. Commercial apple rootstocks M26 and MM111 have been reported to be drought-tolerant rootstocks [9]. One suggestion is that drought tolerance, at least in part, is determined by root dry matter production [13], which is in agreement with the work of Atkinson et al. [6] with apple plants (*Malus domestica*). They used the new rootstock selections, AR295-6, AR360-19 and AR628-2, which produced fewer fine and coarse roots in response to water deficit, whereas in rootstocks AR69-7 and M26, root production increased. This suggests that water deficit influences the production of coarse and fine roots differently and that the response varies with rootstocks. An increase in root growth might produce a greater root surface area leading to an increase in water absorption. Since roots are the only means of acquiring water from the soil, their growth, density and size

Table 1. Shoot fresh weight and shoot dry weight in peach seedlings during water deficit and recovery periods

Cultivar	Treatment	Shoot fresh weight (g)			Shoot dry weight (g)		
		Day beginning	Last day of 5th week	Last day of 2-week recovery	Day beginning	Last day of 5th week	Last day of 2-week recovery
Red Angkhang	Full watering	210.0	300.1	456.0	99.6	134	215.2
	Water deficit		291.6	240.9		129.3	129.9
43060 T1	Full watering	150.5	305.1	351.8	70.6	140.5	170.5
	Water deficit		262.7	337.5		134.3	169
43087 T2	Full watering	204.5	320.3	425.0	95.9	154.7	206.4
	Water deficit		249.4	264.0		141.8	139.9
42047 T1	Full watering	247.5	326.1	369.4	122.25	156.3	182.6
	Water deficit		278.9	252.1		159	128.9
Significance:							
Cultivar		ns[1]	ns	ns	ns	ns	ns
Water deficit		-	*	*	-	ns	ns
Interaction		-	ns	ns	-	ns	ns
CV		26.1	13.9	16.3	33.89	17.4	11.5

Note: ns = not significant; * indicates significant difference from control at $P \leq 0.05$; CV = coefficient of variation
[1]Between water treatments

Table 2. Increases in shoot length and root dry weight in peach seedlings during water deficit and recovery periods

Cultivar	Treatment	Increased shoot length (cm)		Root dry weight (g)		
		week 0-5	week 5-7	After 5 weeks		
				Total Root	Tap Root	Fine Root
Red Angkhang	Full watering	17	19.2	116.6	97.1	19.5
	Water deficit	10.8	11.8	122.7	102.8	19.9
43060T1	Full watering	16.5	18.4	128.8	107.2	21.7
	Water deficit	5.8	7.8	115.3	94.6	20.7
43087T2	Full watering	17.1	21.8	139.2	108.4	30.8
	Water deficit	10.6	12.2	126.9	103.9	23
42047T1	Full watering	19.5	21.6	145.6	125.8	19.8
	Water deficit	9.8	22.8	158.4	128.6	29.8
Significance:						
Cultivar		ns[1]	ns	ns	ns	ns
Water deficit		*	ns	ns	ns	ns
Interaction		ns	ns	ns	ns	ns
CV		41.5	24.9	14.4	15.7	16.0

Note: ns = not significant; * indicates significant difference from control at $P \leq 0.05$; CV = coefficient of variation
[1]Between water treatments

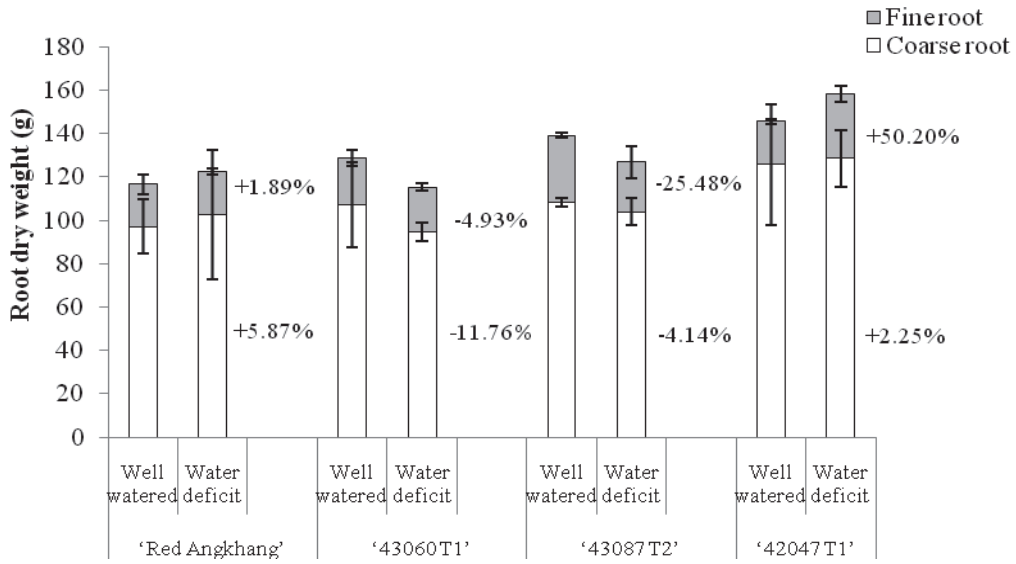

Figure 1. Dry weight of total roots, coarse roots and fine roots of well-watered and water-deficit peach seedlings after 5 weeks of water deficit

represent key responses by plants to drought stress. In our experiment, the increased root dry weight in Red Angkhang and 42047T1 may be considered a characteristic response to drought.

In Rosaceae fruit trees, many researches have reported the accumulation of sorbitol during drought stress [1, 14-16]. In the current study, before the water-deficit period, the sugar concentration was not significantly different among cultivars. However, at the end of the water deficit period, there were significant differences in the levels of soluble sugars, sorbitol and fructose among cultivars, but not after re-watering (Table 3). The increase in soluble sugars and fructose confirms earlier findings that soluble sugars accumulate in leaves during the drought stress of many fruit trees [14, 17, 18]. The highest accumulation of sorbitol was in the water-deficit 42047T1 cultivar, in which the sorbitol level increased significantly compared to other cultivars (Table 3). The accumulation of sorbitol differs depending on the degree of stress exposure or the genetic background [14, 19, 20]. The results in this study demonstrate that 42047T1 adjusts the osmotic pressure by accumulating sorbitol in order to maintain turgor when the plant encounters stress. This is in agreement with another work on peach [1], in which sorbitol was reported to accumulate in both the mature leaves and shoot tips of stressed plants from the second week of treatment, reaching up to 80% of the total solutes involved in osmotic adjustment. In the peach 'Ohatsumomo', sorbitol also accumulates in leaves during water stress [16], and in Japanese pear, the leaves respond to salt and low temperature stress by predominantly synthesising sorbitol [20]. Thus, the increase in the level of sorbitol in 42047T1 in response to water stress indicates that sorbitol plays a role in drought resistance in this cultivar.

Table 3. Soluble sugars (sucrose, fructose and glucose), sorbitol and fructose concentrations in peach seedlings during water-deficit and recovery periods

Cultivar	Treatment	Soluble sugars (mg g^{-1} fresh wt)			Fructose (mg g^{-1} fresh wt)			Sorbitol (mg g^{-1} fresh wt)		
		Day beginning	Last day of 5th week	Last day of 2-week recovery	Day beginning	Last day of 5th week	Last day of 2-week recovery	Day beginning	Last day of 5th week	Last day of 2-week recovery
Red Angkhang	Full watering	30.1	21.07	26.7	11.21	15.11	15.68	26.88	31.14	30.28
	Water deficit		27.28	29.5		17.7	20.9		28.93	24.79
43060 T1	Full watering	25.55	25.6	20.89	7.21	18.47	12.15	23.15	29.26	25.97
	Water deficit		28.99	23.87		24.42	14.81		38.45	28.27
43087 T2	Full watering	26.86	26.31	27.27	7.91	17.92	16.4	25.31	34.77	30.3
	Water deficit		29.61	25.24		22.19	18.47		37.51	28.4
42047 T1	Full watering	41.1	34.65	29.26	14.61	25.79	20.28	28.02	35.88	31.8
	Water deficit		43.31	27.07		34.69	19.59		48.18	28.03
Significance:										
Cultivar		ns[1]	*	ns	ns	*	ns	ns	*	ns
Water deficit		-	ns	ns	-	*	ns	-	*	ns
Interaction		-	ns	ns	-	ns	ns	-	*	ns
CV[2]		34.2	18.43	12.78	21.26	18.81	14.84	68.27	7.98	10.77

Note: ns = not significant; * indicates significant difference from control at $P \leq 0.05$; CV = coefficient of variation

[1]Between water treatments

CONCLUSIONS

By using the 8 parameters (shoot fresh weight, total root dry weight, coarse root dry weight, fine root dry weight, shoot length, soluble sugars, sorbitol and fructose) which show the most significant difference after water deficit for cluster analysis, the degree of drought tolerance of peach seedlings in this study can be separated into 2 groups. The first group has better tolerance under water deficit and consists of Red Angkhang, which increases its root dry weight, and cultivar 42047T1, which increases its root dry weight and also accumulates the highest amount of sorbitol. The second group consists of cultivars 43060T1 and 43087T2, whose the root dry weight decreases and there is no sorbitol accumulation. Compared with the local Red Angkhang cultivar, the new hybrid 42047T1 therefore appears to have better potential for drought tolerance than the other new hybrids 43060T1 and 43087T2.

We suggest that the root dry weight and sorbitol concentration can be used for screening drought tolerant peach rootstocks in northern Thailand.

ACKNOWLEDGEMENTS

This work was funded by the Centre for Advanced Agriculture and Food Research, Kasetsart University, Bangkok and the Royal Project Foundation. We gratefully acknowledge the Royal Angkhang Agricultural Station for providing the plant materials and other facilities.

REFERENCES

1. R. L. Bianco, M. Reiger and S-J S. Sung, "Effect of drought on sorbitol and sucrose metabolism in sinks and sources of peach", *Physiol. Plantarum*, **2000**, *108*, 71-78.
2. Y. Kanayama, "Molecular biology of sugar metabolism and its regulation in fruit", *J. Japan. Soc. Hort. Sci.*, **1998**, *67*, 1203-1208.
3. A. Moing, N. Langlois, L. Svanella, A. Zanetto and J-P. Gaudillere, "Variability in sorbitol: Sucrose ratio in mature leaves of different *Prunus* species", *J. Amer. Soc. Hort. Sci*., **1997**, *122*, 83-90.
4. Y. Kanayama, R. Moriguchi, M. Deguchi, K. Kanahama and S. Yamaki, "Effects of environmental stresses and abscisic acid on sorbitol-6-phosphate dehydrogenase expression in Rosaceae fruit trees", *Acta Hort.*, **2007**, *738*, 375-382.
5. N. Mohammadkhani and R. Heidari, "Drought-induced accumulation of soluble sugars and proline in two maize varieties", *World Appl. Sci. J.*, **2008**, *3*, 448-453.
6. C. J. Atkinson, M. Policarpo, A. D. Webster and A. M. Kuden, "Drought tolerance of apple rootstocks: Production and partitioning of dry matter", *Plant Soil*, **1999**, *206*, 223-235.
7. D. Wongtanet and U. Boonprakob, "Effect of rootstocks on growth of peaches in the highland of northern Thailand", *Acta Hort.*, **2010**, *872*, 327-332.
8. M. Rieger, R. L. Bianco and W. R. Okie, "Responses of *Prunus ferganensis*, *Prunus persica* and two interspecific hybrids to moderate drought stress", *Tree Physiol.*, **2003**, *23*, 51-58.
9. C. J. Atkinson, A. D. Webster, M. Policarpo and A. Kuden, "Drought sensitivity of apple rootstocks", *Acta Hort.*, **1997,** *451*, 171-178.
10. M. Karkacier, M. Erbas, M. K. Uslu and M. Aksu, "Comparison of different extraction and detection methods for sugars using amino-bonded phase HPLC", *J. Chromatogr. Sci.*, **2003***, 41*, 331-333.

11. F. C. Silva, A. Shavaleva, J. P. Maroco, M. H. Almeida, M. M. Chaves and J. S. Pereira, "Responses to water stress in two *Eucalyptus globulus* clones differing in drought tolerance", *Tree Physiol.*, **2004**, *24*, 1165-1172.
12. R. T. Fernandez, R. L. Perry and J. A. Flore, "Drought response of young apple trees on three rootstocks: Growth and development", *J. Amer. Soc. Hort. Sci.*, **1997**, *122*, 14-19.
13. W. C. Olien and A. N. Lakso, "A comparison of the dwarfing character and water relations of five apple rootstocks", *Acta Hort.*, **1984**, *146*, 151-158.
14. Z. Wang and G. W. Stutte, "The role of carbohydrates in active osmotic adjustment in apple under water stress"*, J. Amer. Soc. Hort. Sci*., **1992**, *117*, 816-823.
15. T. G. Ranney, N. L. Bassuk and T. H. Whitlow, "Osmotic adjustment and solute constituents in leaves and roots of water-stressed Cherry (*Prunus*) trees", *J. Amer. Soc. Hort. Sci.*, **1991**, *116*, 684-688.
16. S. Cui, K. Sadayoshi, Y. Ogawa and N. Nii, "Effect of water stress on sorbitol content in leaves and roots, anatomical changes in cell nuclei, and starch accumulation in leaves of young peach trees", *J. Japan. Soc. Hort. Sci*., **2004**, *73*, 25-30.
17. M. L. Rodrigues, M. M. Chaves, R. Wendler, M. M. David, W. P. Quick, R. C. Leegood, M. Stitt and J. S. Pereira, "Osmotic adjustment in water stressed grapevine leaves in relation to carbon assimilation", *Aust. J. Plant Physiol.*, **1993**, *20*, 309-321.
18. S. K. Arndt, W. Wanek, S. C. Clifford and M. Popp, "Contrasting adaptations to drought stress in field-grown *Ziziphus mauritiana* and *Prunus persica* trees: Water relations, osmotic adjustment and carbon isotope composition", *Aust. J. Plant Physiol.*, **2000**, *27*, 985-996.
19. Z. Wang, B. Quebedeaux and G. W. Stutte, "Partitioning of [^{14}C]glucose into sorbitol and other carbohydrates in apple under water stress", *Aust. J. Plant Physiol.*, **1996**, *23*, 245-251.
20. M. Deguchi, M. Watanabe and Y. Kanayama, "Increase in sorbitol biosynthesis in stressed Japanese pear leaves", *Acta Hort.*, **2002**, *587*, 511-517.

Maejo Int. J. Sci. Technol. **2014**, *8*(02), 198-206

Maejo International Journal of Science and Technology

ISSN 1905-7873
Available online at www.mijst.mju.ac.th

Full Paper

Effects of organic carbon source and light-dark period on growth and lipid accumulation of *Scenedesmus* sp. AARL G022

Doungpen Dittamart [1], Chayakorn Pumas [1, 2], Jeeraporn Pekkoh [1, 2] and Yuwadee Peerapornpisal [1, 2, *]

[1] Department of Biology, Faculty of Science, Chiang Mai University, Chiang Mai, 50200 Thailand
[2] Science and Technology Research Institute, Chiang Mai University, Chiang Mai, 50200 Thailand

* Corresponding author, e-mail: yuwadee.p@cmu.ac.th; tel: +66 (0)53 941950 ext.119; fax: +66 (0)53 852 259

Received: 8 March 2013 / Accepted: 4 August 2014 / Published: 13 August 2014

Abstract: The levels of different organic carbon supplements in a mixotrophic culture were optimised to enhance biomass and lipid accumulation in *Scenedesmus* sp. AARL G022. The supplement nutrients, viz. glucose, glycerol and sodium acetate, were compared with non-organic carbon supplement (photoautotrophic culture). The most suitable carbon source was found to be 0.05M glucose, giving a yield of 2.78 ± 0.86 $g.L^{-1}$ of biomass and 233.68 ± 35.34 $mg.L^{-1}$ of crude lipid. The highest yield of biomass (4.04 ± 0.36 $g.L^{-1}$) was obtained from a light-dark cycle of 24:0 hr. The highest crude lipid yield of 396.35 ± 11.60 $mg.L^{-1}$ was obtained from a light-dark cycle of 16:8 hr. The optimised condition for culturing *Scenedesmus* sp. AARL G022 is to cultivate it under a mixotrophic condition using 0.05M of glucose supplement with a light-dark cycle of 16:8 hr.

Keywords: *Scenedesmus* sp. AARL G022, algal bio-oil, mixotrophic cultivation

INTRODUCTION

Algal biofuels are generating considerable interest around the world. Microalgae grow faster than terrestrial plants, frequently doubling their biomass in one day, and can accumulate lipids to as high as 50% of the cell dry weight and express less demand for arable land [1-3]. These lipids can be converted into biodiesel by a chemical process called transesterification and this biodiesel can be used directly or as a blend with diesel fuel for diesel engines [4, 5]. Hence microalgal biomass has the potential to be used as raw material for bio-oil production and it has thus been widely recognised as feedstock for third-generation biofuels [1]. However, it is difficult to cultivate and harvest these

algae in a cost-efficient manner. To achieve economic feasibility of this process, the algal biomass and its lipid content have to be increased and the operation cost has to be reduced [6]. Many factors affect the biomass and lipid productivity of microalgae, for example nitrogen source and concentration [7], light intensity [8], light-dark period [9] and trophic condition [6]. Some microalgae can use organic carbon sources as well as carbon dioxide for growth under mixotrophic conditions, in which the microalgae obtain energy from photosynthesis and oxidation of organic compounds. This indicates that the microalgae are able to live under either photoautotrophic or chemoheterotrophic conditions, or both. The CO_2 released by microalgae via respiration can be trapped and reused under photoautotrophic cultivation [10]. Therefore, it is evident that mixotrophic cultivation can shorten the growth cycle and increase biomass yield more efficiently than can photoautotrophic or chemoheterotrophic culture, separately or combined [11]. Hence a higher growth rate and lipid accumulation in microalgae are promoted [12].

Glucose has normally been used as carbon source in mixotrophic culture but other carbon sources such as crude glycerol from the biodiesel industry, sugars from industrial or agricultural wastes and cane molasses are also found to be promising for the cultivation of mixotrophic algae.

Scenedesmus sp. AARL G022 has recently been reported as a fast growing strain whose large cells are easily harvested and tolerant towards contamination. However, the lipid content in this alga was not so high when compared with other microalgae [13]. For this reason, this research is aimed to analyse the effects of organaic carbon (glucose, glycerol and sodium acetate) and light-dark cycle on the growth and lipide accumulation of *Scenedesmus* sp. AARL G022 grown under laboratory conditions.

MATERIALS AND METHODS

Culture and Growth Conditions

The axenic culture of *Scenedesmus* sp. AARL G022 was obtained from the culture collection of Applied Algal Research Laboratory, Department of Biology, Chiang Mai University. The alga was isolated from a natural water source in Chiang Mai. It was morphologically identified under a compound microscope and maintained in 100 mL of algal medium [14] on an orbital shaker at 25° under constant illumination with a fluorescent lamp (10.8 $\mu moles.m^{-2}.s^{-1}$).

The cultivation was performed in a flask containing 700 mL of the medium supplemented with glucose, glycerol or sodium acetate as the organic carbon source. Each of the carbon sources was supplied in three concentrations: 0.01, 0.02 and 0.05 M. Each experiment was conducted in triplicate. The culturing was performed in a temperature-controlled incubator at 25±2° under continuous illumination with fluorescent lamp (10.8 $\mu moles.m^{-2}.s^{-1}$). The growth was spectrophotometrically measured at optical density of 665 nm and the cells were counted on a haemacytometer counting chamber under a compound microscope (Olympus Normaski) every two days. When each culture reached the stationary phase, the cells were harvested by centrifugation and dried at 60° for 48 hr. The change in cell morphology was observed under the compound microscope and recorded.

Effect of Light-Dark Period

To study the effect of photo-period on growth and lipid accumulation, *Scenedesmus* sp. AARL G022 was grown in a temperature controlled incubator at 25±2° under photoautotrophic (continuous illumination), chemoheterotrophic (no illumination) and mixotrophic conditions with light-dark cycles of 8:16, 12:12, 16:8 and 24:0 hr. In the chemoheterotrophic and mixotrophic cultures, 0.05M glucose was supplied as the organic carbon source.

Biomass Yield and Lipid Extraction

To measure the biomass yield, the microalgal culture (20 mL) was filtered using a pre-weighed GF/C filter paper (Whatman) and dried in an oven at 60° until a constant weight was reached (approximately 2-3 days). The biomass obtained was expressed in grams per litre ($g.L^{-1}$).

The algal lipid content was analysed following the protocol of Bligh and Dyer [15]. Dry algal biomass (approximately 0.1 g) was soaked in 15 mL of chloroform: methanol (2:1 v/v) at room temperature for 24 hr. The resulting solution, after being separated by centrifugation at 6,000 rpm for 10 min. to remove cell sludge, was added with 0.9% NaCl solution (5 mL), allowed to stand for a few minutes and the organic phase was collected. The organic solvent was then evaporated, the remaining crude lipid was dried at 50° and the weight of the lipid was obtained and expressed as per cent of dry biomass and millgrams per litre of the culture.

Statistical Analysis

Statistical comparison between the groups was done by one-way analysis of variance (ANOVA) and Duncan's multiple-range test, using SPSS for Windows version 14.0. The *p*-values that were less than 0.05 were considered significant.

RESULTS AND DISCUSSION

Effect of Organic Carbon

It was observed that under mixotrophic conditions, *Scenedesmus* sp. AARL G022 showed a higher growth rate than that under photoautotrophic conditions (control). The optical density and cell concentration under different concentrations of glucose supplement are demonstrated in Figures 1A and 1B. The glucose supplement enhanced both the number of cells and the OD_{665}. The highest growth rate was observed with 0.05M glucose, followed by 0.02M, 0.01M and non-glucose supplement (photoautotrophic control) respectively. The highest biomass of 2.78±0.86 $g.L^{-1}$ was observed with 0.05M glucose supplement and was 17 times higher than control (Table 1). This result indicates that the stationary growth rate was due to the limitation of carbon source and thus the growth performance would increase with increase in the substrate concentration. According to a previous study, microalgae could be cultivated under glucose up to 0.17M [16]. However, it needs to be noted that a high glucose supplement could inhibit microalgal growth [17] as well as increase the capital cost.

Figures 1C and 1D show the cultures supplemented with glycerol at different concentrations. It is interesting to note that the number of cells from all glycerol concentrations and from the photoautotrophic control was not different, although the highest OD_{665} of 0.41 was obtained when the cells were cultured with the 0.01M glycerol supplement. In contrast, the 0.05M glycerol supplement gave the highest biomass and lipid content (Table 1).

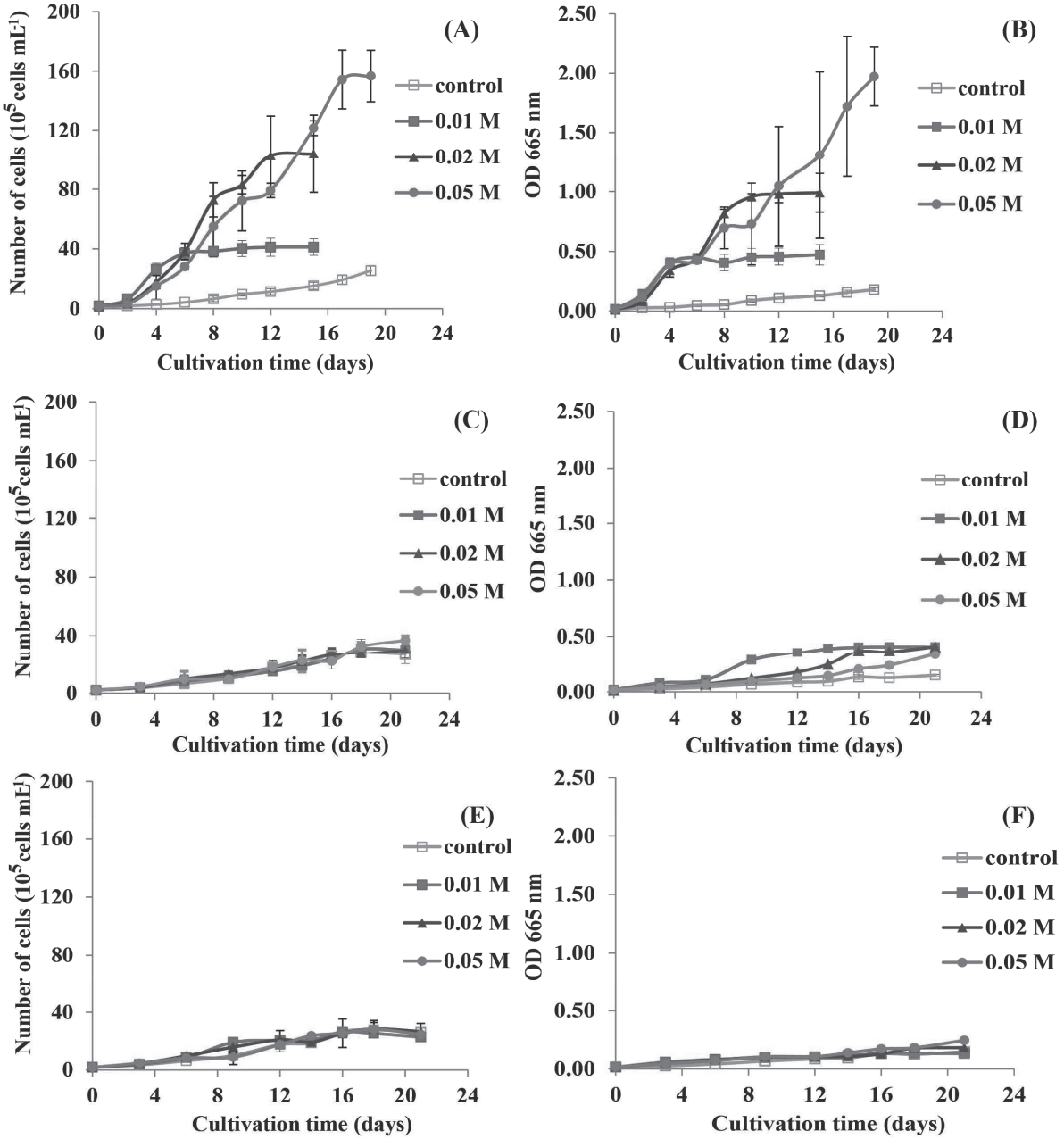

Figure 1. Growth of *Scenedesmus* sp. AARL G022 at 25±2° under continuous illumination in different carbon sources: glucose (A, B); glycerol (C, D); sodium acetate (E, F). Data represent mean ± SD of three replicates.

Table 1. Biomass and crude lipid yield from *Scenedesmus* sp. AARL G022 under continuous illumination at 25±2°

Carbon source	Concentration	Biomass ($g.L^{-1}$)	Crude lipid	
			($mg.L^{-1}$)	(% of biomass)
Glucose	control	0.16±0.02 ^{d}	22.55±6.12 ^{bc}	13.49±3.41 ^{a}
	0.01 M	0.35±0.01 ^{c}	38.61±8.56 ^{b}	11.07±2.18 ^{ab}
	0.02 M	1.07±0.06 ^{b}	74.09±13.57 ^{b}	6.77±3.57 ^{b}
	0.05 M	2.78±0.86 ^{a}	233.68±35.34 ^{a}	8.43±1.56 ^{ab}
Glycerol	control	0.12±0.02 ^{d}	17.58±0.98 ^{d}	14.49±2.12 ^{a}
	0.01 M	0.26±0.06 ^{c}	42.10±9.42 ^{c}	16.11±1.61 ^{a}
	0.02 M	0.38±0.09 ^{b}	62.74±14.64 ^{b}	17.06±0.89 ^{a}
	0.05 M	0.47±0.21 ^{a}	67.90±28.26 ^{a}	14.52±0.02 ^{a}
Sodium acetate	control	0.12±0.02 ^{a}	17.58±0.98 ^{b}	14.49±2.12 ^{a}
	0.01 M	0.25 ±0.11 ^{ab}	33.39±10.95 ^{a}	13.89±1.51 ^{a}
	0.02 M	0.25± 0.05 ^{ab}	31.69±6.27 ^{a}	12.68±0.07 ^{a}
	0.05 M	0.30±0.06 ^{a}	35.73±0.80 ^{ac}	12.08 ±1.97 ^{a}

Note: Data represent mean ± SD of three replicates. Different letters indicate significant differences among different concentrations of each carbon source using ANOVA and post hoc Duncan's multiple-range test ($p < 0.05$).

In mixotrophic cultivation, especially with glucose and glycerol supplements, the microalgae could obtain energy from both photosynthesis and oxidation of organic carbon compounds. Thus, they could utilise some part of the energy for cell division, but the excess energy was stored in the form of lipid granules, which could be obviously noticed under a differential microscope. This was also reflected in the morphology, as it resulted in the cells becoming swollen (Figure 2). In addition, some coenobic colonies were observed to be separated into single cells, resulting in non-significant different colony concentrations during the treatment. Moreover, the cells had become enlarged. The cell colour was also observed to change from green to yellow, and the cells were found to be full of lipid vesicles. The lipid-soluble compounds from the autotrophic cells appeared blackish green, what with chlorophyll and carotenoid as the major components, whereas those from the mixotrophic cells appeared light yellow, which was mainly because of the lipid compounds [18]. Therefore, the spectrophotometrical measurement at 665 nm, which corresponds to the chlorophyll concentration in cells, may not be completely correlated to the true algal biomass in mixotrophic culture. A more accurate assessment of growth in the algal mixotrophic cultivation should be performed by dry biomass measurement.

For the sodium acetate supplement, the values of cell concentration, OD_{665}, biomass and lipid content were not significantly different from those under the photoautotrophic condition (Figures 1E, 1F and Table 1). It is true that acetate can be used as a carbon source via acetyl CoA, which can then be changed to pyruvate and further oxidised in the metabolic pathway. However, the result obtained was found to be opposed to that of previous studies which found that sodium acetate could promote both growth and lipid accumulation in many microalgae such as *Phaeodactylum tricornutum* [17], *Brachiomonas submarina* [19] and *Chlorella vulgaris* [11], while *Scenedesmus* sp. AARL G022 seemed unaffected by sodium acetate supplement.

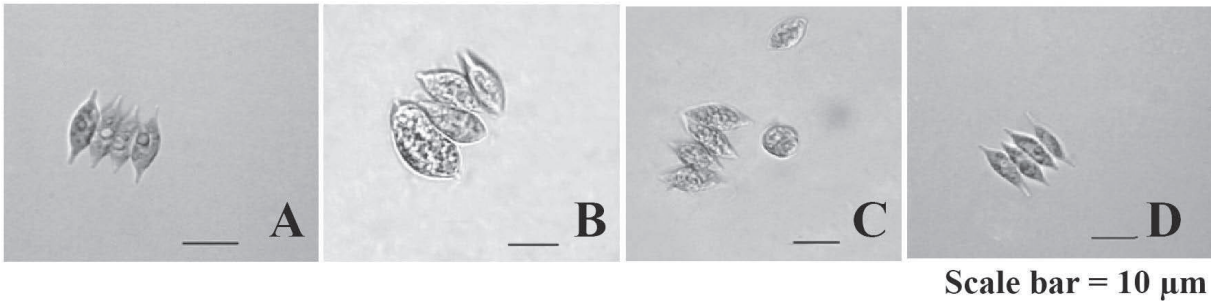

Figure 2. Morphological change of the *Scenedesmus* sp. AARL G022 colony in
A) Photoautotrophic cultivation
B) Mixotrophic cultivation with 0.05 M glucose
C) Mixotrophic cultivation with 0.05 M glycerol
D) Mixotrophic cultivation with 0.05 M sodium acetate

Glucose is the product obtained from the photosynthesis of microalgae; thus, *Scenedesmus* sp. AARL G022 uses glucose directly as an energy source for cell division, rather than stores it in the form of lipid, as evidenced from the supplementation of glucose, which reduced lipid accumulation from 13.49% in the photoautotrophic condition to 8.43% at the 0.05M concentration of glucose supplement. However, the total lipid content was found to increase up to 233.68 $mg.L^{-1}$, which was approximately 10 times that of the control due to the increase in biomass. This is different from that in the case of glycerol supplement, which seems to enhance lipid content and lipid accumulation compared to glucose. Even when the glycerol supplement promoted the algal biomass to become 3-4 times higher than that of the control, its lipid accumulation was not reduced compared to control and this led to a high lipid content in the biomass. This result corresponds to the findings that glycerol can promote the growth of microalgae [20]. The algae, *Schizochytrium limacinum* [21] and *Scenedesmus* sp. [22], were also reported to be capable of glycerol fermentation. In addition, glycerol was also found to enhance fatty acid production in the diatom *Phaeodactylum tricornutum* UTEX-640 [17]. Triglycerides are the main constituents of lipid in algae and it is most probable that glycerol is an intermediate in triglyceride synthesis in algal metabolism. In this study it is clear that glucose supplement promotes cell growth and glycerol supplement enhances lipid accumulation. It would be interesting, therefore, to study the combined effect of glucose-glycerol supplement on both algal growth and lipid content.

Effect of Light-Dark Period

Previous studies have shown that photo-period affects microalgal lipid and biomass production [9, 23]. From our study of the cultures of *Scenedesmus* sp. AARL G022 under photoautotrophic, chemoheterotrophic and mixotrophic conditions, it was found that the alga under mixotrophic condition with a light-dark cycle of 24:0 hr produced the highest number of cells (Figure 3), while the highest biomass was obtained under 24:0 hr and 16:8 hr light-dark cycles (Table 2). However, the highest crude lipid was obtained under 16:8-hr light-dark cycle. Apparently this is because in the light condition (24:0-hr cycle), microalgae perform photoreduction which absorbs energy from light and stores it in energy-carrying molecules such as ATP and NADPH. These energy-pool molecules can be used for the synthesis of biomolecules that promote the growth of the microalgae [9]. Under 16:8-hr cycle, the alga has a dark period in which light-independent reactions can be performed via the Calvin cycle which also operates during the dark phase of photosynthesis.

These chemical reactions convert carbon dioxide and other compounds into glucose by using ATP and NADPH from the photoreduction. Microalgae can oxidise supplemented glucose for energy and then store some excess energy in the form of lipids.

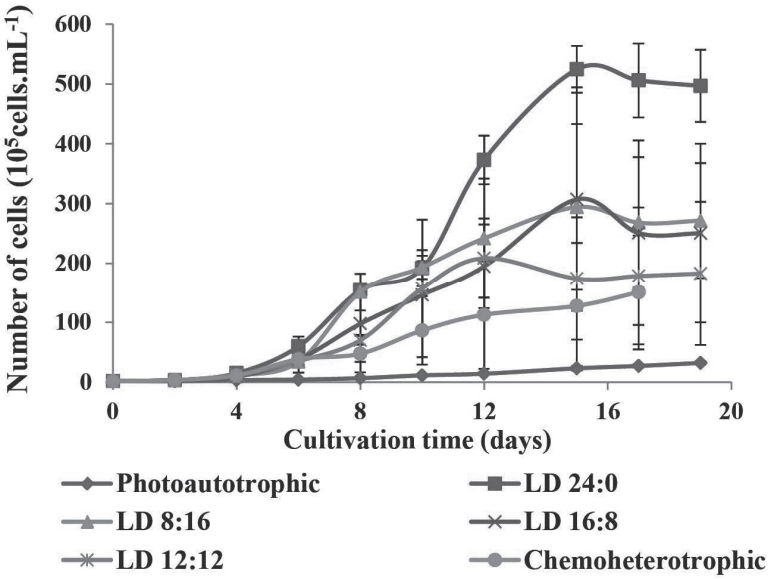

Figure 3. Growth of *Scenedesmus* sp. AARL G022 in the different light-dark cycle (LD) compared with photoautotrophic and chemoheterotrophic cultivation with 0.05M glucose

Table 2. Biomass and crude lipid yield from *Scenedesmus* sp. AARL G022 under different trophic conditions with 0.05M glucose of at 25±2°

	Biomass (g.L^{-1})	**Crude lipid**	
		(mg.L^{-1})	**(% of biomass)**
Photoautotrophic	0.14±0.01 ^{c}	22.57±0.84 ^{d}	15.98±2.30 ^{a}
Chemoheterotrophic	1.94±0.87 ^{b}	158.04±10.89 ^{c}	9.22±4.72 ^{b}
Mixotrophic			
LD 8:16	2.12±0.52 ^{b}	185.00±91.92 ^{c}	8.449 ±2.27 ^{b}
LD 12:12	1.56±0.57 ^{b}	129.16±58.43 ^{c}	8.426 ±2.29 ^{b}
LD 16:8	3.56±0.11 ^{a}	396.35±11.60 ^{a}	11.155±0.13 ^{b}
LD 24:0	4.04±0.36 ^{a}	297.29±51.20 ^{b}	7.471±1.84 ^{b}

Note: Data represent mean ± SD of three replicates. Different letters in the same column indicate significant differences between groups using ANOVA and Duncan's multiple-range test ($p < 0.05$).

Although *Scenedesmus* sp. AARL G022 under mixotrophic cultivation with 0.05M glucose had only a moderate lipid content, its biomass yield was boosted substantially, resulting in high lipid productivity at 396.35 mg.L^{-1} (Table 2). This is comparable with values for species such as *Phaeodactylum tricornutum* (biomass 1.16 g.L^{-1}, 29% lipid content and 336.4 mg.L^{-1} lipid productivity) [17], but lower than values for species such as *Chlorella vulgaris* (biomass 4.8 g.L^{-1}, 13% lipid content and 624 mg.L^{-1} lipid productivity) [11]. In previous studies, it was found that other than the glucose supplement, stress condition and change of nitrogen source could also enhance the productivity. Under a nitrogen-limited condition, *Scenedesmus* sp. 11-1 showed the highest biomass yield of up to 3.88 g.L^{-1} with a lipid content of 41.1% [8], while values of the

specific growth rate and total lipid content of *Scenedesmus dimorphus* and *S. quadricauda* increased when the nitrogen source was changed from nitrate to urea [7]. Thus, a change in the nitrogen source and concentration in a mixotrophic culture may be worth further investigation.

CONCLUSIONS

The optimised condition for culturing *Scenedesmus* sp. AARL G022, a promising organism for bio-oil production, is to cultivate it under a mixotrophic condition with a light-dark cycle of 16:8 hr using 0.05M of glucose supplement. However, glucose is an expensive carbon source so the algal biomass and lipid product are still expensive to be used as raw materials for bio-oil production. Further study should focus on decreasing the media cost by using low-cost nitrogen, phosphorus and organic carbon sources.

ACKNOWLEDGEMENTS

This work was supported by the National Research Council of Thailand (NRCT) under the management of Institute for Science and Technology Research and Development, Chiang Mai University. It was also partially financed by the Energy Policy and Planning Office, Ministry of Energy, Thailand. We thank the Department of Biology, Faculty of Science, Chiang Mai University and the Graduate School for their support.

REFERENCES

1. Y. Chisti, "Biodiesel from microalgae", *Biotechnol. Adv.*, **2007**, *25*, 294-306.
2. X. Li, H. Xu and Q. Wu, "Large-scale biodiesel production from microalga *Chlorella protothecoides* through heterotrophic cultivation in bioreactors", *Biotechnol. Bioeng.*, **2007**, *98*, 764-771.
3. X. Miao and Q. Wu, "Biodiesel production from heterotrophic microalgal oil", *Bioresour. Technol.*, **2006**, *97*, 841-846.
4. C.L. Peterson, M. Feldman, R. Korus and D.L. Auld, "Batch type transesterification process for winter rape oil", *Appl. Eng. Agr.*, **1991,** *7*, 711-716.
5. Y. Zhang, M. A. Dube, D. D. McLean and M. Kates, "Biodiesel production from waste cooking oil: 1. Process design and technological assessment", *Bioresour. Technol.*, **2003,** *89*, 1-16.
6. A. Bhatnagar, S. Chinnasamy, M. Singh and K.C. Das, "Renewable biomass production by mixotrophic algae in the presence of various carbon sources and wastewaters", *Appl. Energ.*, **2011,** *88*, 3425-3431.
7. R. C. D. Goswami and M. C. Kalita, "*Scenedesmus dimorphus* and *Scenedesmus quadricauda*: two potent indigenous microalgae strains for biomass production and CO_2 mitigation—A study on their growth behavior and lipid productivity under different concentration of urea as nitrogen source", *J. Algal Biomass Utln.*, **2011**, *2*, 42-49.
8. J. Liu, C. Yuan, G. Hu and F. Li, "Effects of light intensity on the growth and lipid accumulation of microalga *Scenedesmus* sp. 11-1 under nitrogen limitation", *Appl. Biochem. Biotechnol.*, **2012**, *166*, 2127-2137.
9. J.-V. Pérez-Pazos and P. Fernández-Izquierdo, "Synthesis of neutral lipids in *Chlorella* sp. under different light and carbonate conditions", *C.T.F. Cienc. Tecnol. Futuro*, **2011**, *4*, 47-58.

10. T. M. Mata, A. A. Martins and N. S. Caetano, "Microalgae for biodiesel production and other applications: A review", *Renew. Sustain. Energy Rev.*, **2010**, *14*, 217-232.
11. T. Heredia-Arroyo, W. Wei, R. Ruan and B. Hu, "Mixotrophic cultivation of *Chlorella vulgaris* and its potential application for the oil accumulation from non-sugar materials", *Biomass Bioenergy*, **2011**, *35*, 2245-2253.
12. M. C. Cerón García, A. S. Mirón, J. M. F. Sevilla, E. M. Grima and F. G. Camacho, "Mixotrophic growth of the microalga *Phaeodactylum tricornutum:* Influence of different nitrogen and organic carbon sources on productivity and biomass composition", *Process Biochem.*, **2005**, *40,* 297-305.
13. K. Janta, J. Pekkoh, S. Tongsiri, C. Pumas and Y. Peerapornpisal, "Selection of some native microalgal strains for possibility of bio-oil production in Thailand", *Chiang Mai J. Sci.*, **2013**, *40,* 593-602.
14. J. R. Stein, "Handbook of Phycological Methods: Culture Methods and Growth Measurements", Cambridge University Press, Cambridge, **1979**.
15. E. G. Bligh and W. J. Dyer, "A rapid method of total lipid extraction and purification", *Can. J. Biochem. Physiol.*, **1959**, *37*, 911-917.
16. P. F. Ip, K. H. Wong and F. Chen, "Enhanced production of astaxanthin by the green microalga *Chlorella zofingiensis* in mixotrophic culture", *Process Biochem.*, **2004**, *39*, 1761-1766.
17. H. Wang, R. Fu and G. Pei, "A study on lipid production of the mixotrophic microalgae *Phaeodactylum tricornutum* on various carbon sources", *Afr. J. Microbiol. Res.,* **2012**, *6,* 1041-1047.
18. Q. Y. Wu, S. Yin, G. Y. Sheng and J. M. Fu, "A comparative study of gases generated from stimulant thermal degradation of autotrophic and heterotrophic *Chlorella*", *Prog. Nat. Sci.*, **1992**, *2*, 311-318 (in Chinese).
19. X. Yang, X. Zeng, Y. Ji and Q. Liu, "Effects of sodium nitrate and sodium acetate concentrations on the growth and fatty acid composition of *Brachiomonas submarina*", *J. Ocean Univ. Qingdao*, **2003**, *2*, 75-78.
20. J. Y. Cheng and N. J. Antia, "Enhancement by glycerol of phototrophic growth of marine planktonic algae and its significance to the ecology of glycerol pollution", *J. Fish. Res. Board Can.*, **1970**, *27*, 335-346.
21. D. J. Pyle, R. A. Garcia and Z. Wen, "Producing docosahexaenoic acid (DHA)-rich algae from biodiesel-derived crude glycerol: Effects of impurities on DHA production and algal biomass composition", *J. Agric. Food Chem.*, **2008,** *56,* 3933-3939.
22. H. W. Yen, C. H. Sun and T. W. Ma, "The Comparison of lutein production by *Scenesdesmus* sp. in the autotrophic and the mixotrophic cultivation", *Appl. Biochem. Biotechnol.*, **2011**, *164*, 353-361.
23. E. Jacob-Lopes, C. H. G. Scoparo, L. M. C. F. Lacerda and T. T. Franco, "Effect of light cycles (night/day) on CO_2 fixation and biomass production by microalgae in photobioreactors" *Chem. Eng. Process. Process Intensif.*, **2009**, *48*, 306-310.

Maejo Int. J. Sci. Technol. **2014**, *8*(02), 207-220

Maejo International Journal of Science and Technology

ISSN 1905-7873
Available online at www.mijst.mju.ac.th

Full Paper

Single-phase and multiphase models for temperature and relative humidity calculations during forced convection in a rubber-sheet drying chamber

Racha Dejchanchaiwong [1, 2], Yutthana Tirawanichakul [1, 3], Supawan Tirawanichakul [1, 2] and Perapong Tekasakul [1, 4, *]

[1] Energy Technology Research Centre (ETRC), Faculty of Engineering, Prince of Songkla University, Hat Yai, Songkhla 90112, Thailand
[2] Department of Chemical Engineering, Faculty of Engineering, Prince of Songkla University, Hat Yai, Songkhla 90112, Thailand
[3] Department of Physics, Faculty of Science, Prince of Songkla University, Hat Yai, Songkhla 90112, Thailand
[4] Department of Mechanical Engineering, Faculty of Engineering, Prince of Songkla University, Hat Yai, Songkhla 90112, Thailand

*Corresponding author, e-mail: perapong.t@psu.ac.th

Received: 29 August 2013 / Accepted: 4 August 2014/ Published: 25 August 2014

Abstract: Computational fluid dynamics modelling of single-phase and multiphase flows was used to simulate the temperature and relative humidity at various locations in an empty rubber-sheet drying chamber. In all planes, unlike the single-phase model, the multiphase model's temperature distribution is relatively uniform, and the temperature deviations are 0.01-4.73°C in the bottom plane, 0.02-4.05°C in the middle plane, and 0.01-3.84°C in the top plane. The single-phase model results in temperature deviations of 0.55-6.63°C, 0.02-6.02°C and 0.36-3.89°C in the bottom, middle and top planes respectively. Thus, the multiphase model is deemed superior. The inclusion of water vapour in the multiphase model increases the agreement between model and experimental temperature data. The largest temperature deviations occur at the centre-frontal positions of all planes owing to the turbulence of the hot gas at the inlet. In all planes the relative humidity is almost uniform, except near the centre-frontal area of the bottom plane. Clearly, the multiphase model is more appropriate for simulating chambers containing rubber sheets, though the diffusion of moisture from rubber sheets needs to be considered as well.

Keywords: natural rubber, rubber-sheet drying, multiphase model

INTRODUCTION

Multiphase flow is the simultaneous flow of fluids at different states or with different phases. Multiphase models have been widely used in engineering applications. However, to date, most numerical simulations and physical modelling are based on single-phase methods. Nonetheless, computational modelling of multiphase flow has been used to study complex multi-component systems. The use of computational fluid dynamics (CFD) is increasingly becoming popular in modelling fluid flow and heat and mass transfer because CFD is an accurate, effective and cost-efficient method [1-5]. Simultaneous heat and mass transfer under transient conditions is common in drying processes and CFD simulations have been widely used to analyse problems of fluid flow in drying processes [6-12]. Understanding fluid flow and heat transfer in the natural-rubber smoking process will help improve rubber's drying process and quality. Several previous studies have reported the use of the CFD modelling of single-phase fluid flow and heat transfer in rubber-smoking rooms [13, 14]. In this study, we used CFD simulation of single-phase and multiphase models to obtain the temperature and relative humidity in an empty rubber-sheet drying chamber and to assess the effect of a second phase (vapour).

SIMULATION APPROACH

Velocity, temperature and moisture can be determined by solving the continuity, momentum and energy equations respectively for fluid flow and heat and mass transfer, along with appropriate boundary conditions.

Governing Equations

Fluid flow can be described by the governing partial differential equations of mass, momentum and energy. Results are determined by solving these equations simultaneously. The governing equations for incompressible flow and Newtonian fluid are given by the following [15]:

Continuity equation

$$\frac{\partial \rho}{\partial t} + \nabla \cdot (\rho \bar{\mathbf{u}}) = 0 \quad (1)$$

Momentum equation

$$\frac{\partial (\rho \bar{\mathbf{u}})}{\partial t} + \nabla \cdot (\rho \overline{\mathbf{u}\mathbf{u}}) = -\nabla P + \nabla \cdot \left[\mu_{eff} \left(\nabla \bar{\mathbf{u}} + \nabla \bar{\mathbf{u}}^{T} \right) - \frac{2}{3} \nabla \cdot \bar{\mathbf{u}} I \right] - \rho g \beta \left(\bar{T} - \bar{T}_{o} \right) \quad (2)$$

Energy equation

$$\frac{\partial (\rho E)}{\partial t} + \nabla \cdot \left(\bar{\mathbf{u}} (\rho E + P) \right) = \nabla \cdot \left(\lambda_{eff} \nabla \bar{T} - \sum_{j} H_j \mathbf{J}_j + \left(\bar{\boldsymbol{\tau}}_{eff} \cdot \bar{\mathbf{u}} \right) \right) + S_E \quad (3)$$

where $\bar{\mathbf{u}}$ is the vector velocity (m/s), P is the pressure (N/m^2), ρ is the density (kg/m^3), g is the gravitational acceleration vector (m/s^2), β is the thermal expansion coefficient, μ_{eff} is the effective viscosity (kg/m s), $\bar{\mathbf{u}}^{T}$ is the transposed mean velocity (m/s), $\bar{T}_0$ is the system surrounding temperature (reference temperature, K), $\bar{T}$ is the temperature (K), I is the unit tensor, λ_{eff} is the effective conductivity (W/m K), t is the time (s), $\mathbf{J}_j$ is the diffusion flux of species j (kg/m^{2}s),

H_j is the enthalpy of species j (J/kg), $\bar{\tau}_{eff}$ is the effective stress tensor, S_E is the source term, and E is the total energy:

$$E = H - \frac{p}{\rho} + \frac{u^2}{2} \tag{4}$$

where H is the enthalpy (J/kg), u is the velocity (m/s), and $\frac{u^2}{2}$ represents the kinetic energy.

For turbulent flow, Reynolds stress and turbulent heat flux can be calculated using the standard $k-\varepsilon$ model [13]. The equations for the kinetic energy of turbulence (k in the $k-\varepsilon$ model) and its dissipation rate (ε) are the following [15, 16]:

k Equation

$$\frac{\partial(\rho k)}{\partial t} + \frac{\partial(\rho \bar{\mathbf{u}}_i k)}{\partial x_i} = \frac{\partial}{\partial x_i}\left[\left(\mu + \frac{\mu_t}{\sigma_k}\right)\frac{\partial k}{\partial x_i}\right] + P_k + G - \rho\varepsilon \tag{5}$$

ε Equation

$$\frac{\partial(\rho \varepsilon)}{\partial t} + \frac{\partial(\rho \bar{\mathbf{u}}_i \varepsilon)}{\partial x_i} = \frac{\partial}{\partial x_i}\left[\left(\mu + \frac{\mu_t}{\sigma_\varepsilon}\right)\frac{\partial \varepsilon}{\partial x_i}\right] + C_1 \frac{\varepsilon}{k}(P + C_3 G) - C_2 \rho \frac{\varepsilon^2}{k} \tag{6}$$

where the model constants are:

$$C_\mu = 0.09, C_1 = 1.44, C_2 = 1.92, C_3 = 1.0, \sigma_k = 1.0 \text{ and } \sigma_\varepsilon = 1.217$$

The $\rho\varepsilon$ term in Eq. (5) is the destruction rate, μ is the viscosity (kg/m s), P_k is the shear production [13] and G is the buoyancy production [13]:

$$P_k = \mu_t \frac{\partial \bar{\mathbf{u}}_i}{\partial xj}\left(\frac{\partial \bar{\mathbf{u}}_i}{\partial x_j} + \frac{\partial \bar{\mathbf{u}}_i}{\partial x_i}\right) \tag{7}$$

$$G = g_i \beta \frac{\mu_t}{\mathrm{Pr}}\left(\frac{\partial \bar{T}}{\partial x_i}\right) \tag{8}$$

where Pr is the Prandtl number. The eddy viscosity (μ_t, kg/m s) is defined from dimensional analysis as

$$\mu_t = \rho C_\mu \frac{k^2}{\varepsilon} \tag{9}$$

Mass Transfer in Air

In this study, the fluid in the empty rubber-sheet drying chamber is a mixture of air, which is the continuous phase, and the droplets of vapour, which is the dispersed phase. Both can be described by Fick's law of mass transfer [17]:

$$\frac{\partial(\rho Y)}{\partial t} + \nabla \cdot (\rho \bar{\mathbf{u}}) Y = -\nabla \cdot \bar{\mathbf{J}} + S \tag{10}$$

$$\bar{\mathbf{J}} = -\left(\rho D_m + \frac{\mu}{Sc}\right)\nabla Y \tag{11}$$

where $\bar{\mathbf{J}}$ is the diffusion flux (kg/m^{2}s), Y is the mass fraction of water vapour in air (kg water/kg dry air), D_m is the diffusion coefficient of water vapour in air (m^2/s), and Sc is the Schmidt number of turbulent flow.

CFD Programme

We performed 3D simulations using the ANSYS Fluent, version 13, CFD software. The finite volume method in the programme was used to calculate the temperature and relative humidity distributions in the model chamber. The force convective terms were discretised using a first-order upwind scheme [13]. The pressure-velocity coupling was solved using the SIMPLE discretisation algorithm [13].

COMPARISON

The temperature and relative humidity in the model chamber using the single-phase and multiphase models were derived and compared with the experimental results to assess the agreement.

Experiments

The drying chamber dimensions are 1.2 m × 1.2 m × 1.2 m, as shown in Figure 1. The inlet air was heated by eight electrical heater sets (6 x 600W and 2 x 2kW). Temperatures at 32 positions, as shown in Figure 2, were measured by type-K thermocouples. The air relative humidity was measured using a probe (Rense, HT-740-T-1) at the location shown in Figure 2. A hot wire-type anemometer (Testo, 405-V1) was used to measure the air velocity at three points at the inlet of the chamber.The average value was used as the boundary condition at the inlet in the simulation. All data were continuously recorded using a data logger (Data-Taker, DT 605) at 1 min. intervals.

We investigated the temperature and relative humidity distribution in the drying chamber. The results, as shown in Figure 3, show that the temperature in each plane in the drying chamber increased rapidly during the initial stage and then gradually until a steady state was attained. The largest average temperature difference between any planes is 4°. The relative humidity, as anticipated, decreased with increasing temperature, as shown in Figure 4. The initial and final relative humidity values are 61.1% and 28% respectively.

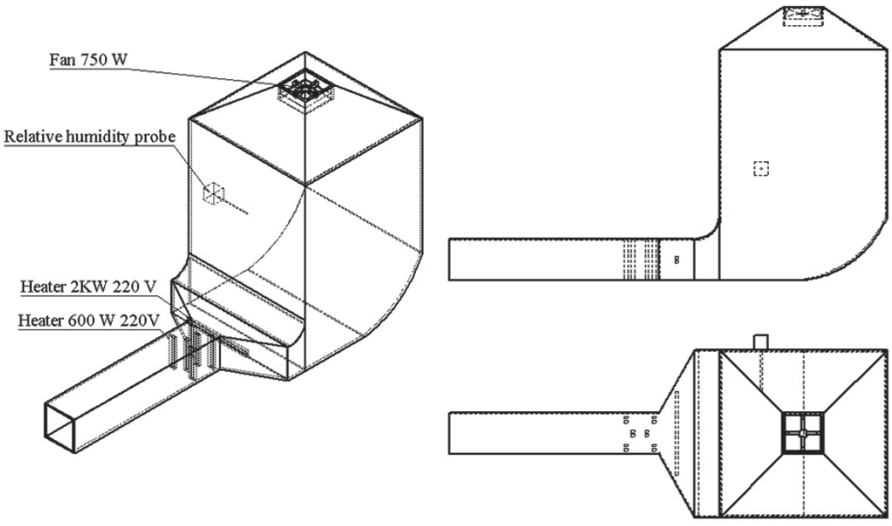

Figure 1. Schematic of the model rubber-sheet drying chamber

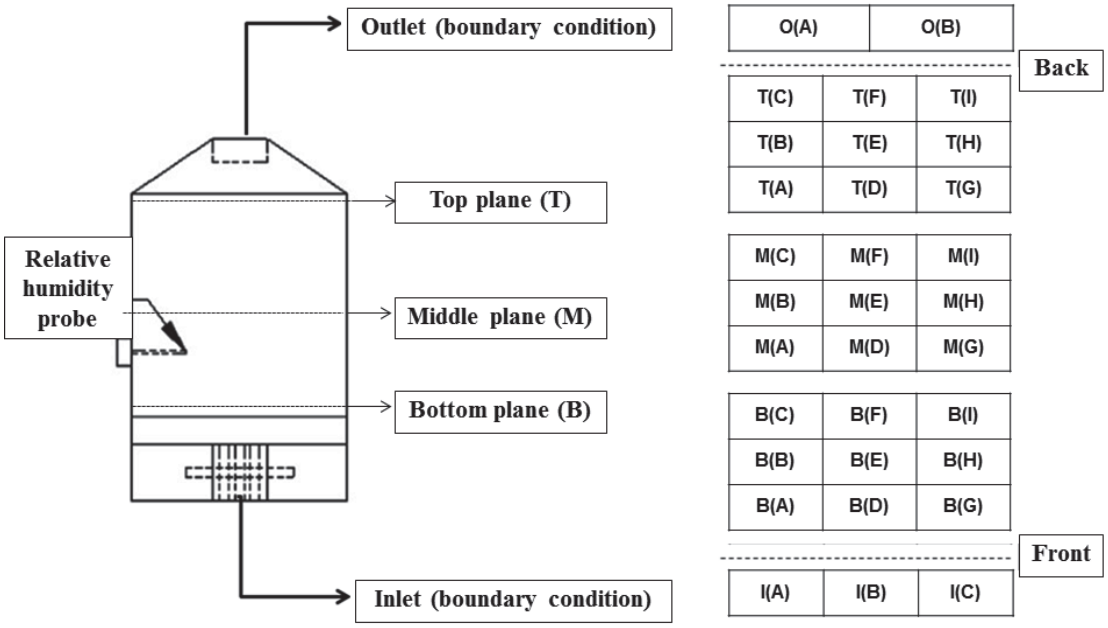

Figure 2. Positions of temperature and relative humidity probes in each plane

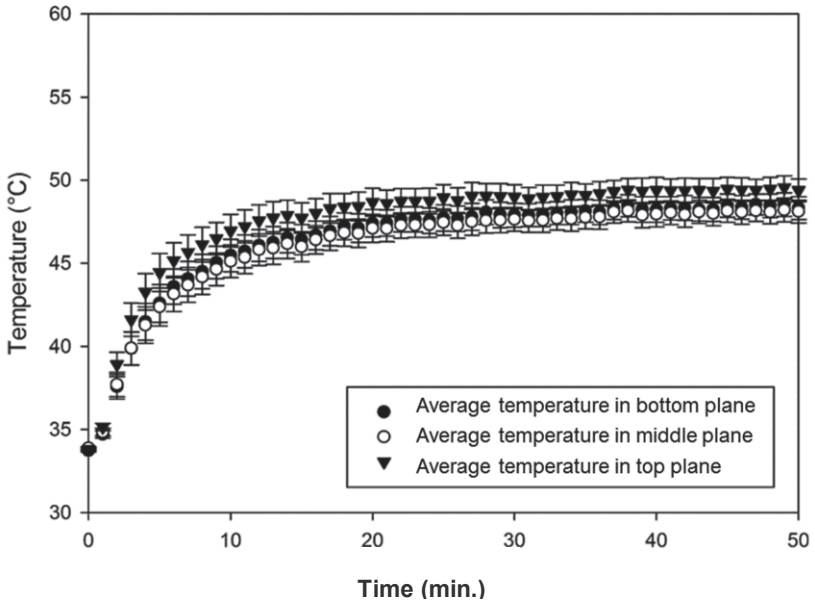

Figure 3. Average temperature as a function of time in the model drying chamber

Simulation

The model flow is fully symmetrical along the central plane of the chamber. The symmetrical condition is considered in the simulation to minimise the discrepancies when using the 3D half-size chamber in Figure 5. To minimise the computational time and avoid nonconvergence, we used the 3D half-size model in the simulations. The element-type tetrahedral and patch conformation algorithms were used to set the grid cells. The initial and boundary conditions in the simulations are described in the next section. Simulations were performed until steady state was reached; that is, after about 50 min.

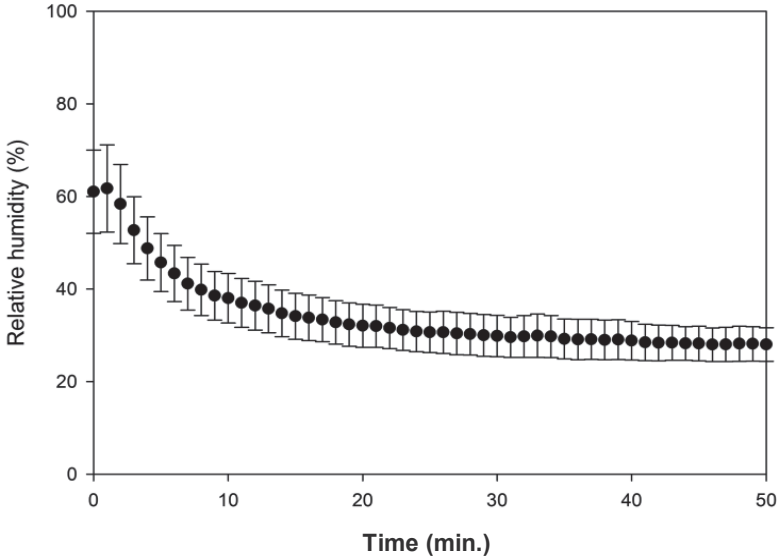

Figure 4. Relative humidity as a function of time in the model drying chamber

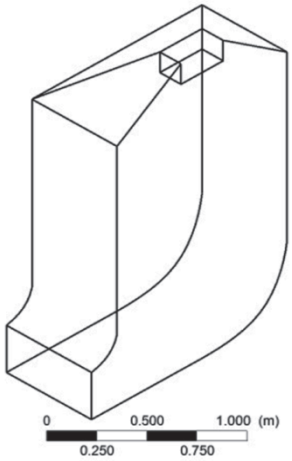

Figure 5. 3D half-size chamber used in the simulations

Initial and Boundary Conditions

Initial conditions

The initial temperature obtained from the experiments was 30.2°. The initial volume fraction of water vapour in air was 0.030416 (m^3 of water vapour/m^3 of dry air). This value was calculated from the measured relative humidity of 60% and the dry-bulb temperature of 33.0°. Thus,

$$v = w_s \left[\frac{\rho_{dry-dair}}{\rho_{water-vapour}} \right] \quad (12)$$

where v is the volume fraction of water vapour, w_s is the humidity ratio ($kg_{water\ vapour}/kg_{dry\ air}$), $\rho_{water-vapour}$ is the density of water vapour, and $\rho_{dry-air}$ is the density of dry air.

Boundary conditions

At the inlet, the experimental constant inlet air velocity was 0.725 m/s. The user-defined function of the inlet temperature and vapour volume fraction were used as boundary conditions.

At the outlet, the pressure was set at zero. The experimental outlet temperature data as a function of time were fitted and used as boundary conditions in the user-defined function. At the wall, experimental heat flux data as a function of time were fitted and used as boundary conditions in the user-defined function.

Computational Validation

A grid sensitivity test was performed using three different mesh schemes, as shown in Table 1. For the bottom-plane temperature, the comparison between the simulation and experiments is shown in Figure 6. The simulation results using the coarse grid are not sufficiently accurate when compared with the experimental results. The simulation results using the medium and fine grids agree well with the experimental results. Discrepancies of 0.01-1.05% are seen using the medium grid, which is deemed satisfactory compared with the fine grid scheme. Therefore, the minimal grid refinement of 83,649 was used in the simulation.

Table 1. Grid schemes used in the convergence test

	Case 1 (coarse)	Case 2 (medium)	Case 3 (fine)
Node	9,530	17,397	32,695
Element	59,469	83,649	163,601

RESULTS AND DISCUSSION

Temperature

Single-phase models have been rigorously evaluated by other researchers; hence we concentrated on the multiphase model. Nevertheless, we also compared the temperature predictions of the single-phase and multiphase models.

Multiphase model vs experiment

The multiphase model temperature distribution in the bottom, middle and top planes, initially and after 50 min. at steady state, is shown in Figure 7. The initial and steady state temperature is respectively 33.85° and 49.64°. The temperature distribution in any plane is uniform with no significant differences between planes. The temperature deviations between experiments and simulations are 0.01-4.73° for the bottom plane, 0.02-4.05° for the middle plane, and 0.01-3.84° for the top plane, as shown respectively in Figures 8-10. The largest deviation of 4.73° occurs at the centre-frontal position of the bottom plane, which is denoted as B(D) in Figure 2, and is attributed to the proximity of the hot-gas inlet where the temperature is highly variable. However, the boundary temperature conditions in the simulations are constant. The centre-frontal position in the middle plane, denoted as M(D), is still affected by the hot gas from the inlet, as shown in Figure 9. The hot-gas effect decreases in the top plane where the temperature is rather uniform throughout, as shown in Figure 10. The comparison of the experimental and model temperatures shows acceptable agreement; thus, we can use the multiphase model to simulate the temperature distribution in the drying chamber.

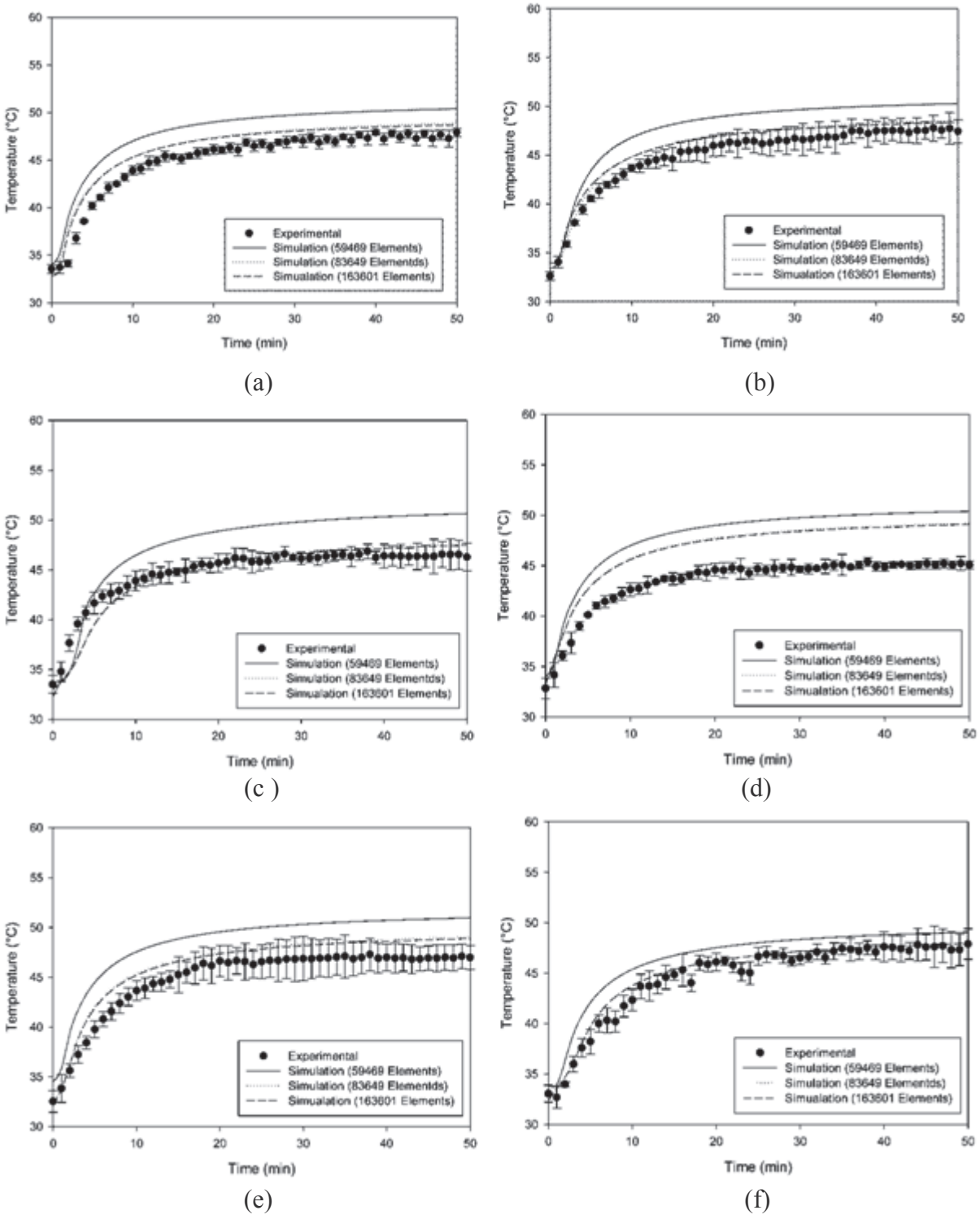

Figure 6. Plots of temperature as a function of time for experimental and simulation data for the multiphase model using the coarse (59,469 elements), medium (83,649 elements) and fine (163,601 elements) grid schemes in the bottom plane: (a) position B(A); (b) position B(B); (c) position B(C); (d) position B(D); (e) position B(E); (f) position B(F)

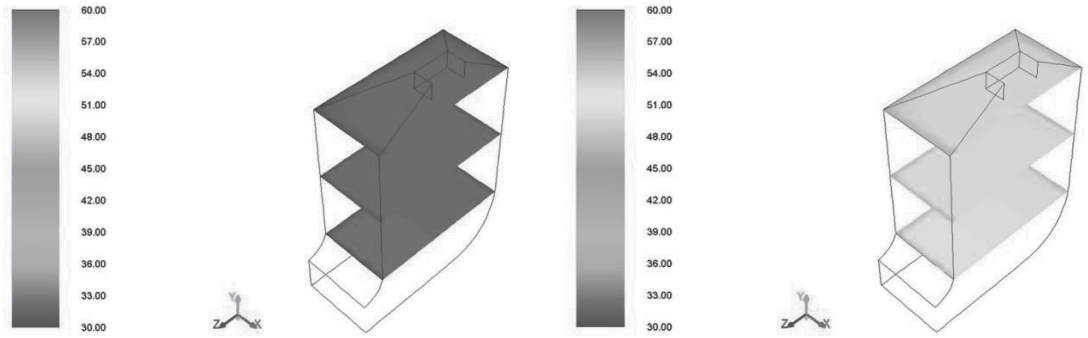

(a) (b)

Figure 7. Temperature profile of bottom, middle and top planes in the model chamber at 0 min. (a) and 50 min. (steady state) (b)

Multiphase model vs single-phase model

The single-phase and multiphase model temperatures were compared with the experimental data for the largest deviation scenario (at the centre-frontal positions of all planes) and the smallest deviation scenario (at B(F), centre-back position of the bottom plane) and shown in Figures 11-13. The deviations at B(D) are 1.66-6.63° and 0.51-4.73° for the single-phase model and the multiphase model respectively. At B(F), the deviations for the multiphase model are minimal at 0.01-2.47°, whereas those of the single-phase model are 0.96-6.27°. Similar results are obtained in the middle and top plane, as shown in Figures 12 and 13 respectively. Initially, the multiphase model shows better agreement in the middle plane while the differences in the top plane are not clear. Overall, the multiphase model outperforms the single-phase model. The inclusion of humidity in the multiphase model decreases the air temperature compared with the single-phase model.

Relative Humidity

The relative humidity (RH) predicted by the multiphase model is shown in Figures 14 and 15. The RH distribution in the bottom, middle and top planes at the beginning and after 50 min. at steady state are shown in Figures 14 (a) and 14 (b) respectively. In all planes, the RH values are mostly uniform except near the centre-frontal area of the bottom plane. The largest deviation is initially seen with higher RH variation in the bottom plane, as shown in Figure 14. Apparently, the flow turbulence at the inlet induces variations in the moisture distribution. Moreover, the RH difference between minimum and maximum is initially much higher than that at steady state. The experimental and multiphase model data are compared in Figure 15. The deviations range between 0.56-10.45%, suggesting acceptable agreement and the suitability of the multiphase model.

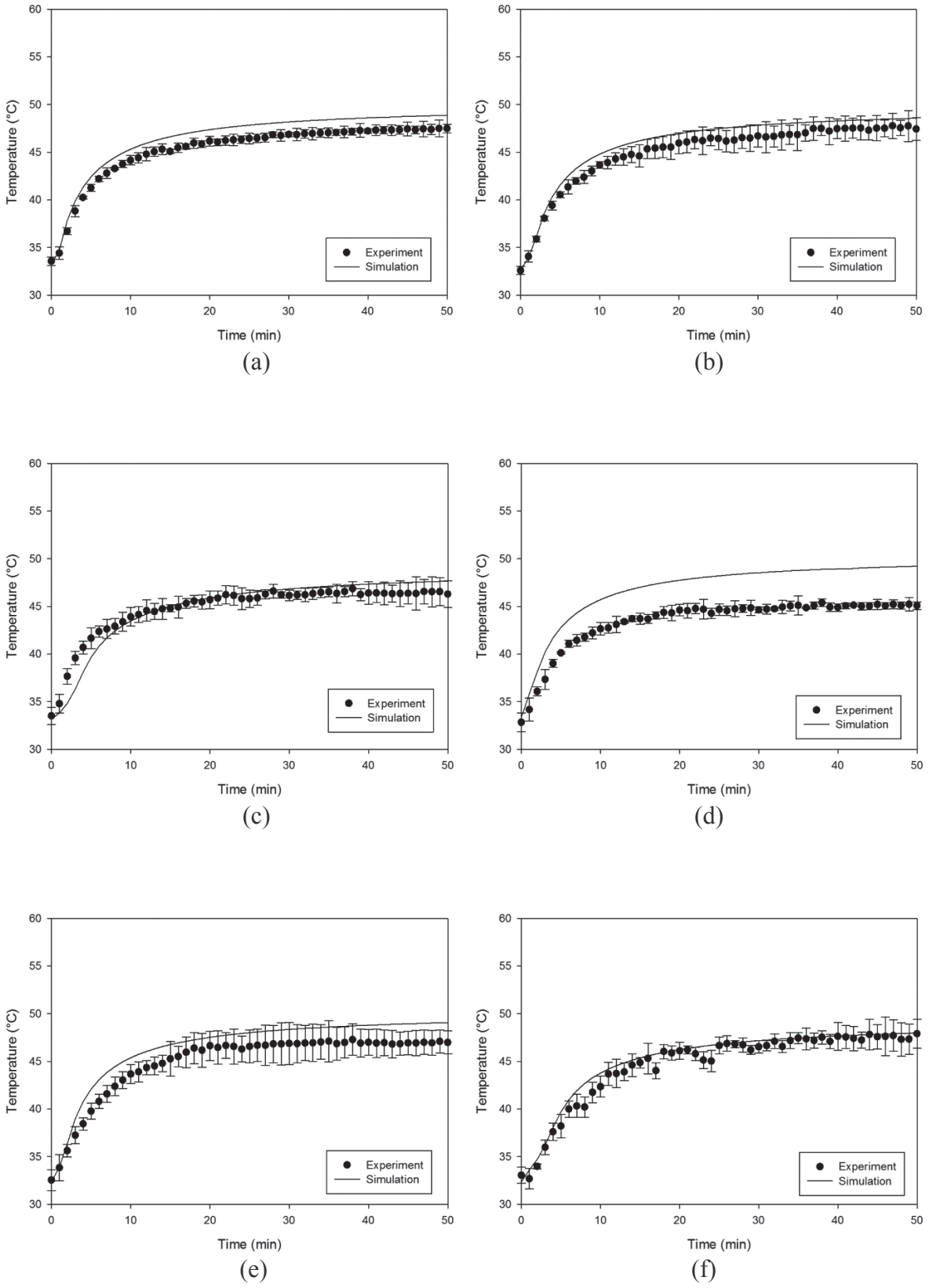

Figure 8. Plots of temperature as a function of time for the experiment and multiphase model in the bottom plane: (a) position B(A); (b) position B(B); (c) position B(C); (d) position B(D); (e) position B(E); (f) position B(F)

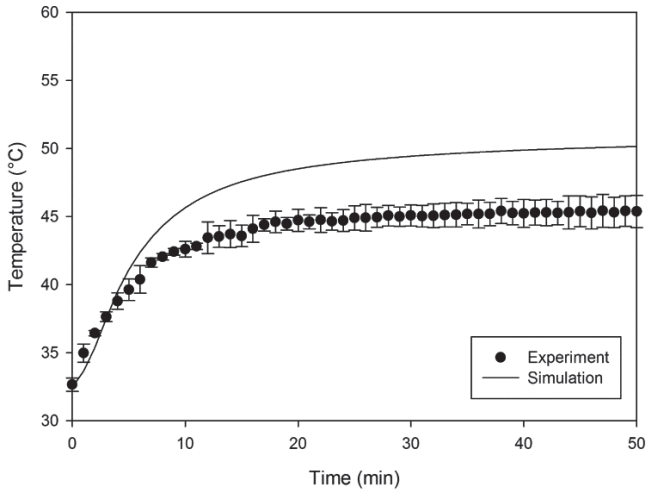

Figure 9. Plots of temperature as a function of time for the experiment and multiphase model in the middle plane (position M(D))

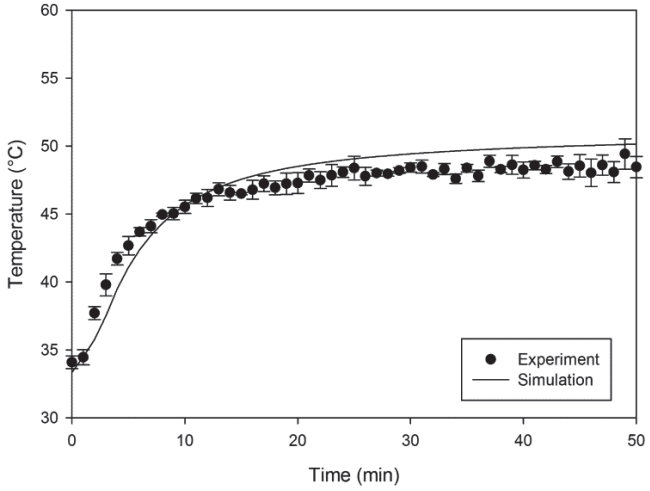

Figure 10. Plots of temperature as a function of time for the experiment and multiphase model in the top plane (position T(D))

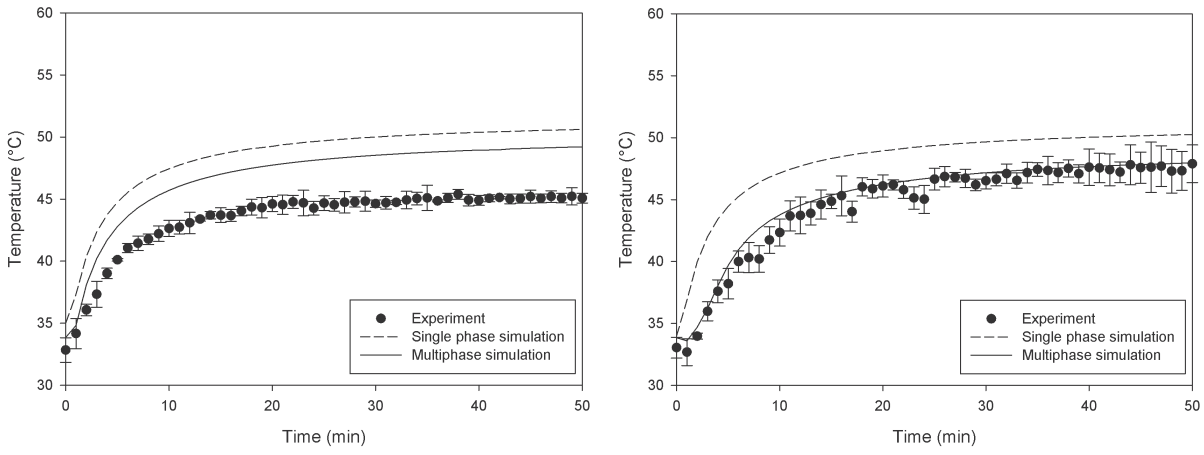

Figure 11. Plots of emperature as a function of time for the experiment and simulations in the bottom plane: (a) position B(D); (b) position B(F)

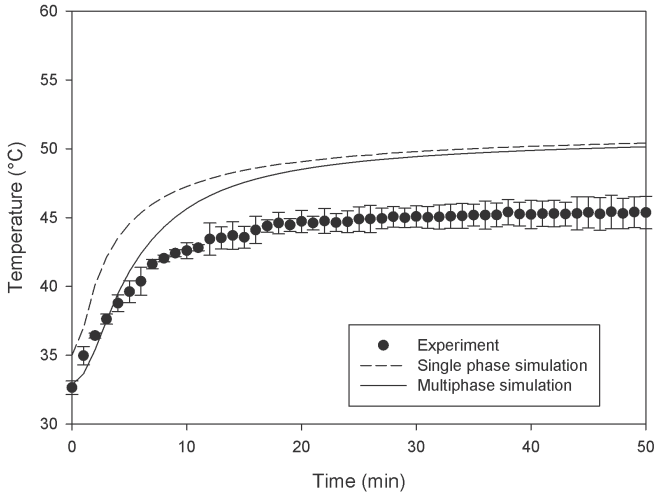

Figure 12. Plots of temperature as a function of time for the experiment and simulations in the middle plane (position M(D))

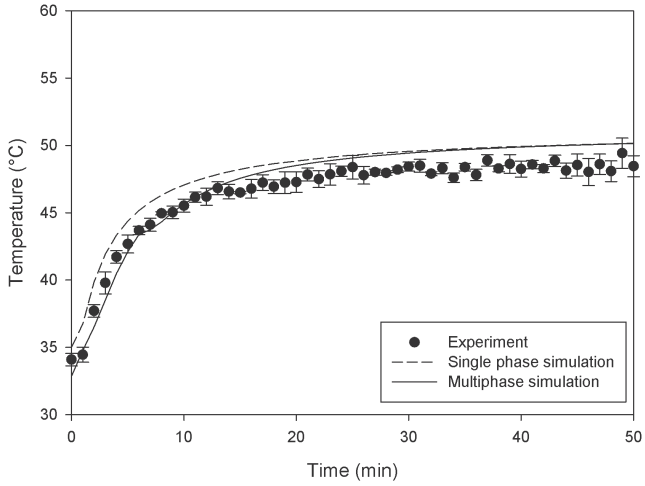

Figure 13. Plots of temperature as a function of time for the experiment and simulations in the top plane (position T(D))

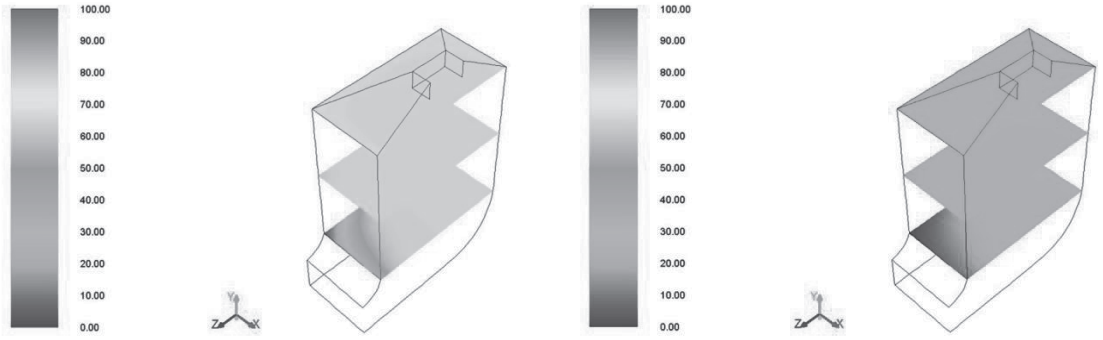

(a) (b)

Figure 14. Relative humidity (%) profile of the bottom, middle and top planes in the drying chamber at 0 min. (a) and 50 min. (steady state) (b)

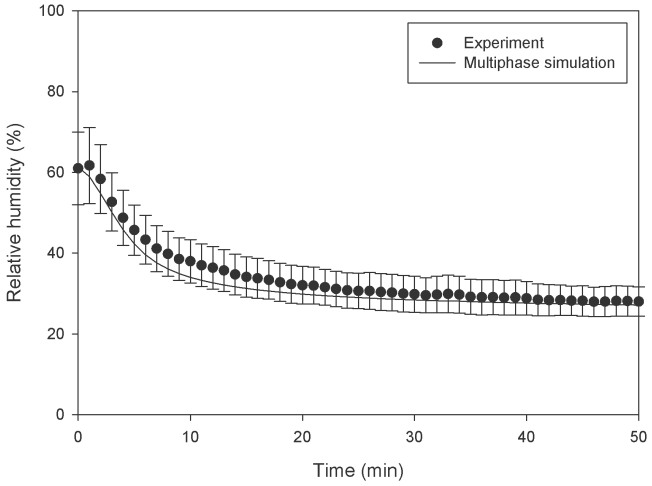

Figure 15. Plots of relative humidity as a function of time in the drying chamber

CONCLUSIONS

Temperature and relative humidity distributions in a model rubber-sheet drying chamber were simulated using CFD. For temperature, the multiphase model is superior to the single-phase model. The largest temperature deviation is seen at the centre-frontal location owing to the turbulence of the hot gas at the inlet. As for relative humidity, the multiphase model well reproduces the experimental results. The multiphase model can thus be used to simulate and reliably predict the temperature and relative humidity distribution in a chamber containing rubber sheets. Nonetheless, the diffusion of moisture from the sheets has to be included in the simulation to obtain the optimal conditions for energy savings.

ACKNOWLEDGEMENTS

This study was supported by the Higher Education Research Promotion and National Research University Project of Thailand, Office of the Higher Education Commission. We also thank Mr. Wiwat Sutiwipakorn for editing the manuscript.

REFERENCES

1. C. Y. Wang and P. Cheng, "A multiphase mixture model for multiphase, multicomponent transport in capillary porous media—I. Model development", *Int. J. Heat Mass Transf*., **1996**, *39*, 3607-3618.
2. V. Mathiesen, T. Solberg and B. H. Hjertager, "An experimental and computational study of multiphase flow behavior in a circulating fluidized bed", *Int. J. Multiphase Flow*, **2000**, *26*, 387-419.
3. P. Spicka, M. M. Dias and J. C. B. Lopes, "Gas-liquid flow in a 2D column: Comparison between experimental data and CFD modelling*"*, *Chem. Eng. Sci*., **2001**, *56*, 6367-6383.
4. S. Venkateswaran, J. W. Lindau, R. F. Kunz and C. L. Merkle, "Computation of multiphase mixture flows with compressibility effects", *J. Comput. Phys*., **2002**, *180*, 54-77.
5. M. V. Tabib, G. Lane, W. Yang and M. P. Schwarz, "CFD study of single phase and multiphase (liquid–liquid) pump-mixer: Analyzing design parameters, flow structures and turbulence", *Chem. Eng. Sci*., **2012**, *80*, 55-69.

6. B. Xia and D. W. Sun, "Applications of computational fluid dynamics (CFD) in the food industry: A review", *Comput. Electron. Agric*., **2002**, *34*, 5-24.
7. P.-S. Mirade, "Prediction of the air velocity field in modern meat dryers using unsteady computational fluid dynamics (CFD) models", *J. Food Eng*., **2003**, *60*, 41-48.
8. E. Mathioulakis, V. T. Karathanos and V. G. Belessiotis, "Simulation of air movement in a dryer by computational fluid dynamics: Application for the drying of fruits", *J. Food Eng*., **1998**, *36*, 183-200.
9. J. Smolka, A. J. Nowak and D. Rybarz, "Improved 3-D temperature uniformity in a laboratory drying oven based on experimentally validated CFD computations", *J. Food Eng*., **2010**, *97*, 373-383.
10. J. Cui and S. Wang, "Application of CFD in evaluation and energy-efficient design of air curtains for horizontal refrigerated display cases", *Int. J. Therm. Sci*., **2004**, *43*, 993-1002.
11. P.-S.Mirade, A. Kondjoyan and J.-D. Daudin, "Three-dimensional CFD calculations for designing large food chillers", *Comput. Electron. Agric*., **2002**, *34*, 67-88.
12. T. A. G. Langrish and D. F. Fletcher, "Spray drying of food ingredients and applications of CFD in spray drying", *Chem. Eng. Process*., **2001**, *40,* 345-354.
13. M. Promtong and P. Tekasakul, "CFD study of flow in natural rubber smoking-room: I. Validation with the present smoking-room", *Appl. Thermal Eng*., **2007**, *27*, 2113-2121.
14. P. Tekasakul and M. Promtong, "Energy efficiency enhancement of natural rubber smoking process by flow improvement using a CFD technique", *Appl. Energ*., **2008**, *85,* 878-895.
15. H. K. Versteeg and W. Malasekera, "An Introduction to Computational Fluid Dynamics: The Finite Volume Method", Pearson Education, Essex, **1995**.
16. J. D. Anderson, "Computational Fluid Dynamics: The Basics with Applications", McGraw-Hill, New York, **1995**.
17. R. B. Bird, W. E. Stewart and E. N. Lightfoot, "Transport Phenomena", 2nd Edn., John Wiley and Sons, New York, **2007**.